

**REACTION OF METHANE IN A DIELECTRIC  
BARRIER DISCHARGE PLASMA REACTOR**

By

GREGORY D. HOLLAND

Bachelor of Science

Oklahoma State University,

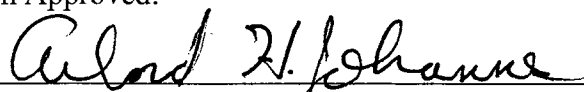
Stillwater, Oklahoma

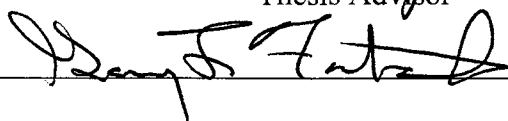
1995

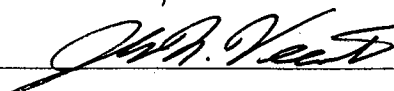
Submitted to the faculty of the  
Graduate College of  
Oklahoma State University  
In partial fulfillment of  
The requirements for  
The Degree of  
DOCTOR OF PHILOSOPHY  
December, 2002

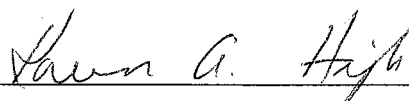
REACTION OF METHANE IN A DIELECTRIC  
BARRIER DISCHARGE PLASMA REACTOR

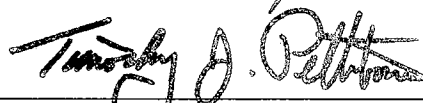
Dissertation Approved:

  
Thesis Advisor









Dean of the Graduate College

## ACKNOWLEDGMENTS

I wish to express my gratitude to my major advisor, Dr. AJ Johannes for his guidance and assistance throughout my graduate program. I would also like to thank the other members of my committee, Dr. Gary Foutch, Dr. Karen High, and Dr. John Veenstra for all of their time and assistance. The staff of the School of Chemical Engineering, both past and present, also deserves special recognition for all of the assistance they have provided me. I am also grateful to the School of Chemical Engineering and to the Oklahoma State University Environmental Institute for their years of financial support.

A special debt of gratitude goes to my parents, Lonnie and Linda Holland. This goal could never have been accomplished without their endless love and financial support in times of need. For all that you have ever done, I thank you.

Last but certainly not least, I would like to thank my loving wife for her patience and devout encouragement during the final phases of this research.

## TABLE OF CONTENTS

1. . INTRODUCTION .....	1
1.1. Objectives of the Study.....	3
1.2. Outline of Work.....	3
2. BACKGROUND INFORMATION AND LITERATURE REVIEW .....	5
2.1. Background Information.....	5
2.1.1. Thermodynamic Considerations .....	5
2.1.2. Plasma .....	6
2.1.3. Non-equilibrium Plasma Reactors .....	10
2.1.4. Chemical Reactions .....	16
2.2. Hydrocarbon Reactions in Electric Discharge.....	18
2.3. Electric Discharge Models.....	22
2.4. Research at Oklahoma State University .....	24
3. EXPERIMENTAL APPARATUS AND PROCEDURE .....	27
3.1. Experimental Method .....	27
3.1.1. Dielectric Barrier Discharge Reactor.....	27
3.1.2. Gas Chromatograph .....	31
3.1.3. Temperature Measurements.....	32
3.1.4. Pressure Measurements.....	32
3.1.5. Mass Flow Measurements.....	32
3.1.6. Power Supply .....	33
3.1.7. Step-up Transformer .....	33
3.1.8. Voltage Measurements.....	33
3.1.9. Current Measurements .....	33
3.2. Experimental Procedure.....	34
4. RESULTS AND DISCUSSION – EXPERIMENTAL .....	37
4.1. Residence Time .....	37
4.2. Operating Frequency .....	39
4.3. Electric Field Strength .....	42
4.4. Circuit Variables.....	44
4.5. Scaling the Dielectric Barrier Discharge Process.....	47
4.5.1. Flow Rate.....	47

4.5.2. Dual Reactor Study .....	49
4.6. Additional Observations .....	54
5. EXPERIMENTAL RECOMMENDATIONS .....	57
6. METHANE PLASMA MODEL FRAMEWORK.....	60
6.1. Model Overview .....	60
6.1.1. Residence Time.....	62
6.1.2. Discharge Frequency and Period .....	62
6.1.3. Temperature .....	62
6.1.4. Pressure .....	63
6.2. Electron Density .....	63
6.3. Electric Field.....	63
6.4. Reactions.....	63
7. RESULTS AND DISCUSSION – MODELING.....	66
7.1. Base Case for Scaled Parameters.....	66
7.2. Residence Time .....	69
7.3. Operating Frequency .....	74
7.4. Hydrogen Production.....	78
7.5. Sensitivity Analysis .....	78
8. METHANE PLASMA MODEL RECOMMENDATIONS.....	81
9. CONCLUSIONS.....	82
REFERENCES .....	85
APPENDIX A – Experimental Data.....	89
APPENDIX B – Calibration Data.....	97
APPENDIX C – MATLAB Routines .....	100
APPENDIX D – Reactions .....	109
APPENDIX E – Bisection Subroutine.....	112

APPENDIX F – Sensitivity Analysis .....	115
---	-----

## LIST OF TABLES

1. Ranges of Variables Studied.....	4
2. Characteristic Parameters for Glow Discharges .....	12
3. Characteristic Parameters for Corona Discharges .....	13
4. Characteristic Parameters for Dielectric Barrier Discharges .....	15
5. Reactor Dimensions .....	30
6. Gas Chromatograph Operating Parameters .....	32
7. Calculated Hydrogen Mole Fractions .....	54
8. Carbon Fraction Comparison: Experiment vs. Model Base Case at 250 Hz, 27 kV, and 3.1 seconds .....	66
9. Carbon Fraction Comparison: Experiment vs. Model Base Case at 250 Hz, 27 kV, and 2.2 seconds .....	69
10. Carbon Fraction Comparison: Experiment vs. Model Base Case at 250 Hz, 27 kV, and 5.1 seconds .....	70
11. Carbon Fraction Comparison: Experiment vs. Model Base Case at 200 Hz, 27 kV, and 3.1 seconds .....	74
12. Carbon Fraction Comparison: Experiment vs. Model Base Case at 300 Hz, 27 kV, and 3.1 seconds .....	74
13. Hydrocarbon Sensitivity to Model Variables, Final Composition at 250 Hz and 3.1 seconds .....	78

## LIST OF FIGURES

1. Equilibrium Composition for a Mixture of C <sub>1</sub> to C <sub>5</sub> Hydrocarbons at 1 Atm ...	6
2. Comparison of Maxwellian, Boltzmann, and Druyvesteyn Electron Energy Distribution Functions .....	9
3. Debye Length Plasma Classification .....	9
4. Relationship Between Mean Electron Energy, Reduced Field, and Effective Breakdown Field for Xenon.....	10
5. Typical Glow Discharge Device and Discharge Regions.....	11
6. Electric Field Lines for a Point-plate Corona Discharge .....	12
7. Point-Plate Corona Discharge Device .....	12
8. Typical RF Discharge Configurations .....	13
9. Single Dielectric Barrier (Semi-Corona) Discharge Devices .....	14
10. Dual Dielectric Barrier (Ozonizer) Discharge Devices .....	15
11. Diagram of Experimental Setup.....	29
12. Close-up Image of Plasma Reactor While Not in Operation.....	30
13. Close-up Image of Plasma Reactor While in Operation.....	30
14. The Effect of Residence Time on Methane Conversion and Product Distribution at 250 Hz and 27 kV .....	38
15. The Effect of Residence Time on Product Selectivity at 250 Hz and 27 kV...	38
16. The Effect of Frequency on Methane Conversion and Product Distribution at 3.1 seconds and 27 kV .....	41
17. The Effect of Frequency on Product Selectivity at 3.1 seconds and 27 kV.....	41
18. The Effect of Electric Field on Methane Conversion and Product Distribution at 3.1 seconds and 250 Hz .....	43
19. The Effect of Electric Field on Product Selectivity .....	43
20. The Primary Voltage of the Transformer as a Function of the Secondary Voltage of the Transformer.....	45
21. The Voltage Across a 3-ohm Resistor on the Primary Side of the Transformer as a Function of the Secondary Voltage of the Transformer .....	46
22. The Current at the 120-Volt Wall Source as a Function of the Secondary Voltage of the Transformer.....	46
23. The Primary Voltage of the Transformer for Two Different Retention Times at Two Different Frequencies .....	47
24. The Voltage Across a 3-ohm Resistor on the Primary Side of the Transformer for Two Different Retention Times at Two Different Frequencies .....	48
25. The Current at the 120-Volt Wall Source as a Function of the Secondary Voltage of the Transformer for Two Different Retention Times at Two Different Frequencies.....	48



26. The Power at the 120-Volt Wall Source as a Function of the Secondary Voltage of the Transformer for Two Different Retention Times at Two Different Frequencies.....	49
27. Comparison of Methane Conversion and Product Distribution for Dual Reactor and Single Reactor Configurations at 3.2 seconds, 250 Hz, and 27 kV.....	51
28. Comparison of Product Selectivity for Dual Reactor and Single Reactor Configurations at 3.2 seconds, 250 Hz and 27 kV.....	51
29. The Primary Voltage of the Transformer as a Function of the Secondary Voltage of the Transformer for Dual Reactor and Single Reactor Configurations at 3.2 seconds and 250 Hz.....	52
30. The Voltage Across a 3-ohm Resistor on the Primary Side of the Transformer for Dual Reactor and Single Reactor Configurations at 3.2 seconds and 250 Hz .....	52
31. The Current at the 120-Volt Wall Source as a Function of the Secondary Voltage of the Transformer for Dual Reactor and Single Reactor Configurations at 3.2 seconds and 250 Hz.....	53
32. The Power at the 120-Volt Wall Source as a Function of the Secondary Voltage of the Transformer for Dual Reactor and Single Reactor Configurations at 3.2 seconds and 250 Hz.....	53
33. Two Types of Solid Deposits Inside the Reactor.....	56
34. Flowchart Showing Separate Stages of Plasma Model.....	61
35. Detailed Trace of CH <sub>4</sub> Carbon Fraction over a Five-Discharge Interval.....	67
36. Detailed Trace of CH <sub>3</sub> • Carbon Fraction over a Five-Discharge Interval .....	68
37. Detailed Trace of C <sub>2</sub> H <sub>6</sub> Carbon Fraction over a Five-Discharge Interval .....	68
38. Detailed Trace of C <sub>2</sub> H <sub>5</sub> • Carbon Fraction over a Five-Discharge Interval.....	69

## NOMENCLATURE

$\epsilon_0$  = Electron Energy (eV)

$m_e$  = Electron Mass

$v$  = Electron Velocity

$\lambda_D$  = Debye Length (m)

$k$  = Boltzmann's Constant

$T$  = Absolute Temperature

$e$  = Charge of Electron

$n$  = Number Density ( $\text{cm}^{-3}$ )

$D$  = Diffusion Coefficient ( $\text{cm}^2/\text{s}$ )

$\mu$  = Ionic Mobility ( $\text{cm}^2/\text{Vs}$ )

$E$  = Electric Field Strength (V/cm)

$E/n$  = Reduced Electric Field (Td)

$nd$  = Effective Breakdown Field ( $\text{cm}^{-2}$ )

eV = Electron Volt (1 eV =  $1.60\text{E-}19$  J)

$p_0$  = Pressure

# CHAPTER 1

## INTRODUCTION

Many investigators have attempted to convert methane to higher molecular weight hydrocarbons. The economic potential for such conversions is significant. Natural gas is the least expensive petroleum resource in the U.S. and wellhead prices historically have been very low. Any economic process that could convert natural gas to a higher molecular weight product such as ethane, ethylene, propane, or oxygenates such as methanol would increase the value of these reserves.

The remote location of many natural gas reserves also creates a hindrance to their economic development. Transportation of methane through compressed gas lines is costly and inefficient. The ability to convert natural gas to a liquid product before transport would allow compressors to be replaced with pumps and improve the cost-benefit ratio.

The most commonly studied method for converting natural gas to a higher value product involves a catalytic reaction of methane and oxygen. In this process, ethane, ethylene, and small amounts of higher molecular weight hydrocarbons are formed. However, the production of undesirable oxidation products such as carbon monoxide and carbon dioxide reduces the efficiency of this type of process. Typical reaction conditions for these processes are temperatures ranging from 900 – 1100 K and pressures from 2 – 10 atmospheres.

Previous studies indicate the primary coupling reactions required to form ethane or other higher molecular weight hydrocarbons from methane are free radical reactions

[1-3]. If the methyl radical concentrations could be kept high with little or no oxygen present, the coupling reactions would be maximized and the oxidation products would be minimized. A dielectric barrier discharge (DBD) has the potential to do this. Although DBD was first studied over 100 years ago, the only resulting large-volume industrial application to date is ozone production. Research conducted at Oklahoma State University has proven that this technology can create free radicals from methane and produce higher molecular weight hydrocarbons from propane [4-5].

DBD processes possess three characteristics that are important for the economic production of longer-chain hydrocarbons from methane. The first is that no oxygen is required for the production of free radicals. Bond cleavage occurs when high-energy free electrons collide with one of the heavier molecular species. The second is that operating temperatures are near ambient because the generated plasma is not in thermal equilibrium with the molecules of the product stream. The free electrons acquire substantial kinetic energy in the alternating electric field of the plasma reactor. Uncharged molecular species are unaffected by this field. Electron impact provides the mechanism for energy transfer. Uncharged molecules gain very little kinetic energy from the electrons because of the large mass differential. Since the neutral molecules of the system do not acquire appreciable kinetic energy, the temperature of the product stream remains near ambient and typically is only a few degrees warmer than the inlet stream [6]. This ability to operate at ambient temperatures eliminates the need for costly heat-recovery equipment. The third characteristic is that operating pressures are near atmospheric pressure. Unlike some other non-equilibrium plasma processes (e.g. glow discharge), DBD can operate at relatively high pressures ( $\geq 1$  atmosphere), eliminating the need for a costly vacuum

system. This ability to operate at positive gage pressures also eliminates the concerns of contamination from leaks.

### **1.1 Objectives of the Study**

The first objective of this study was to determine if the carbon-hydrogen bonds of methane could be broken in the DBD plasma reactor and to investigate the effects of frequency, applied voltage, and residence time on the conversion and product selectivity when methane was exposed to dielectric barrier discharge. The second objective was to develop a scaled kinetic model for methane reactions that occur in the dielectric barrier discharge.

### **1.2 Outline of Work**

The experimental phase involved acquisition and assembly of the various components of the reaction system and analytical apparatus. The reaction system included the methane source, tubing, reactor, flare, power supply, and luminous tube transformer. The analytical system included the gas chromatograph used for identification and quantification of the product gases and the electrical probes used to measure various power and energy variables. Once these systems were in place, experiments were conducted to measure product composition when the reactor was operated at ambient pressure and temperature for the range of variables shown in Table 1.

The modeling phase involved building a database of relevant chemical reactions and solving them as a stiff set of coupled ordinary differential equations using *MATLAB*. Electron impact rates were scaled to match a single set of operating conditions used as a

basis. Model predictions then were compared to experimental results for various operating conditions. A sensitivity analysis was conducted to investigate the stability of the model framework for each of the unknown variables. Recommendations for future research are also presented.

TABLE 1  
RANGES OF VARIABLES STUDIED

Variable	Range
Frequency	200-300 Hz
Electric Field	108-154 kV/cm
Residence Time	2.2-5.1 seconds

## CHAPTER 2

### BACKGROUND INFORMATION & LITERATURE REVIEW

#### 2.1 Background Information

##### 2.1.1 Thermodynamic Considerations

Traditional methods of methane conversion take advantage of the equilibrium compositions of various hydrocarbons at high temperatures. The methane feed is heated to the desired temperature, the gas is allowed to reach equilibrium and then the temperature is quickly lowered. Figure 1 shows the equilibrium compositions calculated using Outokompu's *HSC Chemistry* program (Ver. 3.0) when a Gibbs minimization is performed over a range of 0 to 3000 °C at atmospheric pressure. The hydrogen-to-carbon ratio is maintained at 4:1, the same as for methane molecules. Methane is the primary hydrocarbon up to 500 °C. Small amounts of isobutane and ethylene form near 1000 °C, but quickly diminish as the temperature is raised. Acetylene becomes the primary hydrocarbon from 1500 to 2000 °C and cyclopropane becomes the primary hydrocarbon above 2500 °C. The changes in hydrogen composition reflect the changes in the saturation of the dominant hydrocarbon(s).

A temperature of 648 °C is required to convert 5% of the methane to other components at equilibrium. A temperature of 736 °C is required to convert 10% of the methane to other components at equilibrium. An equilibrium conversion of 50% is not realized until 1050 °C.

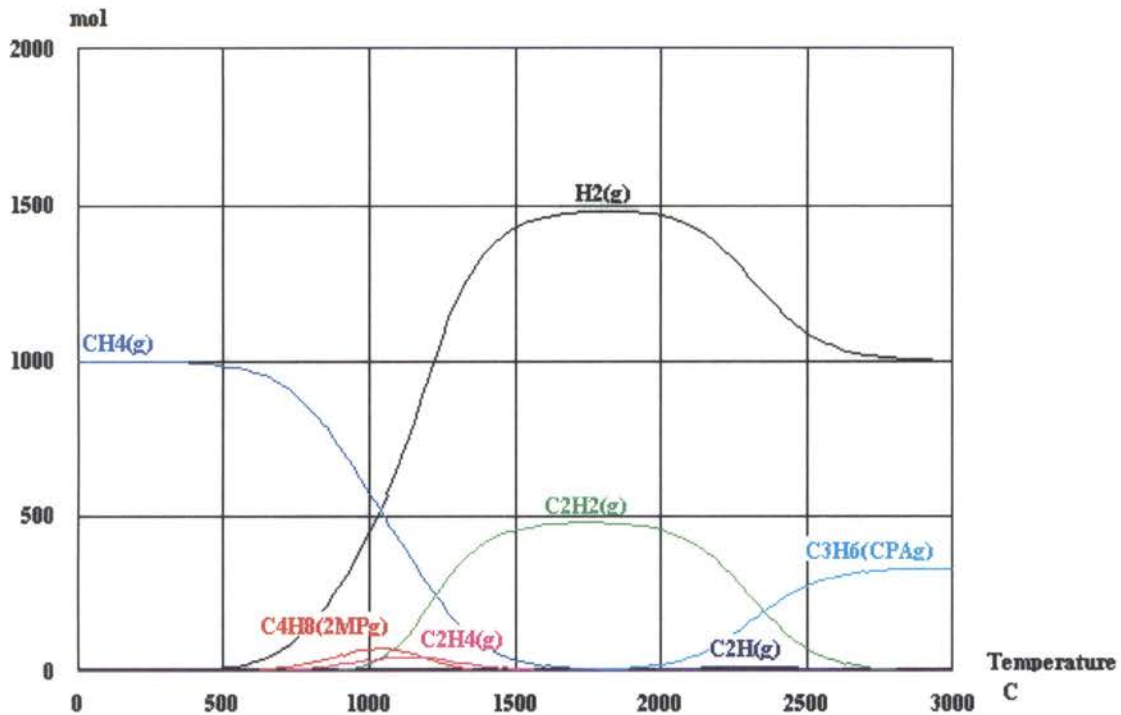


Figure 1. Equilibrium Composition for a Mixture of  $C_1$  to  $C_5$  Hydrocarbons at 1 Atmosphere

### 2.1.2 Plasma

A plasma is an ionized or partially ionized gas and differs from ordinary gas in that it is a good conductor of electricity and is affected strongly by an electric or magnetic field. However, the wide range of fundamental plasma parameters results in various plasma classifications.

If the free electrons are in thermodynamic equilibrium with the gas molecules, then the plasma is considered an equilibrium or thermal discharge (e.g. thermal arc). If the free electrons are not in thermodynamic equilibrium with the neutral gas molecules, the plasma is considered a non-equilibrium discharge (e.g. corona discharge). Eliasson et al. provide an excellent comparison of non-equilibrium plasma processes [7].



Plasma also can be separated into disruptive and non-disruptive discharges. Disruptive discharges have a highly localized current flow (e.g. spark discharge). Non-disruptive discharges have a relatively low current flow diffused over the entire surface of the discharge gap (i.e., glow discharge).

A more rigid plasma classification scheme can be established by considering the following three factors: electron energy, electron density, and Debye length [8]. Electron energy ( $\epsilon$ ) is defined as:

$$\epsilon_o = \frac{1}{2}(m_e v^2) \quad (1)$$

where ( $m_e$ ) is the electron mass and ( $v$ ) is the electron velocity. Electron energy is sometimes expressed as an effective electron temperature ( $T_e$ ). One electron volt (eV) is equal to an effective electron temperature of approximately 11,600 K.

It should also be noted that electron energies typically are reported as mean values; they are not mono-energetic. Electron energy distributions frequently are non-Maxwellian, and in all cases, the majority of the electrons populate low-energy levels with a relatively small population in the high-energy tail as shown in Figure 2.

In partially ionized plasmas such as DBD, the energy distribution function maxima often coincide with the energy required for electronic excitation (2-3 eV). Electronic excitation leads to photon emission upon relaxation of the molecule and produces a visible glow from the plasma region. Only a relatively small fraction of the electrons in a weakly ionized plasma possess the energy typically required for dissociation (6-14 eV).

Electron density ( $n_e$ ) is defined as the number of free electrons per unit volume and typically may range from  $10^{12}$  to  $10^{26} \text{ m}^{-3}$ . The Debye length ( $\lambda_D$ ) characterizes the screening effect on the field of a charged particle by oppositely charged particles, and typically may range from  $10^{-10}$  to  $10^{-1} \text{ m}$ . Much larger ranges are possible for electron density and Debye length and may occur in natural processes (stellar plasmas and lightning). For parallel plate geometry Debye length is defined as:

$$\lambda_D = \epsilon_0 kT / (e^2 n_e) = D\epsilon_0 / \mu e n_e$$

General plasma types can be classified with these variables as shown in Figure 3 [8].

Another commonly used parameter for non-equilibrium plasmas is the reduced field ( $E/n$ ) which is the electric field divided by the neutral gas density and is often measured in units of Townsends (Td). One Td is equal to  $1 \times 10^{-17} \text{ V-cm}^2$ . The electron energy and the breakdown strength of a plasma are both determined by the reduced field as shown in Figure 4. Typical gases such as  $\text{O}_2$  and  $\text{N}_2$  break down around 100 Td [7]. One major advantage of silent discharge is the ability to control the mean electron energy by adjusting the product of gas density and gap width ( $nd$ ) [6].

Based on these comparisons, silent electric discharge can be classified as a non-equilibrium, non-disruptive discharge with relatively low electron energies and intermediate electron densities.

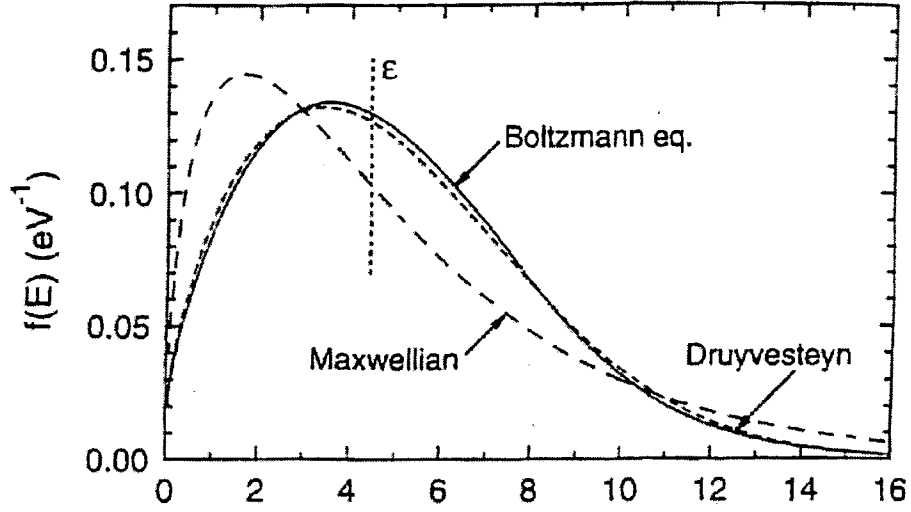


Figure 2. Maxwellian Electron Energy Distribution Function Compared with Boltzmann and Druyvesteyn Distribution Functions [9]

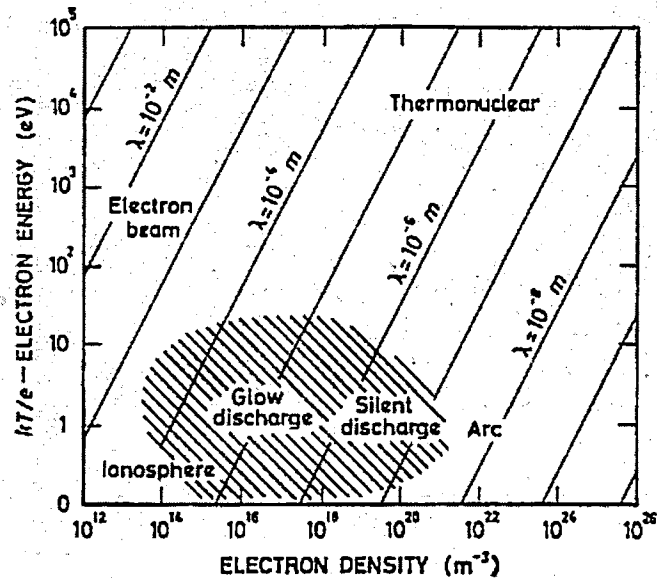


Figure 3. Debye Length Plasma Classification [8]

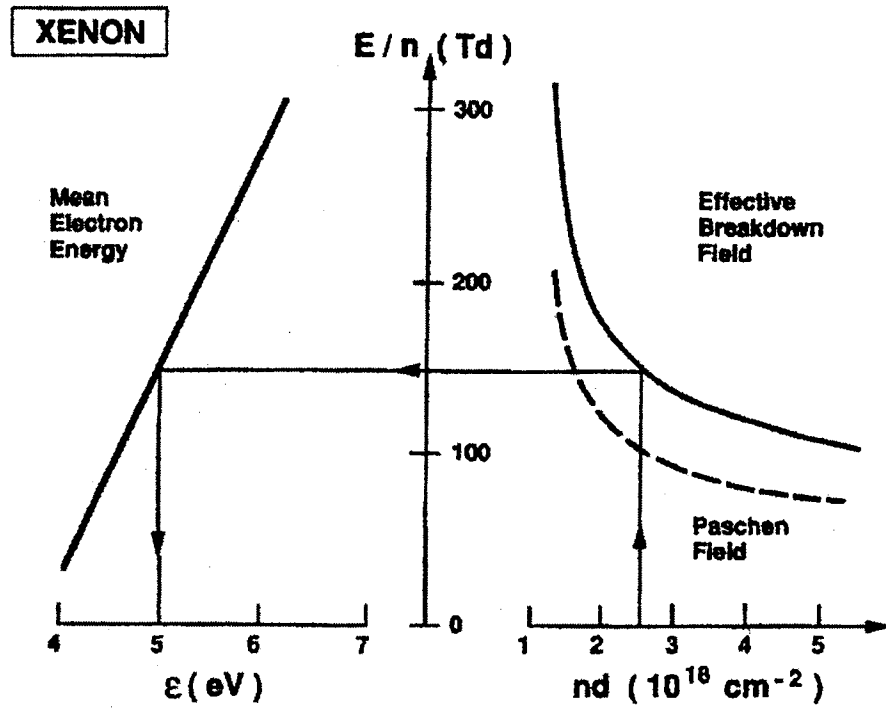


Figure 4. Relationship Between Mean Electron Energy, Reduced Field, and Effective Breakdown Field for Xenon [6]

### 2.1.3 Non-equilibrium Plasma Reactors

A brief description of different non-equilibrium plasma types and reactor configurations encountered in the literature is presented here and compared to plasma type and reactor configuration used in this research.

*Glow discharge* is a non-disruptive discharge in which a low temperature, low-pressure (vacuum) discharge is produced by applying a direct current between two electrodes inside the reaction chamber. This is the type of plasma generated by modern neon signs. Glow discharges are an important tool for plasma chemical studies but have not been used for industrial production because of the low pressures and low flow rates involved. A typical glow discharge

configuration is shown in Figure 5. Characteristic parameters for glow discharges are shown in Table 2.

*Corona discharge* is a non-disruptive discharge in which a low temperature discharge is produced at atmospheric pressures by strong electric fields generated at highly curved electrode surfaces. Electrode configuration may be a point-point, point-plate (Figures 6 and 7), or a wire-in-tube configuration. Characteristic parameters for corona discharges are shown in Table 3.

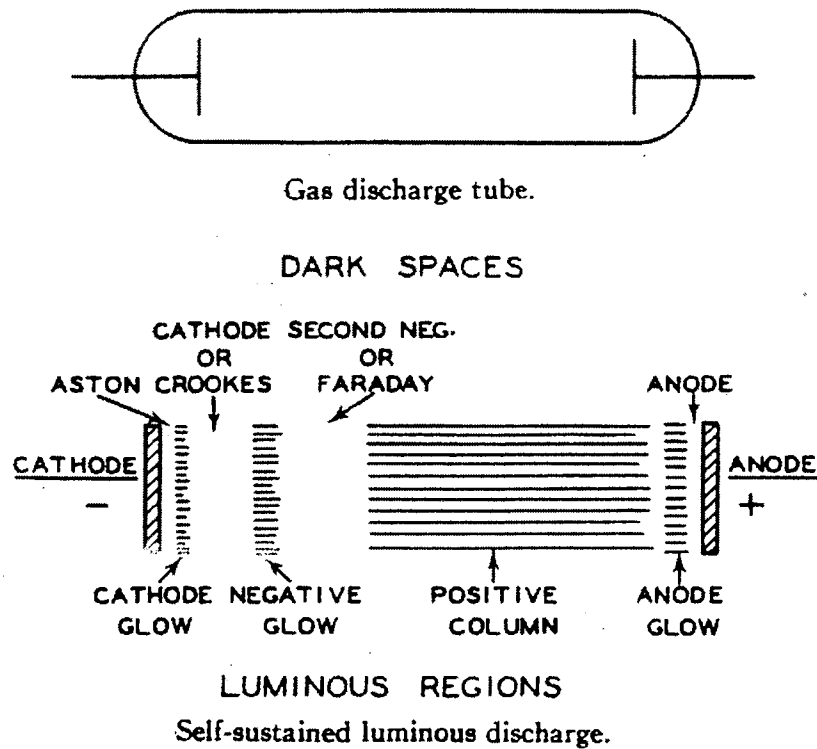


Figure 5. Typical Glow Discharge Device and Discharge Regions [10]

TABLE 2  
CHARACTERISTIC PARAMETERS FOR GLOW DISCHARGES [7]

Pressure	< 10 mbar
Electric Field	10 V/cm
Reduced Field	50 Td
Mean Electron Energy	0.5 to 2 eV
Electron Density	$10^8$ to $10^{11}$ cm <sup>-3</sup>
Degree of Ionization	$10^{-6}$ to $10^{-5}$

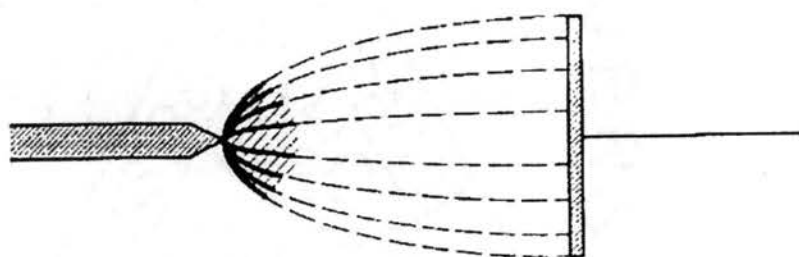


Figure 6. Electric Field Lines for a Point-plate Corona Discharge [7]

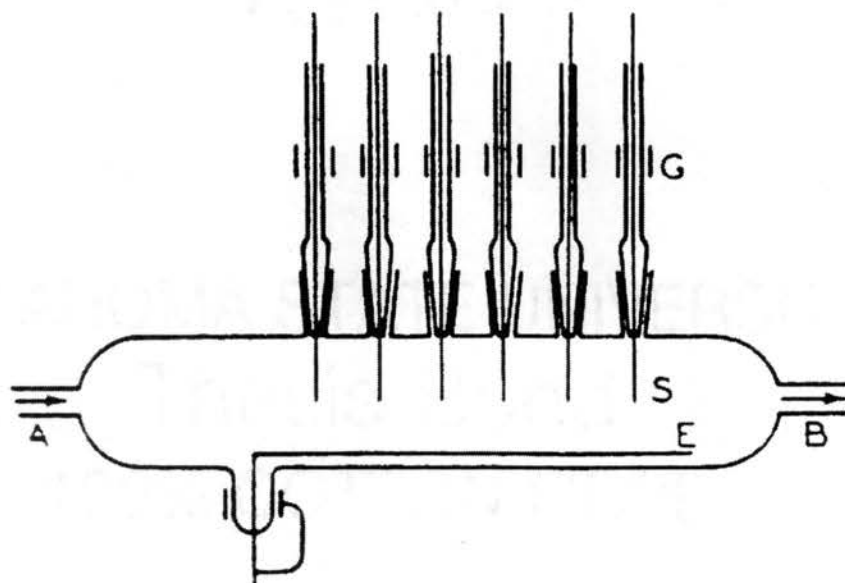


Figure 7. Point-Plate Corona Discharge Device. S = Point Electrodes; E = Plate Electrodes; G = Guard Electrodes; A = Gas Entrance; B = Exit for Reaction Products [10]

TABLE 3  
CHARACTERISTIC PARAMETERS FOR  
CORONA DISCHARGES [7]

Pressure	1 bar
Electric Field	0.5 to 50 kV/cm, variable
Reduced Field	2-200 Td, variable
Mean Electron Energy	5 eV, variable
Electron Density	$10^{13} \text{ cm}^{-3}$
Degree of Ionization	small, variable

*Electrodeless discharge* is a discharge produced by passing a high frequency alternating current through a solenoid that is made of heavily insulated wire and is wrapped around the glass reaction chamber as shown in Figure 8. This high-frequency current produces a strong alternating electric field within the reaction chamber, parallel to the axis of the solenoid. No electrodes are contained within the plasma chamber. Electrodeless discharge also may be referred to as RF (radio frequency) or inductive discharge. This should not be confused with microwave plasmas which are thermal, equilibrium discharges.

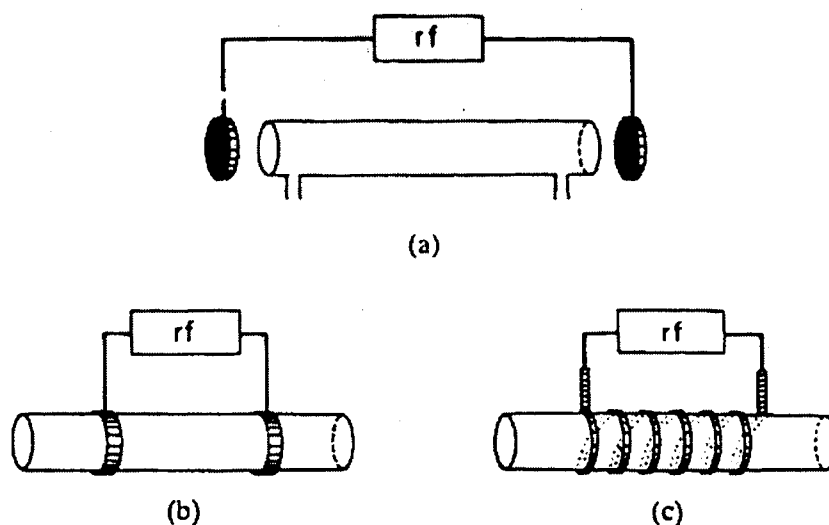


Figure 8. Typical RF Discharge Configurations [7]

*Dielectric barrier discharge* (DBD) was used for this research. DBD is a silent electric discharge in which a low temperature discharge is produced at atmospheric pressures by placing one or more dielectric barriers between the electrodes and generating a large electric field using a high voltage alternating current. If a single dielectric barrier is placed between the electrodes and the inner electrode is a wire, as in Figure 9, the configuration often is referred to as a semi-corona discharge. If two dielectric barriers are used without a wire inner electrode, as in Figure 10, the setup is sometimes referred to as an ozonizer discharge. Characteristic parameters for DBD are shown in Table 4.

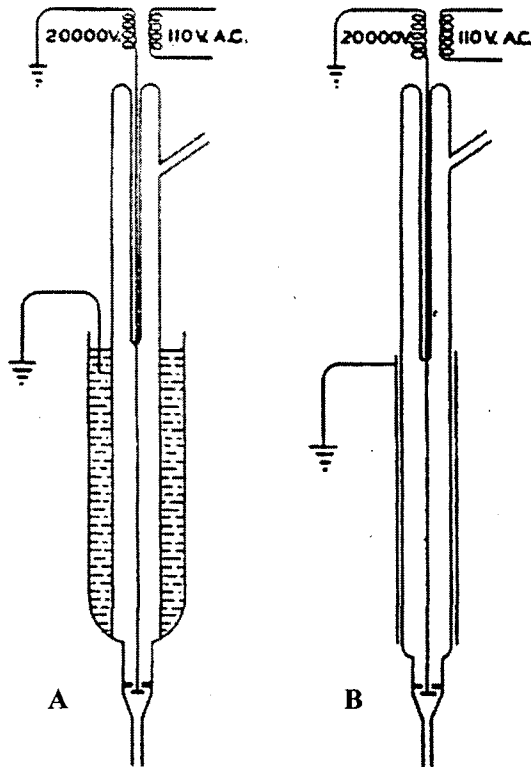


Figure 9. Single Dielectric Barrier (Semi-Corona) Discharge Devices. (A) Inner Electrode is a Fine Wire and Outer Electrode is a Water-Jacket; (B) Outer Electrode is a Metal Foil. [10]



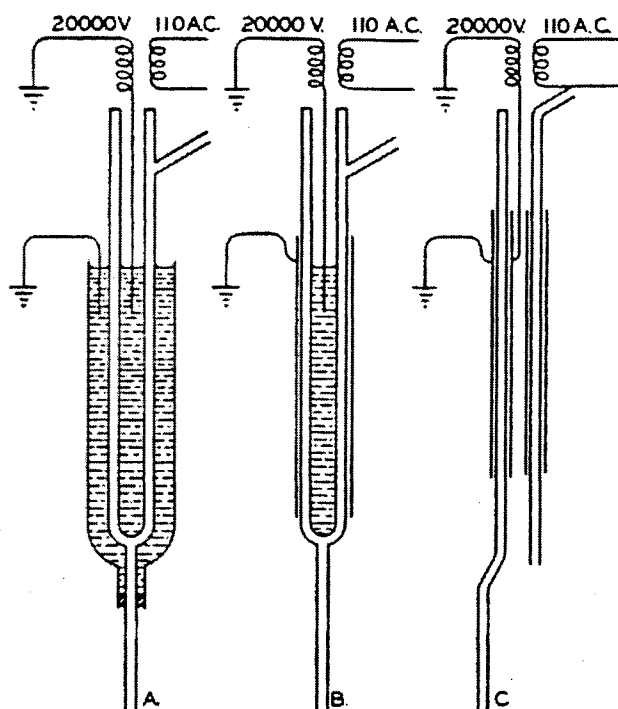


Figure 10. Dual Dielectric Barrier (Ozonizer) Discharge Devices. All-Glass Ozonizers, Cylindrical Type: (A) Two Water Electrodes; (B) Metal Outer and Water Inner Electrode; (C) Two Metal Electrodes. [10]

TABLE 4  
CHARACTERISTIC PARAMETERS FOR  
DIELECTRIC BARRIER DISCHARGES [7]

Pressure	1 bar
Electric Field	0.1 to 100 kV/cm
Reduced Field	1 to 500 Td
Electron Energy	1 to 10 eV
Electron Density	$10^{14} \text{ cm}^{-3}$
Degree of Ionization	$10^{-6}$ to $10^{-5}$

DBD can be formed at ambient temperatures and pressures by generating a strong alternating electric field across a gas-filled space and separating the electrodes by one or more dielectric barriers. The dielectric barrier acts as an insulator and prevents a direct current flow from one electrode to the other. As

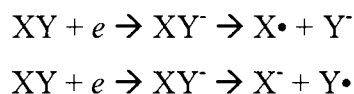
the electric field increases at the beginning of an alternating current (AC) half-cycle, an induced charge builds up on the interior of the reactor wall. Once the electric field reaches a critical value, the gap is no longer able to provide sufficient insulation. The reaction chamber is then filled with micro-discharges as the induced charges attempt to cancel each other. These high-energy electrons impact neutral gas molecules, resulting in electronic excitation, ionization, and dissociation. Many of these impacts result in the production of secondary electrons that are subsequently accelerated by the electric field and may result in additional impacts. The generated charge is transported quickly across the chamber and accumulates on the dielectric surfaces, producing an opposing electric field that eventually will extinguish the micro-discharges. Activated species continue to react even after the micro-discharges have been extinguished. As the electric field reverses polarity, the induced charge increases, breakdown occurs again, and electrons are accelerated back through the gas as the process is repeated.

#### 2.1.4 Chemical Reactions

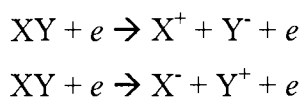
This section provides examples of common hydrocarbon reactions that occur within silent electric discharge [8]. This is not an exhaustive list of possible reactions, only a representative example of known reaction processes. These and other reaction mechanisms may be found in the literature [8,10].

One ionization process that can occur at the lowest electron energy levels is the formation of negative ions by electron resonance capture. Dissociation of

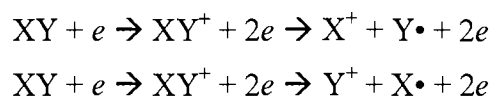
this negative ion may then result in the formation of a smaller negative ion and a free radical:



Electron resonance capture occurs at energies on the order of 6-7 eV and therefore occurs at reasonable efficiencies in silent electric discharges. At electron energies of approximately 10-14 eV, fragmentary ionization may occur:

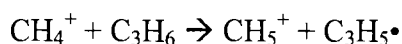


At even higher electron energies, a positive molecule may be formed which can then dissociate into a fragmentary positive ion and a free radical:



Additional types of reactions occur once these initial reactants are formed and often are grouped as follows:

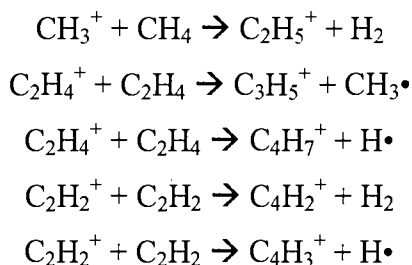
*Atom transfer* – a single atom is removed by a positive ion. These bimolecular ionic reactions can be important in the formation of free radicals.



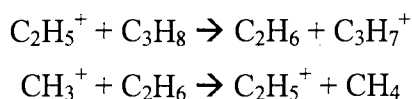
*Symmetrical transfer* – essentially the same as atom transfer, except both reactants are the same species.



This group of reactions also includes ion-molecule transfers that may involve dramatic rearrangements of atoms and bonds.



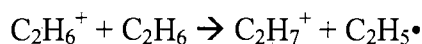
*Negative ion transfer* – ion and molecule interactions involving the exchange of negative hydrogen ions. This occurs almost exclusively with hydrocarbons and tends to produce higher molecular weight species.



*Charge transfer* – a very important source of free radicals in simple diatomic gases.



*Excited ions* – ions that receive additional electron impacts can become excited and form more complex ionic species and free radicals. Symmetric transfers are observed most often but non-symmetric reactions are possible.



## 2.2 Hydrocarbon Reactions in Electric Discharge

This review provides a brief history and representative examples of experiments, not performed at Oklahoma State University, involving the reaction of methane and other hydrocarbons in various types of discharge. Glockler and Lind [10] give a more complete review of early works involving additional chemical reactions in various types

of discharges. Spedding [8] also gives a review of various chemical reactions in non-disruptive, silent electric discharge.

By the end of the 18<sup>th</sup> century, at least two researchers had investigated hydrocarbon reactions using an electric spark discharge. In 1796, Fourcroy subjected three unspecified hydrocarbons to an electric spark, noting the production of oily droplets without deposition of carbon and an increase in gas volume. In 1798, Henry noted the condensation of “gaz hydrogené carboné” when exposed to the electric spark.

In 1869, Bertholet subjected methane to the electric spark and noted the deposition of carbon, liberation of hydrogen, and increase in volume. In 1877 Bertholet also investigated the reactions of methane, ethane and ethylene in a silent electric discharge. He discovered that all three produced free hydrogen, condensed or polymerized hydrocarbons, and small quantities of acetylene. Reaction of ethylene also produced a small quantity of benzene and a liquid characterized as  $C_nH_{1.83n}$ .

In 1874, de Wilde found that acetylene polymerizes more readily in the ozonizer than does ethylene. P. and A. Thenard reported that the polymerization of acetylene to solid occurs with ease, while the polymerization to liquid takes place with more difficulty and under special, unspecified conditions [10].

In 1927, Lind and Glockler began investigating the reactions of many light hydrocarbons using all-glass ozonizer, wire semi-corona, rod semi-corona, and wire corona reactors. Ice water condensation traps were placed between successive reactors to regulate the average molecular weight of the products by removing the higher molecular weight species from the feed. In their study of ethane in the all-glass ozonizer, they found that raising the temperature from 35 °C to 70 °C reduced the average molecular

weight of the products from 467 to 105. They also noted a delayed condensation effect which they attributed to the “open bonds” of unstable species that did not physically condense until they had reacted to form stable, higher molecular weight molecules. Solid carbon dendrites were formed on the inner electrode of the semi-corona reactors, but this solid formation did not occur or was not noticeable in the all-glass ozonizer.

Lind and Glockler continued to investigate the reactions of methane, ethane, propane, n-butane, and ethylene using a series of twelve semi-corona discharge reactors with ice water condensation traps after each reactor. The experiments were carried out at atmospheric pressure, flow rates from 0.45-0.6 liters/hour, and 10-15 kV. They noted an increase in the production of condensed products as the molecular weight of the feed increased. They also noted that the amount of condensed products was greatest in the middle condensers. They suggested that the initial increase of condensation products was due to the accumulation of unreacted activated species and that the subsequent decrease of condensation products was due to the accumulation of hydrogen and methane that diluted the gas and inhibited the reaction of activated species. Two types of solid product were obtained: carbon dendrites that formed on the inner electrode and a resinous, inert solid that formed on the walls. Liquid products were characterized only as distillation fractions. Methane conversion up to 50% was observed [10].

In 1931, Lind and Shultze studied the reaction of methane in an ozonizer at low pressures and short residence times [11-12]. They noted that the total amount of methane reacted in a given time increased rapidly as the pressure was reduced and that liquid products were greater at low pressures.

During the last part of the 20<sup>th</sup> century, improved analytical and diagnostic techniques sparked a renewed interest in discharge processes, including work at Oklahoma State University (see Section 2.2 below). Environmental concerns led to an interest in the oxidation of various compounds such as trichloroethylene, ammonia, and oxides of nitrogen through the use of electric discharge [13-15]. A renewed interest in hydrocarbon addition reactions eventually followed.

Okazaki et al. and Okumoto et al. [16-17] have investigated direct conversion of methane to methanol using silent electric discharge at 250 Hz and voltages up to 25 kV. Major products were methanol and carbon monoxide. Selectivity of methanol was greater at lower oxygen concentrations, and dissociation of oxygen was noted as the primary pre-requisite for methanol formation.

Legrand et al. [18] reacted methane in the afterglow of a 2.45 GHz microwave generator in a discharge tube filled with nitrogen. Metastable states of nitrogen were used to activate methane for the production of ethane, ethylene, acetylene and small amounts of C<sub>3</sub> and C<sub>4</sub> hydrocarbons. They claimed that nitriles were present, but unobservable.

Thanyachotpaiboon et al. [19] studied the conversion of methane to higher hydrocarbons in AC, non-equilibrium plasmas in a planar, single dielectric barrier discharge at 50 Hz and voltages up to 11 kV. Their study examined the influence of residence time and applied voltage on conversion and selectivity. The percent conversion of methane increased significantly at longer residence times. Higher voltages also resulted in higher conversions. Another interesting aspect was that the addition of helium or ethane to the feed greatly enhanced methane conversion.

## 2.3 Electric Discharge Models

By 1967, several researchers had developed experimental methods to measure high-energy electron impact cross sections for methane in electron swarm experiments [1]. By 1977, Kleban and Davis [20-21] were using a two-term Legendre expansion of the Boltzmann equation to model electron drift velocities and diffusion coefficients for polyatomic gases like methane ( $\text{CH}_4$ ) and the deuterium analog of methane ( $\text{CD}_4$ ).

Pitchford et al. [22] conducted their own study on methane and nitrogen. They suggested that a four to eight term Legendre expansion of the Boltzmann equation “was required for convergence of the transport coefficients to the accuracy required for the determination of cross sections from swarm experiments.”

In 1984, Chatham et al. [23] published their work, which measured total and partial electron collisional ionization cross sections for methane ( $\text{CH}_4$ ), ethane ( $\text{C}_2\text{H}_6$ ), silane ( $\text{SiH}_4$ ), and disilane ( $\text{Si}_2\text{H}_6$ ) for electron energies from 30 to 300 eV. This greatly expanded the range over which models could be compared.

The work of Segur et al. [24-25] developed two numerical solution methods of the Boltzmann equation to calculate swarm time-of-flight parameters for nitrogen ( $\text{N}_2$ ) and methane ( $\text{CH}_4$ ). The first solution employed a finite element method (FEM) while the second solution is based on the path differential form of the Boltzmann equation. Both solutions are iterative procedures for which acceleration methods were developed. Good agreement with earlier researchers was found.

Penetrante et al. [26] developed an arbitrary-collision sampling technique for Monte Carlo calculations of diffusion coefficients for electron swarms in gases. Their



method showed excellent agreement with previous results for methane, but discrepancies remained for nitrogen.

Work by Ohmori et al. [27] showed that the two-term Legendre expansion of the Boltzmann equation was not accurate when  $E/p_0$  was on the order of 1 V/cm/Torr. This corresponds to the energy level where a larger number of electrons are in the inelastic cross section region.

Masi et al. [2] used three different approaches to study gas-phase behavior of a methane glow discharge: a traditional thermodynamic equilibrium assumption, a consolidated kinetic method, and a statistical fragmentation method. In the consolidated kinetic method, the electrical properties of the discharge are used to calculate electron energy distribution functions (EEDFs) using a variety of Boltzmann, particle-in-cell (PIC), or Monte Carlo codes [28]. The calculated EEDF is then used to compute electron-molecule impact rates. These impact rates, along with the kinetic constants for conventional thermal reactions, are then solved as a set of ordinary differential equations (ODEs) to determine the system composition. This method can best be applied to systems where parameters such as electron impact cross sections and thermal reaction rate constants are known. The statistical fragmentation method was originally developed for photon ionization processes, but has been extended to low-pressure, weakly ionized plasmas. This method assumes that the energy initially absorbed by a molecule cannot be exchanged with other species and can contribute only to its fragmentation. The system composition is computed by maximizing entropy under the constraints of energy, charge, and atomic mass conservation. The assumption of thermodynamic equilibrium led to

severe errors. The statistical fragmentation theory agreed qualitatively with the detailed kinetic model, which in turn agreed well with experimental results.

Modeling of electron swarm parameters eventually turned to modeling of practical applications like the destruction of hazardous chemicals [29] and the destruction of biological organisms [30]. The terrorist attacks on September 11, 2001 have increased greatly the interest in these applications.

## **2.4 Research at Oklahoma State University**

Many studies on silent electric discharge systems have been performed at Oklahoma State University. These studies have involved a number of different reactor configurations and reactions. A common factor was the placement of at least one dielectric barrier between the electrodes of the reactor and the use of a high-voltage, alternating electric field.

Piatt [4] investigated the potential usefulness of a silent electric discharge reactor as an air purification device for biochemical agents in military vehicles and vessels. A series of destructive and non-destructive tests was performed to develop a kinetic model for methane oxidation and to identify critical variables affecting scale-up. Destruction trends were obtained for a wide range of voltages and frequencies; efficiencies greater than 45% were observed.

Desai [31] investigated the potential utility of a silent electric discharge reactor for the destruction of hydrogen sulfide ( $\text{H}_2\text{S}$ ). Experiments were conducted to identify critical variables affecting the destruction process and to recommend areas for future

investigation. Reaction products were hydrogen gas ( $H_2$ ) and elemental sulfur (S), with destruction efficiencies up to 92%.

Mangrio [32] investigated the feasibility of using a silent electric discharge reactor for the production of titanium dioxide ( $TiO_2$ ) by vapor-phase oxidation of titanium tetrachloride ( $TiCl_4$ ). Ultrafine  $TiO_2$  powders with particle diameters of 0.001-0.1  $\mu m$  were obtained.

Robinowitz [33] studied the production of  $NO_x$  in silent electric discharge systems. Maximum efficiency for conversion was 99.33%. Optimization was achieved by studying the effects of voltage, frequency, and humidity on the reaction system.

Hurst [34] studied the oxidation of carbon tetrachloride in a silent electric discharge reactor. Variables such as voltage, frequency, humidity, and percent excess air were studied to determine optimal operating conditions. Destruction efficiencies up to 94.2% were achieved.

Manning [5] studied hydrocarbon rearrangements and synthesis using a silent electric discharge reactor. By controlling operating variables such as residence time, voltage, and frequency, liquid hydrocarbon products were obtained from pure propane feed.

Sidhu [35] performed additional studies on the production and destruction of  $NO_x$  in a silent electric discharge reactor. The results obtained were comparable to previous studies.

Magunta [36] performed additional studies on the decomposition of  $H_2S$  in a silent electric discharge reactor. The results obtained were comparable to previous studies.

Parker [37] studied the basic parameters of the electrical system used to generate a silent electric discharge and addressed some of the problems associated with operating the reactor at high voltages and frequencies. Recommendations for constructing a more stable system resulted from this work.

Lytle [38] performed additional studies on the electrical system used to generate a silent electric discharge while studying the production and destruction of  $\text{NO}_x$  compounds. The importance of the power factor as it affects the operating parameters was realized in this study.

In summary, much research has been performed with different types of electric discharge, and by researchers in a variety of disciplines: chemistry, physics, electrical engineering, and chemical engineering. Initial work regarding the chemistry and physical mechanism of the plasma has now evolved into application-based research.

## CHAPTER 3

### EXPERIMENTAL APPARATUS AND PROCEDURES

#### 3.1 Experimental Method

A schematic diagram of the apparatus used for this study is shown in Figure 11. Power originated from a 120 V, 60 Hz AC wall plug and was adjusted by a power supply. This power supply controlled the voltage and frequency of the input to the primary side of the high voltage transformer. Voltage and current were measured at the wall plug so that the total power consumption could be calculated. The transformer stepped the voltage up to operating levels. The secondary side (output) of the transformer was connected to the inner and outer electrodes of the reactor and the applied voltage was measured. Voltage and current also were measured on the primary side of the transformer to determine the power consumption in the reactor and transformer. A pressure transducer was used to measure the pressure at the reactor inlet, and a mass flow controller allowed steady, controlled input of the methane feed. Methane purity was 99.99% (research grade). The product gas exiting the reactor was analyzed using an in-line gas chromatograph before being flared. The reactor was contained inside a laboratory fume hood to prevent the possible buildup of dangerous gases. Equipment specifications are given below.

##### 3.1.1 Dielectric Barrier Discharge Reactor

Proper design of the reactor was very important. The geometry and physical parameters of the reactor greatly affected the properties of the electrical

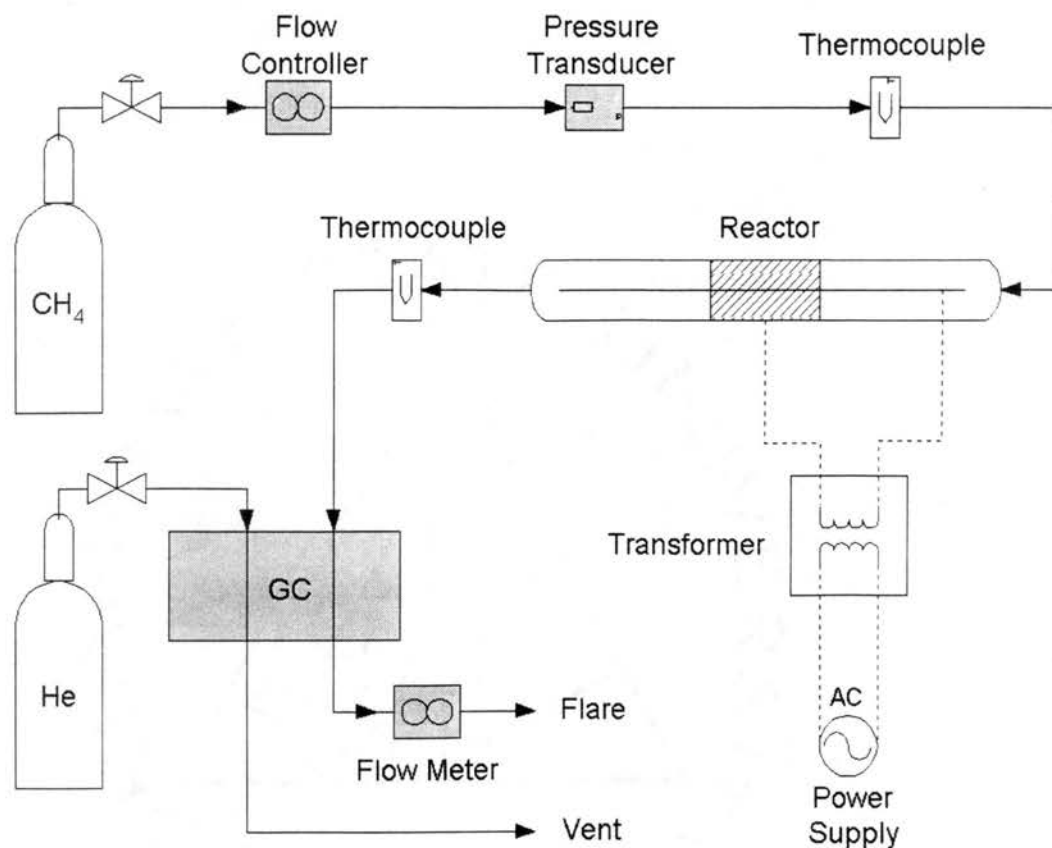


Figure 11. Diagram of Experimental Setup

circuit. Previous studies at Oklahoma State University (OSU) have used a reactor with an annular region for flow between two concentric electrodes. That configuration was retained for this project since it minimized edge effects, provided a more even distribution of the gas flow, and was easier to construct.

A dielectric barrier with a low dielectric constant and a low coefficient of thermal expansion was required for this work. Quartz glass is an extremely pure type of glass and possesses both of these qualities. Quartz glass has been used effectively in previous studies [37]. Some of the previous reactors used at OSU were constructed of Pyrex. On several occasions, reactors constructed from Pyrex failed at point defects where the applied voltage exceeded the integrity of the reactor walls and burn-through occurred.

Another critical factor was electrode design. Previous studies at OSU have used loosely coiled wire or wire mesh electrodes. These types of electrodes did not conform well to the cylindrical shape of the reactor and did not provide a continuous electrode surface area. Small gaps between the electrode material and the dielectric walls caused inefficiencies in the operation of the reactor and increased the capacitance and resistance of the electrical system. Initial attempts to use liquid electrodes in this study resulted in the heating and eventual evaporation of the liquid because of electrical resistance.

Based on these considerations, the final reactor design for this study was a single dielectric barrier reactor (quartz glass tube) with one axial electrode (2-mm brass rod) inside the tube. A second electrode (fine copper wire) was tightly wrapped around the outside of the tube near the midpoint, forming a 3-cm, nearly continuous surface. The reactants flowed through the narrow annulus between the inner electrode and the inner surface of the dielectric barrier. The small annular gap minimized the capacitance of the reactor, keeping the power factor near unity. The reactor was set at a slight downhill slope from inlet to outlet. Reactor dimensions are given in Table 5. Figure 12 shows the reactor while not in operation. The central electrode is visible at each end and the outer electrode is at the center. The black coloration on each side of the central electrode is due to solid buildup (fouling) on the inner walls of the reactor. Figure 13 shows the reactor while it is in operation. The purple light emitted from each side of the central electrode is due to photon emission.

TABLE 5  
REACTOR DIMENSIONS

Dielectric barrier ID	0.5 cm
Dielectric barrier OD	0.7 cm
Reactor Length	30 cm
Diameter of Inner Electrode	0.2 cm
Length of Inner Electrode	30 cm
Length of Outer Electrode	3 cm



Figure 12. Close-up Image of Plasma Reactor While Not in Operation.

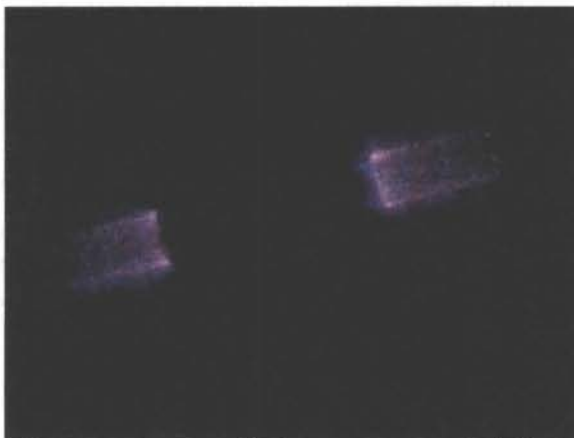


Figure 13. Close-up Image of Plasma Reactor While in Operation.



### 3.1.2 Gas Chromatograph

The gas chromatograph (GC) used in this study was a Varian model 3700 GC with a thermal conductivity detector (TCD) module (part #02-001881-00). The carrier gas was helium at 20 sccm for both the reference and packed column. The packed column was a 9-ft. x 1/8-inch stainless steel column with HayeSep Dip, 100/120 packing. The output device was a Hewlett Packard model 3390A integrator with printout. The GC settings are listed in Table 6. Methane, ethane, propane, isobutane, and n-butane peaks were identified by comparison with the retention times measured for pure component standards. Ethylene, propylene, and pentane peaks were identified based on packed column characteristics and a list of products identified by mass spectrometry at the Phillips Petroleum Company Analytical Lab in Bartlesville. Products were collected using 250-ml glass sample bulbs (Ace Glassware model #7395-44).

TABLE 6.  
GAS CHROMATOGRAPH OPERATING PARAMETERS

Injector Temperature:	170 °C
Column Temperature:	160 °C
Detector Temperature:	200 °C
Filament Temperature:	230 °C
TCD Current:	172.5 mA
Attenuation:	2
Range:	0.5 mV
Output:	negative ( - )
Carrier Gas:	He @ 20 sccm per column

The integrated area for each component peak was converted to a mass fraction using standard weighting factors [39]. The mass fractions were

normalized for all carbon-containing components to calculate the conversion of methane and the carbon fraction of each component.

### 3.1.3 Temperature Measurements

Two Omega type K thermocouples with an Omega DP465 digital readout were used to measure temperatures at the inlet and outlet of the reactor. The thermocouples were calibrated against the Hart Scientific Microtherm 1006 readout and a model 5614 resistor probe. The Hart scientific thermometer had been calibrated against a Minco platinum resistance thermometer at the temperatures of interest.

### 3.1.4 Pressure Measurements

The pressure in the reactor was assumed to be approximately equal to the pressure measured 2-ft. upstream of the reactor inlet using a Sensotec TJE/708-04 pressure transducer and Sensotec 450D digital readout. The pressure transducer was calibrated against the Ruska Model 7215i digital pressure controller.

### 3.1.5 Mass Flow Measurements

Mass flow was controlled using a Brooks 5850 TR Series mass flow controller located upstream of the reactor inlet with a Linde FM4575 Mass Flow Meter control module. A Brooks 5860 TR Series mass flow meter was located downstream, just before the flare, to confirm continuity of gas flow. Both meters were calibrated against an Alltech Digital Flow Meter.

### 3.1.6 Power Supply

The primary voltage to the step-up transformer and the operating frequency of the reactor were regulated using a California Instruments Model-1001TC power supply. The input to the power supply was a standard 120 V, 60 Hz line.

### 3.1.7 Step-up Transformer

A Franceformer Model #15060P luminous tube transformer, mid-point ground, was used to step up the operating voltage for the reactor. The transformer is designed to deliver 15 kV, 3VA from a standard 120 V and 60 Hz input.

### 3.1.8 Voltage Measurements

Measurement of primary and secondary voltage at the transformer was made using a Tektronix P6015A High Voltage/High Frequency Probe (1000x attenuator) with a John Fluke Mfg. Co. Model 8050A digital multimeter. The probe only measures voltage relative to ground so the actual potential difference for both the primary and secondary side was equal to the total magnitude of the voltage trace on the Tektronix 2235 Cathode Ray Oscilloscope (CRO).

### 3.1.9 Current Measurements

Measurement of the total current to the power supply, transformer, and reactor was made using a Weston Electric Instrument Corp. Model #155 ammeter between the power supply and the wall outlet. Measurement of the current

required by just the transformer and reactor was made on the primary side of the transformer by measuring the voltage drop across a 3-ohm resistor located between the power supply and the transformer.

### **3.2 Experimental Procedure**

A few safety precautions should be observed before beginning any experimental work. The two primary sources of danger are high voltage electricity and flammable gases.

The risk of electric shock is especially dangerous at the transformer, where electric potentials of 27,000+ volts may be encountered. Before beginning any experimental procedures, a cursory inspection of the wiring should be made to insure that all electrical leads are securely connected and not exposed such that they could charge other metallic surfaces near the experimental equipment.

The methane feed is highly flammable, and care should be taken to avoid leaks in the gas lines which could be ignited by errant sparks from poorly connected electrical wires. Always insure that the fume hood is in proper working order so that flammable gas concentrations cannot build up if a small, undetected leak occurs. Also insure that all tubing is properly connected before turning on the flow of methane. Methane is denser than air and methane vapors will settle to the lowest level of the room, creating a potential risk of asphyxiation. It should also be noted that high purity methane is odorless because it does not contain the methyl mercaptans associated with typical natural gas sources. The material safety data sheet (MSDS) for methane is available in the lab notebook

next to the door or from the laboratory manager. Detailed procedures are given below.

1. Review all laboratory safety procedures and material safety data sheets.
2. Inspect the equipment to insure that all electrical connections are secure and that there are no leaks in the gas lines.
3. Begin the carrier gas (Helium) flow at 40 standard  $\text{cm}^3/\text{min}$  (sccm). (20 sccm per column). Wait 10 minutes for the GC lines to purge. This insures that no oxygen is present within the TCD that could cause oxidation of the sensitive filaments.
4. Turn on the GC and the TCD. Set the GC to the specifications listed above (Table 6). Allow the GC and TCD temperatures to reach equilibrium and then zero the integrator. While the GC is warming up, turn on the natural gas make-up line and ignite the waste gas flare so that flammable gases are not released into the hood venting system.
5. Set the methane feed flow rate using the mass flow controller and begin the feed gas ( $\text{CH}_4$ ) flow to the reactor. Purge the reactor for at least 1/2-hour to insure that no air (oxygen) remains inside the reactor. This can be done while the GC is warming up.
6. Set the operating frequency on the power supply. Turn on the power supply and slowly increase the amplitude to the desired level. Always reduce the amplitude to zero before changing the frequency settings.
7. Once all experimental settings have been finalized, allow at least 20 minutes for the products to reach the GC sample valve. Record temperature, pressure, current, and voltage measurements. Turn the sample valve clockwise and press START on the integrator. Return the sample valve to the counter-clockwise position.
8. After all peaks have been detected, press STOP on the integrator. If another experiment is to be performed, purge the reactor, adjust any settings that need to be changed and return to step 5.
9. Once the experiments are done, decrease the amplitude and turn off the power supply. Turn off the methane feed to the reactor and the natural gas flare line. Turn off the TCD and GC power but allow the helium carrier gas to continue flowing for approximately 30 minutes. This will allow the filaments to cool sufficiently and prevent oxidation once air diffuses back in through the outlet.

Experiments were performed to examine the effect of residence time, operating frequency, and electric field strength on methane conversion and product selectivity. Two of these variables were kept constant while measurements were made over a range of values for the variable being studied. A total of eight different combinations were examined. These results are presented in Chapter 4.

## **CHAPTER 4**

### **RESULTS AND DISCUSSION EXPERIMENTAL**

In this section, the effects of electric field strength, residence time, and field frequency on methane conversion and product distributions are presented. Reactor behavior, the formation of liquids and solids, scale-up, and power consumption are also discussed.

#### **4.1 Residence Time**

The effect of residence time on product compositions was studied at 2.2, 3.1, and 5.1 seconds. These residence times were calculated assuming turbulent, plug-flow conditions. A calculation of the Reynolds number indicated that the flow would be laminar under normal conditions. However, it is likely that the action of the electric field on the charged particles in the plasma provides some degree of mixing. The effect of residence time on product compositions is shown in Figure 14. The operating frequency was 250 Hz and the applied electric field was 180 kV/cm. Four sets of data were taken at each setting. The error bars show one standard deviation from the average of those four points. The product compositions are shown as carbon fractions – the total amount of carbon for that product divided by the total amount of carbon fed to the reactor as methane. Conversion of methane increased with residence time, as did the carbon fractions for each product. None of the product species showed a decrease with residence time. This trend would be expected if lower molecular weight hydrocarbons are continually combined to form higher molecular weight hydrocarbons. Greater residence

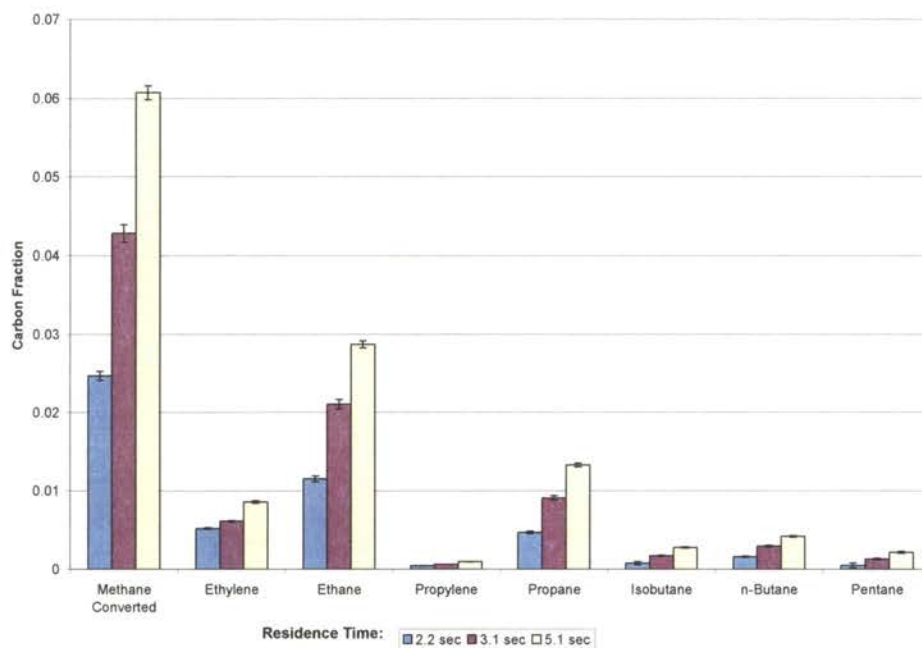


Figure 14. The Effect of Residence Time on Methane Conversion and Product Distribution at 250 Hz and 180 kV/cm.

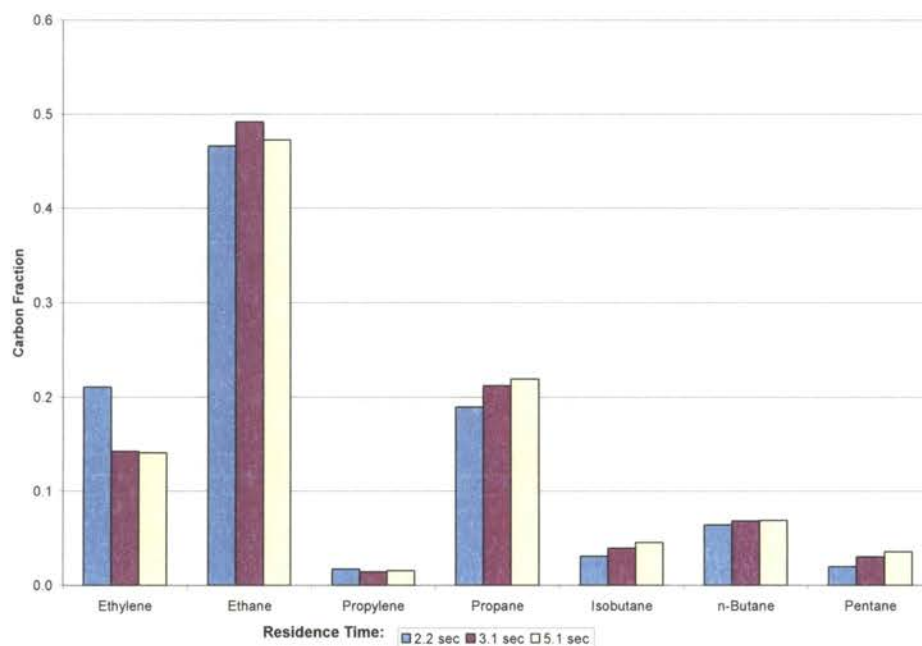


Figure 15. The Effect of Residence Time on Product Selectivity at 250 Hz and 180 kV/cm.



times allow for greater conversion. Kinetic, rather than thermodynamic, considerations dominate the process. Total conversion of methane appears likely if sufficient time were allowed. It is expected that the fraction of lower molecular weight hydrocarbons like ethylene and ethane would eventually decrease once the methane conversion approaches 100%. Without methane, ethylene and ethane formation would cease. However, ethylene and ethane would continue to react and form higher molecular weight species.

The effect of residence time on product selectivity is shown in Figure 15. Selectivity in this study is defined as the total amount of carbon for a product divided by the total amount of carbon (as methane) that reacted. At higher residence times, propane, isobutane, and pentane selectivity increased at the expense of ethylene. Propylene and n-butane selectivity remained essentially constant. Ethane showed the highest selectivity at the intermediate residence time of 3.1 seconds before decreasing. This suggests that the rate of formation for higher molecular weight species as a group is increasing compared to the rate of formation for ethylene, and after 3.1 seconds, ethane. As higher molecular weight species are formed, new reaction mechanisms are possible for the depletion of methane and a smaller fraction of the converted methane goes to ethylene formation.

## **4.2 Operating Frequency**

The effect of the operating frequency was studied at circuit operating frequencies of 200, 250, and 300 Hz. The actual discharge frequency was twice the operating frequency since two sinusoidal peaks occurred during each cycle. The methane feed rate was maintained at 10.5 standard cm<sup>3</sup>/min (sccm). The total residence time was 3.1 seconds and incompressible, constant molar flow was assumed since the calculated

increase in the total number of moles was less than 2.25% for each of the three studies. The effect of operating frequency on methane conversion and product compositions is shown in Figure 16. The applied electric field was 180 kV/cm. Four sets of data were taken at each setting. The error bars show one standard deviation from the average of those four sets of data. The product compositions are shown as carbon fractions. Conversion of methane increased with frequency, as did the carbon fractions for each product. None of the product carbon fractions showed a decrease as the frequency was increased. Increasing the frequency effectively increases the amount of time for electron impacts to occur, and therefore, methane conversion and product formation increases.

The effect of operating frequency on product selectivity is shown in Figure 17. Ethane and ethylene selectivity was higher at low frequencies while propane, isobutane, and pentane selectivity was higher at high frequencies. Selectivity of propylene and n-butane remained essentially constant regardless of frequency. At higher frequencies, propane, isobutane, and pentane were formed at the expense of ethylene and ethane. This suggests that the rate of formation for higher molecular weight species as a group is increasing compared to the rate of formation for ethylene and ethane. As higher molecular weight species are formed, new reaction mechanisms are possible for the depletion of methane and a smaller fraction of the converted methane goes to ethylene and ethane formation.

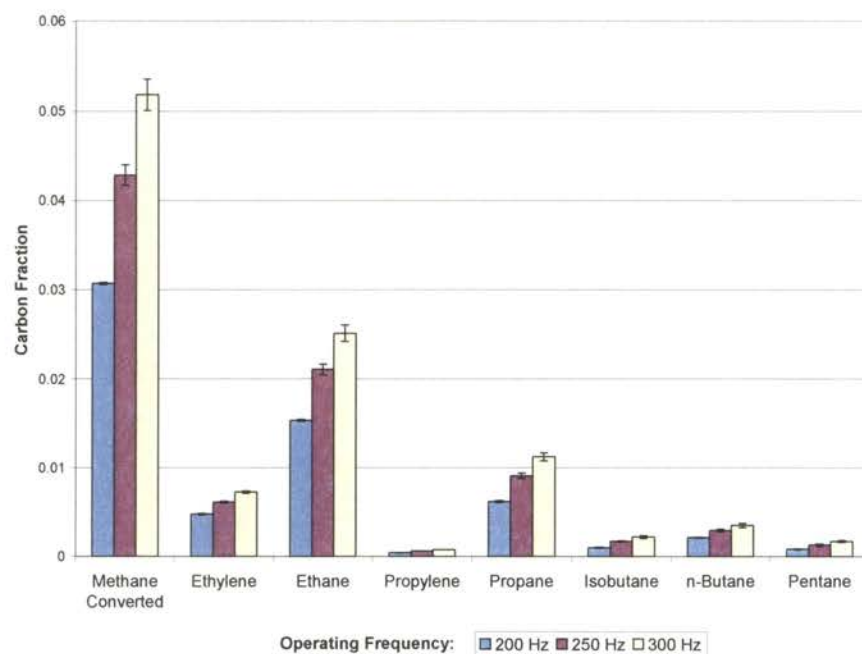


Figure 16. The Effect of Frequency on Methane Conversion and Product Distribution at 3.1 seconds and 180 kV/cm.

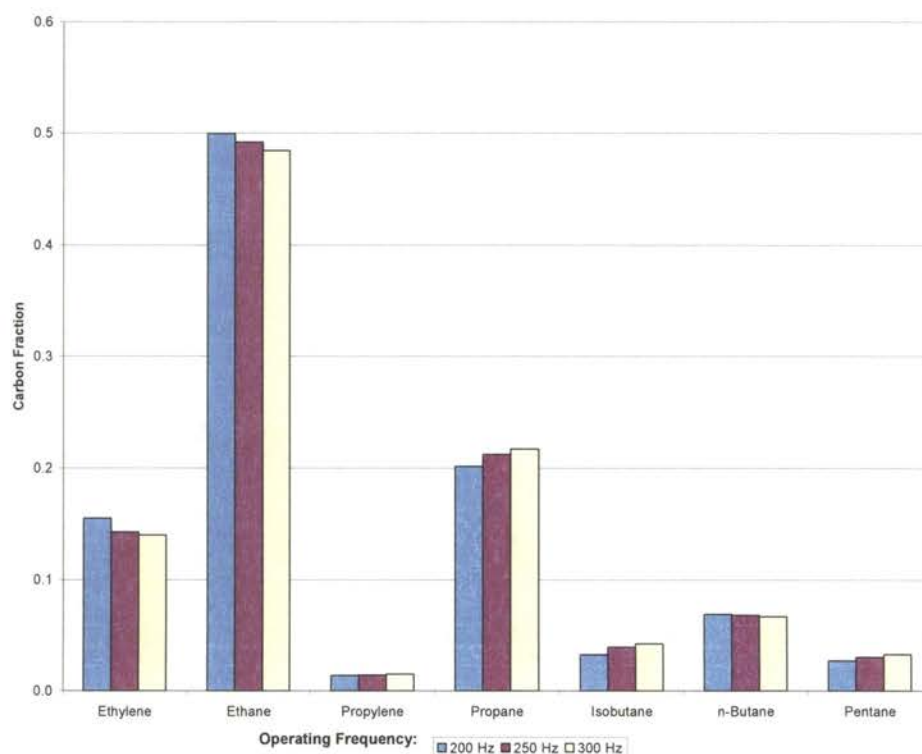


Figure 17. The Effect of Operating Frequency on Product Selectivity at 3.1 seconds and 180 kV/cm.

### 4.3 Electric Field Strength

The effect of the applied electric field strength was studied at 127 kV/cm, 153 kV/cm, and 180 kV/cm (19 kV, 23 kV, and 27 kV applied electric potential respectively). These values were the rms peak-to-peak values at the reactor electrodes divided by the total radial distance between the electrodes. Dielectric losses could not be measured. The methane feed rate was maintained at 10.5 sccm. The total residence time was 3.1 seconds assuming incompressible, constant molar flow. The calculated increase in the total number of moles was less than 2.25% for each of the three studies. Frequency was maintained at 250 Hz, subjecting the reactants to 500 discharges per second, or approximately 1500 total discharges. The effect of the applied electric field strength on methane conversion and product composition is shown in Figure 18. Four sets of data were taken at each setting. The error bars show one standard deviation from the average of those four sets of data. The product compositions are shown as carbon fractions. Methane conversion increased considerably when the electric field was increased from 127 kV/cm to 180 kV/cm. The carbon fraction of each product also increased as the electric field strength was increased. None of the product carbon fractions showed a decrease as the electric field was increased. However, the percent increase of the ethylene and propylene carbon fractions was much less than for other products. Higher electric fields should result in a higher mean electron energy, which would increase the rate of electron impact reactions. An increased rate of electron impact reactions would then result in a higher methane conversion and product formation.

The effect of electric field strength on product selectivity is shown in Figure 19. Ethylene and propylene selectivity was higher at low field strengths while ethane,

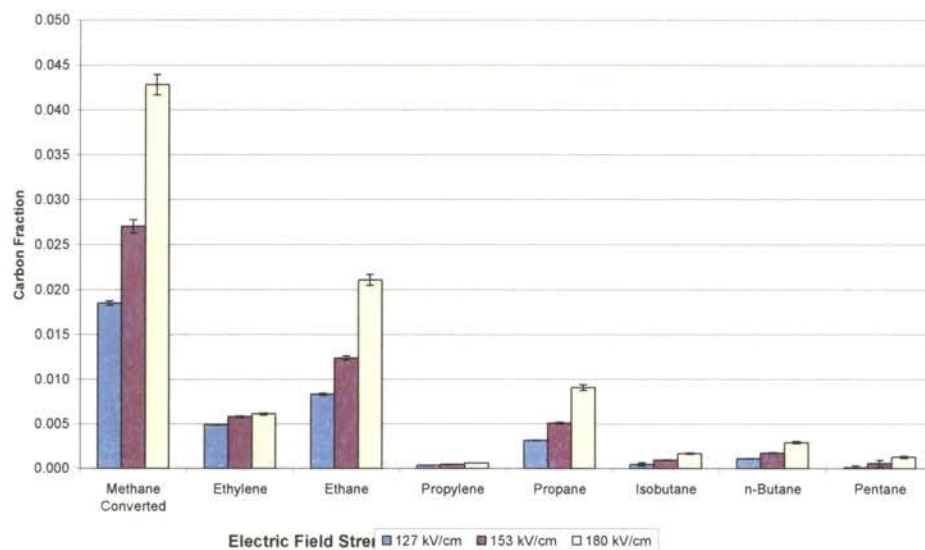


Figure 18. The Effect of Electric Field Strength on Methane Conversion and Product Distribution at 3.1 seconds and 250 Hz.

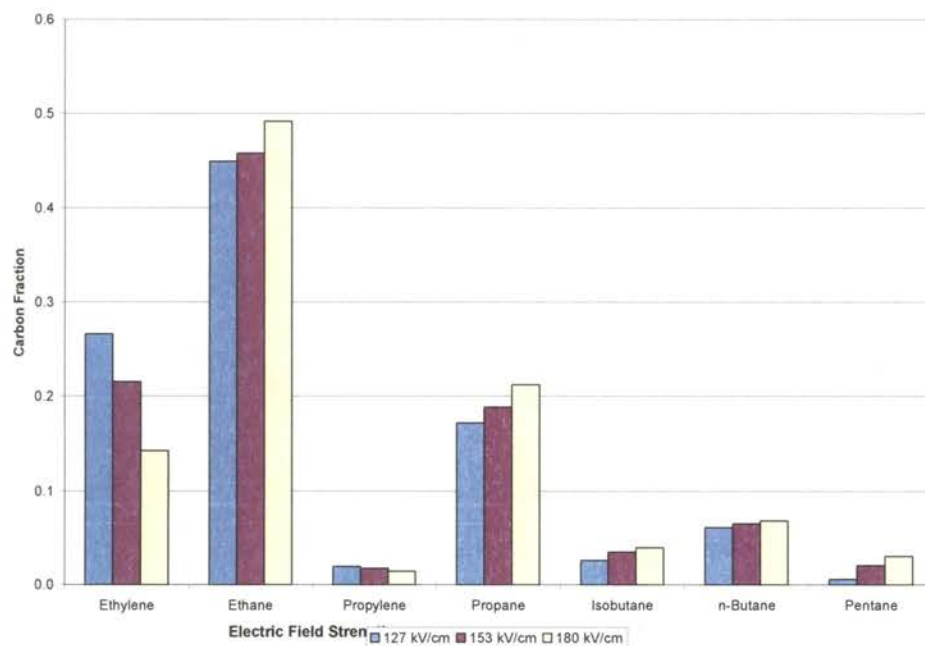


Figure 19. The Effect of Electric Field Strength on Product Selectivity at 3.1 seconds and 250 Hz.

propane, isobutane, n-butane, and pentane selectivity was higher at high field strengths. At higher applied electric fields, saturated hydrocarbon selectivity increased at the expense of unsaturated hydrocarbon selectivity. As with increased residence time and frequency, the formation of higher molecular weight species results in new reaction pathways for the depletion of methane and a smaller fraction of the converted methane goes to ethylene formation.

#### **4.4 Circuit Variables**

The dynamics of the electrical circuit during plasma generation are complex. Circuit variables such as voltage and current often drifted as the electrical system warmed up and reached steady state. Changing the operating parameters changed the circuit parameters. A detailed study of the circuit was beyond the scope of this research, but the following trends are presented in the hope that they could provide insight for future investigations of the circuits used to generate dielectric barrier discharges.

The following plots show how the primary voltage, primary current, voltage at the wall outlet, and current at the wall outlet changed as the reactor was operated at different frequencies and over a range of secondary voltages. The voltage on the primary side of the transformer decreased as the operating frequency was increased at constant secondary voltage, but the voltage on the primary side increased as the secondary voltage was increased at constant operating frequency as shown in Figure 20. The voltage drop across the measuring resistor on the primary side of the transformer increased when either the operating frequency or secondary voltage was increased as shown in Figure 21. This means that the current also increased as either parameter increased. The current at

the wall source decreased as the operating frequency was increased at constant secondary voltage but increased as the secondary voltage was increased at constant operating frequency as shown in Figure 22.

The practical implications are that with the current electrical setup, more power is delivered to the reactor and less total power is required to create a given electric potential at the reactor electrodes for high frequencies than for low frequencies. Since methane conversion also increases with frequency for a given electric field strength (or applied electric potential), this also means that efficiency improves at the higher frequencies examined.

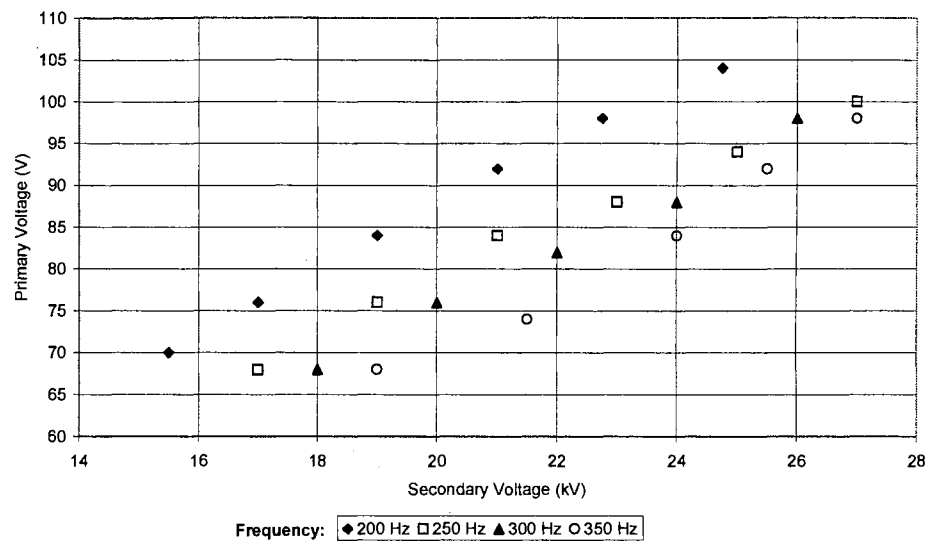


Figure 20. The Primary Voltage of the Transformer as a Function of the Secondary Voltage of the Transformer.

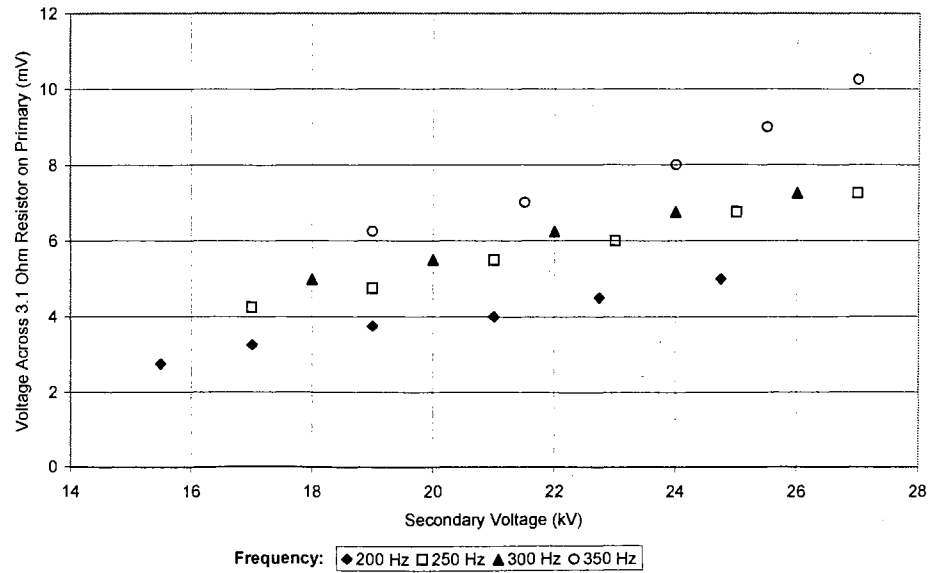


Figure 21. The Voltage Across a 3-ohm Resistor on the Primary Side of the Transformer as a Function of the Secondary Voltage of the Transformer.

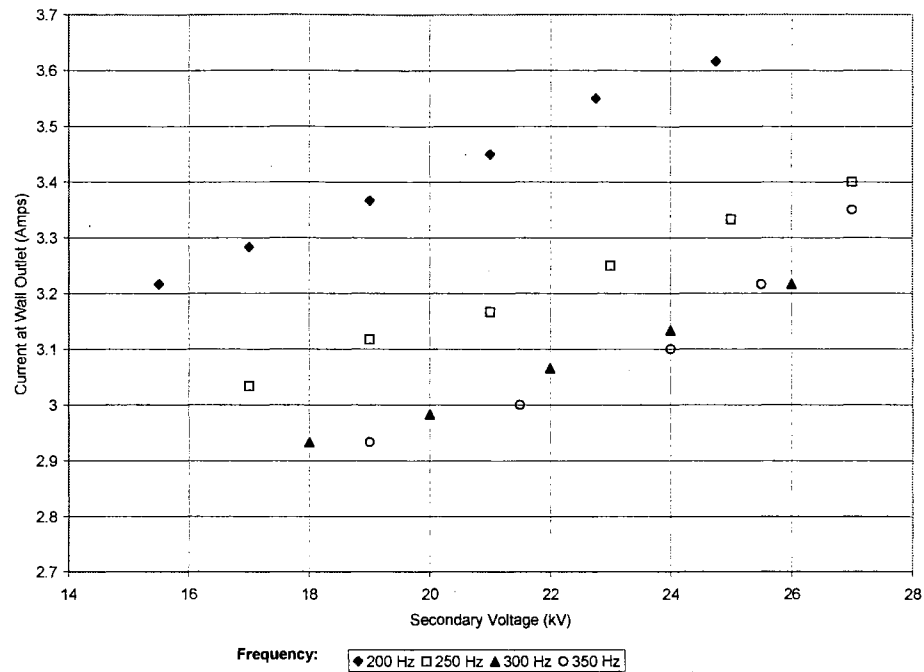


Figure 22. The Current at the 120-Volt Wall Source as a Function of the Secondary Voltage of the Transformer.



## 4.5 Scaling the Dielectric Barrier Discharge Process

One of the biggest questions regarding DBD reactors is how to scale up the process from a bench-scale unit. Industrial-scale applications may require several hundred to several thousand cubic feet of gas to be processed each minute. The requirement for a small discharge gap will necessitate a large number of reactors and a high electrode surface area. A thorough understanding of the electrical characteristics will be required for the construction of industrial scale processes.

### 4.5.1 Flow Rate

In the range of flow rates studied, the methane feed does not appear to affect the electrical characteristics of the circuit. Figures 23-26 show circuit parameters for two

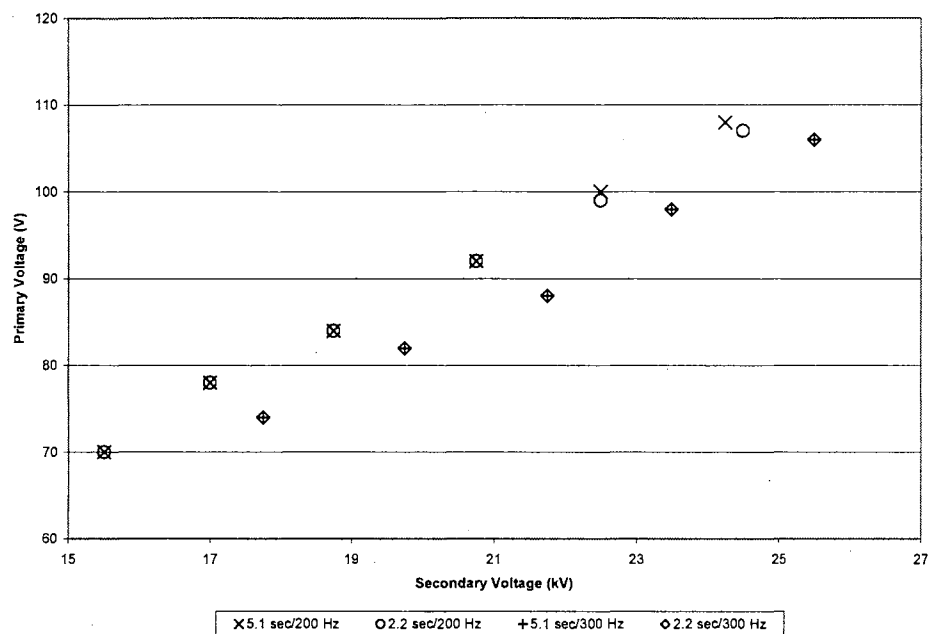


Figure 23. The Primary Voltage of the Transformer for Two Different Retention Times at Two Different Frequencies.

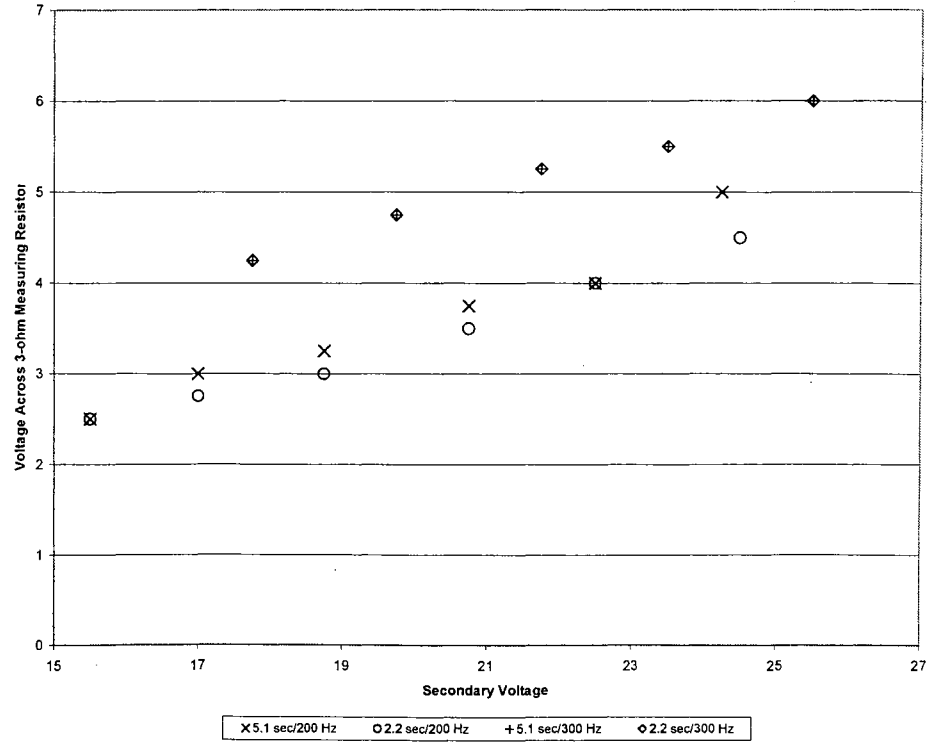


Figure 24. The Voltage Across a 3-ohm Resistor on the Primary Side of the Transformer for Two Different Retention Times at Two Different Frequencies.

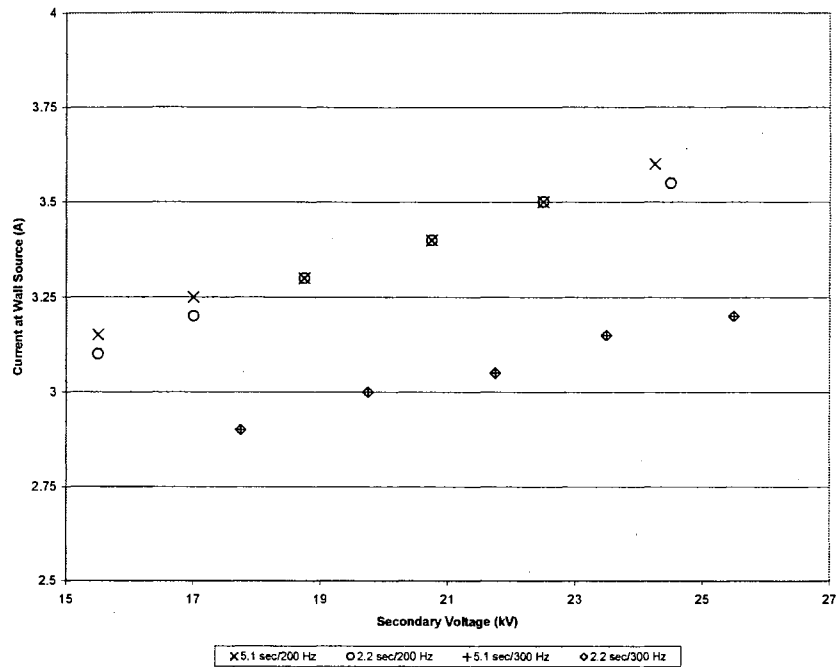


Figure 25. The Current at the 120-Volt Wall Source as a Function of the Secondary Voltage of the Transformer for Two Different Retention Times at Two Different Frequencies.

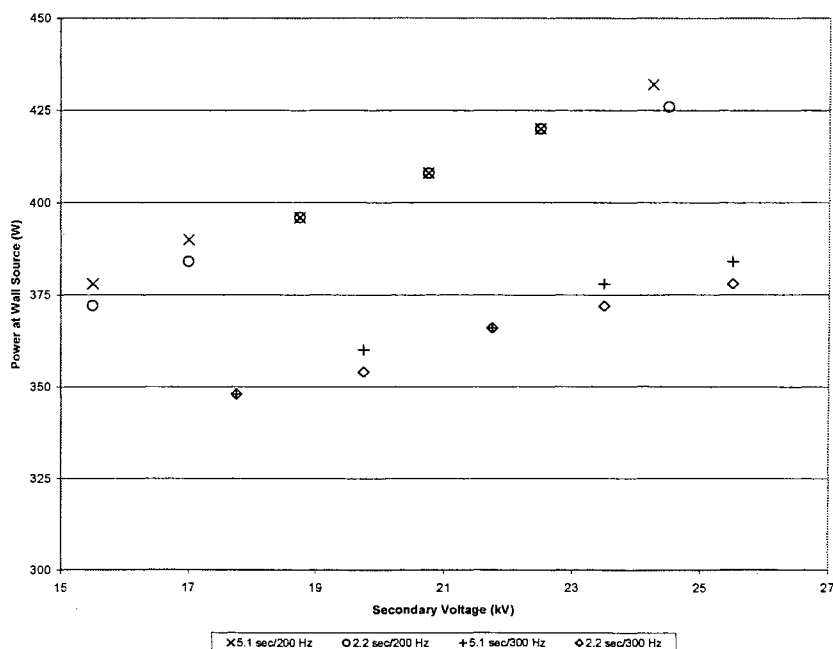


Figure 26. The Power at the 120-Volt Wall Source as a Function of the Secondary Voltage of the Transformer for Two Different Retention Times at Two Different Frequencies.

different flow rates at two different discharge frequencies. At 200 Hz, only small differences are noted for each flow rate and most of the data overlap. At 300 Hz, the same trend is apparent, with almost identical values for both flow rates. As a result, the gas flow rate does not appear to affect power consumption. However, gas flow rate will still affect the total energy input to the stream.

#### 4.5.2 Dual Reactor Study

To study the factors affecting scale-up of the DBD process, two experimental configurations were compared: one with a single reactor and the other with two reactors. The two reactors were connected in parallel electrically, and the flow was split between them using a simple T-connector. Both reactor configurations were operated at the same frequency, with the same applied voltage, and at equivalent retention times. Methane

conversion was considerably higher for the single reactor configuration (Figure 27). Selectivity of ethane, propylene, and isobutane was higher for the dual reactor configuration (Figure 28). Production of n-butane was negligible with the dual reactor configuration.

The use of two reactors connected in parallel would have doubled the capacitance of the secondary circuit and may have resulted in a decreased power factor. Another possibility is that the current to each reactor in the dual reactor configuration may have been only half of the current to the single reactor configuration. Either or both of these considerations could explain the lower conversion achieved in the dual reactor configuration.

The electrical characteristics were measured for each individual reactor, the dual reactor setup, and the open circuit (no connections on the secondary side of the transformer). The results are compared in figures 29-32. Unexpected differences in the values of the individual reactors may be due to the scale of the measurements. The primary voltage was determined by measuring the peak-to-peak distance on the oscilloscope. When the 20-mV/division scale of the oscilloscope and the 1000x step-down function of the probe are factored in, a small difference in the measured peak-to-peak distance becomes magnified. A small drift occurs in all of the circuit variables over time as the power supply heats up. The primary current and the current at the wall source are higher when a single reactor is connected than when the circuit is left open or both reactors are connected. The cause of this is uncertain.

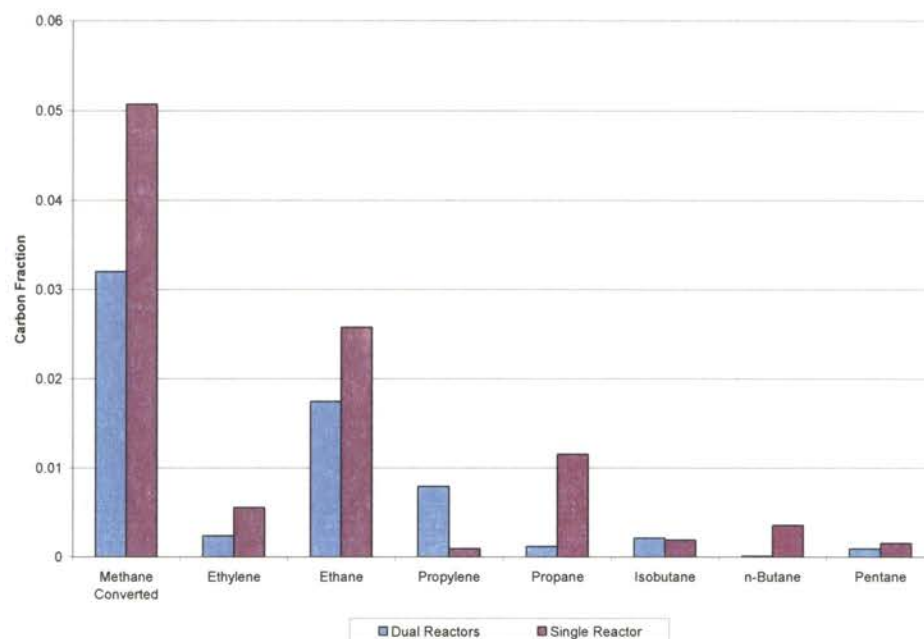


Figure 27. Comparison of Methane Conversion and Product Distribution for Dual Reactor and Single Reactor Configurations at 3.2 seconds, 250 Hz, and 180 kV/cm.

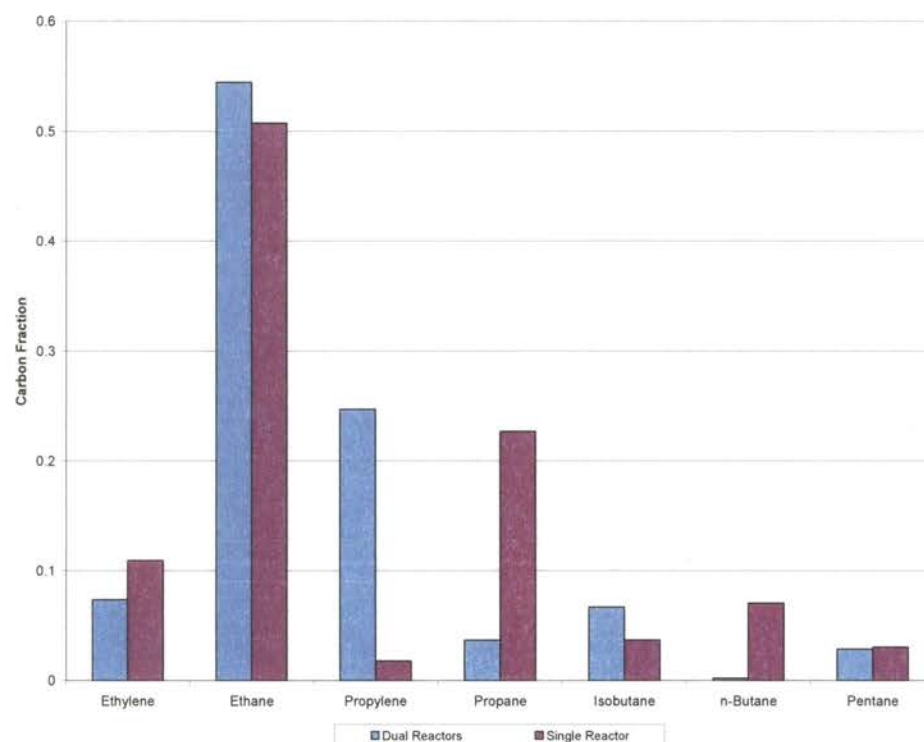


Figure 28. Comparison of Product Selectivity for Dual Reactor and Single Reactor Configurations at 3.2 seconds, 250 Hz and 180 kV/cm.

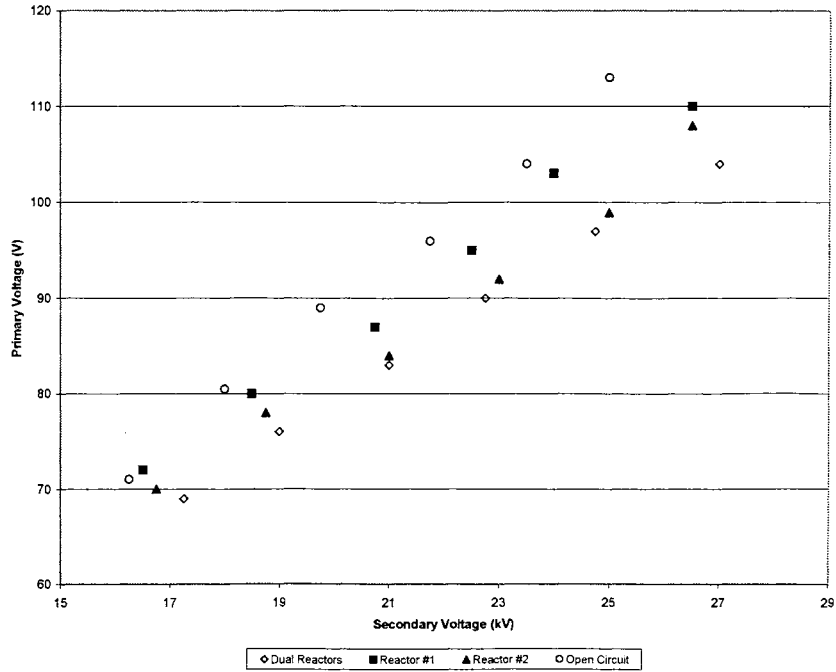


Figure 29. The Primary Voltage of the Transformer as a Function of the Secondary Voltage of the Transformer for Dual Reactor and Single Reactor Configurations at 3.2 seconds and 250 Hz.

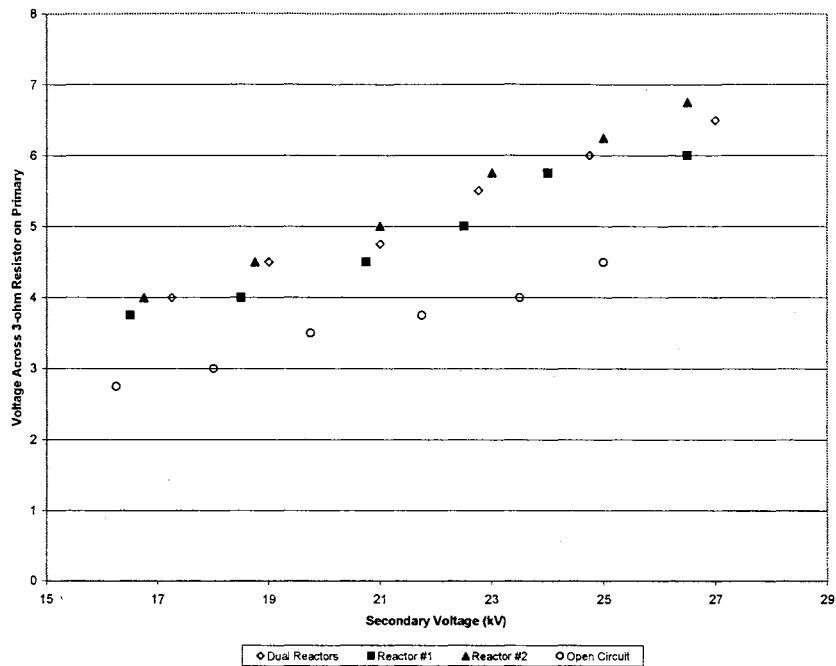


Figure 30. The Voltage Across a 3-ohm Resistor on the Primary Side of the Transformer for Dual Reactor and Single Reactor Configurations at 3.2 seconds and 250 Hz.

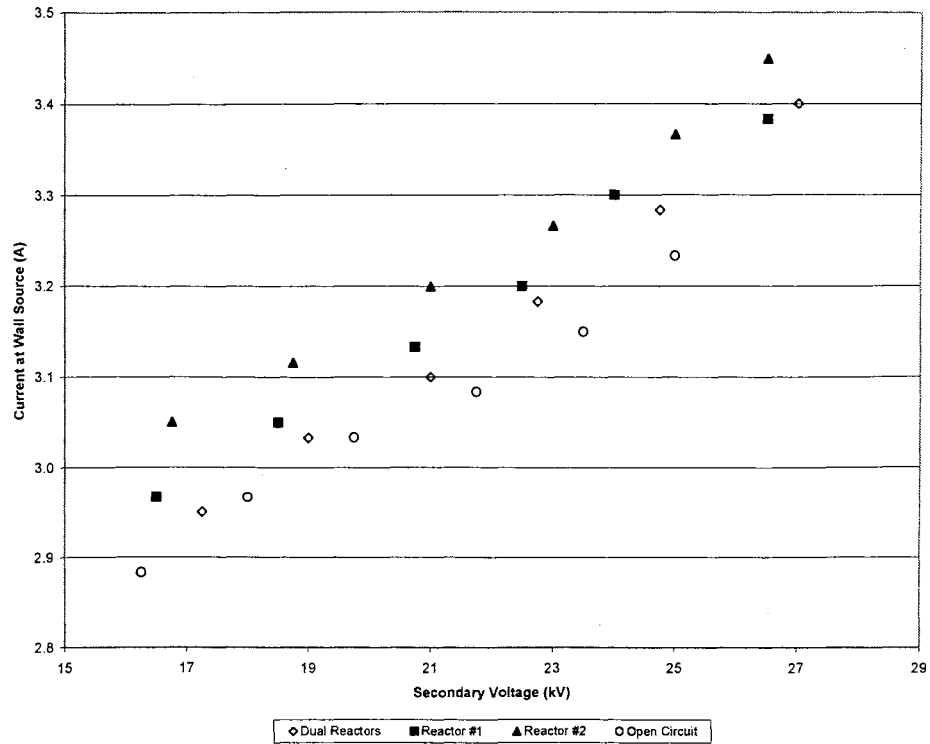


Figure 31. The Current at the 120-Volt Wall Source as a Function of the Secondary Voltage of the Transformer for Dual Reactor and Single Reactor Configurations at 3.2 seconds and 250 Hz.

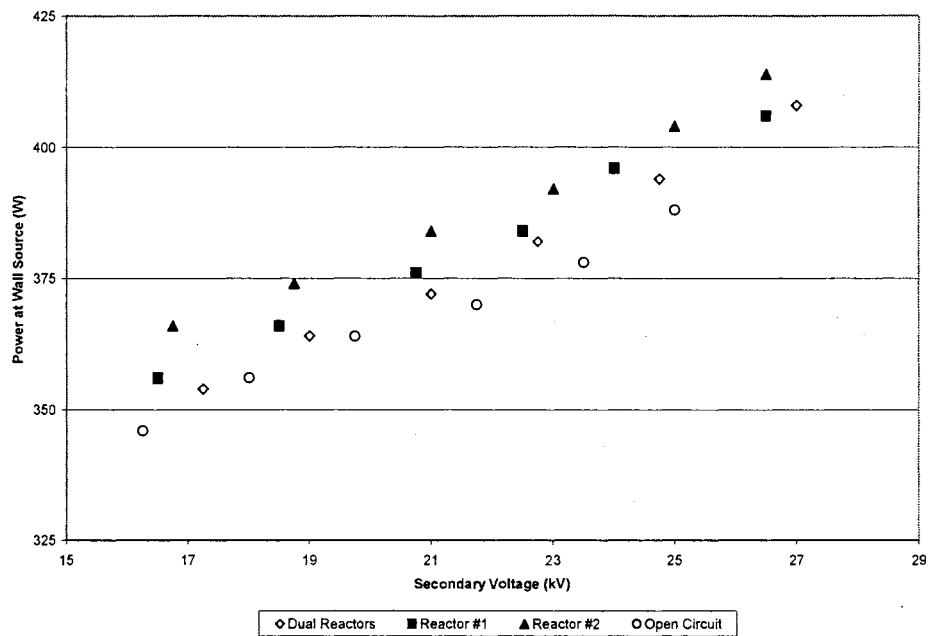


Figure 32. The Power at the 120-Volt Wall Source as a Function of the Secondary Voltage of the Transformer for Dual Reactor and Single Reactor Configurations at 3.2 seconds and 250 Hz.

#### 4.6 Additional Observations

The focus of the previous results has been on carbon fractions. However, it should be noted that a considerable amount of hydrogen should be liberated during the formation of higher molecular weight hydrocarbons from methane. Although the hydrogen fraction could not be measured directly, a hydrogen balance could be used to calculate the hydrogen fraction in the product stream. These calculated hydrogen mole fractions are listed in Table 7. The total moles of hydrogen calculated for each experiment are given in Appendix A with the measured experimental data.

TABLE 7.  
CALCULATED HYDROGEN MOLE FRACTIONS

Experimental Conditions	Hydrogen Mole Fraction
200 Hz, 180 kV/cm, 3.1 seconds	0.039
250 Hz, 180 kV/cm, 3.1 seconds	0.054
300 Hz, 180 kV/cm, 3.1 seconds	0.065
250 Hz, 180 kV/cm, 5.1 seconds	0.076
250 Hz, 180 kV/cm, 2.2 seconds	0.033
250 Hz, 127 kV/cm, 3.1 seconds	0.025
250 Hz, 153 kV/cm, 3.1 seconds	0.036

Although the goal of this research was to form longer-chain gaseous hydrocarbons from methane, the formation of both liquid and solid products also was observed. A very fine mist of liquid droplets was formed inside the reactor on the downstream side of the plasma zone after extended operation at high frequency and voltage. During one experiment, a single drop coalesced in the bottom of the reactor but could not be analyzed.



Figure 33 shows the two distinct types of solid product that were produced inside the reactor. Solids particles (probably carbon) were deposited on both the inner electrode and the reactor wall, forming small ( $\sim 1$  mm long) dendrites on the inner electrode after several hours at high frequency and voltage. A thin, translucent film was also deposited on the wall of the reactor. This film was brittle and uneven in thickness, forming an irregular surface. This film was probably caused by the eventual polymerization of liquid droplets that coalesced on the reactor walls. This film coated not only the area covered by the outer electrode, but also extended upstream and downstream for 1 to 2 cm, covering the end-effect regions. As the solid deposits increased, they seemed to cause a very slight decrease in the efficiency of the reactor.

A weak plasma zone formed at both ends of the reactor. This end-effect was due to the fact that the inner electrode was not covered by a dielectric layer and provided a voltage potential along the entire length of the reactor tube. The electric field of the end-effect regions decreased as the distance from the outer electrode increased. The visible region usually extended about 1 cm from either end of the outer electrode as shown in Figure 13. Occasional sparking along the outer surface of the reactor occurred from the outer electrode toward either end of the reactor.

Overall, the DBD plasma reactor performed above expectations. The dielectric strength of the quartz glass tubing was more than adequate for the electric fields used. The luminous tube transformer remained in perfect working order throughout the experimental work and did not break down the way transformers operated by Parker did at frequencies near 1000 Hz [37]. However, some improvements could still be made and are presented in Chapter 5.

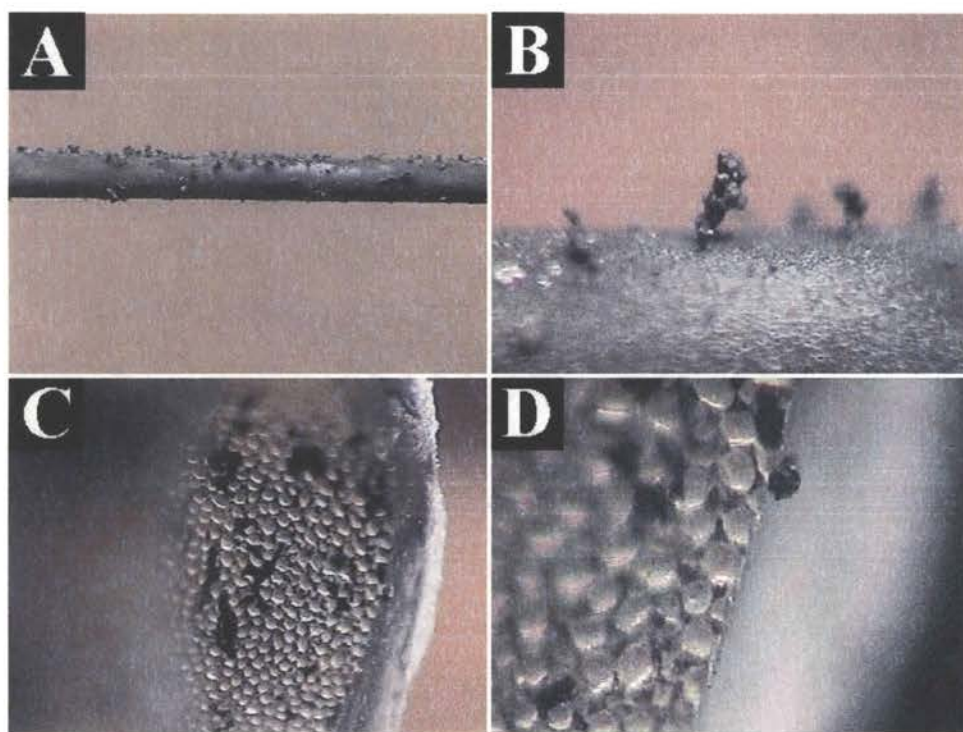


Figure 33. Two Types of Solid Deposits Inside the Reactor. [A] Carbon Deposits on the Inner Electrode. [B] Magnified Image of a Carbon Dendrite Formed on the Inner Electrode. [C] Polymer Film Deposited on the Inner Wall of the Reactor. [D] Magnified Image of the Polymer Film Showing the Irregular "Cobblestone" Surface Features.

## CHAPTER 5

### EXPERIMENTAL RECOMMENDATIONS

The electrical system needs to be examined and understood more thoroughly. Altering one component or operating variable affected the other electrical parameters and ultimately, the conversion and product distribution. Electrical probes must be rated for the appropriate voltages and frequencies. The use of inadequate high-voltage probes resulted in setbacks. Impedance matching should be implemented in plasma studies at Oklahoma State to ensure maximum real power to the reactor. The current experimental configuration does not have the necessary plasma diagnostic equipment for measuring electron density, electron energy, or power input to the reactants. Feng et al. [40] have proposed an automated system for power measurement in the silent discharge. This method uses a specially designed circuit and a PC to integrate a Lissajou plot (charge-voltage trace) of the reactor. This method is recommended for use during future work at Oklahoma State. Once the electrical diagnostic techniques and controls have been improved, construction of a new reactor composed of many more tubes would prove useful for measuring scale-up parameters. The power measurement method of Feng et al. [40] also would permit evaluation of the reactor efficiency.

Although the pressure and temperature of the reactor were monitored in this work, there was no means to control either of those variables. Since both variables affect reaction rates, controlling temperature and pressure could provide additional means to optimize methane conversion or product selectivity in the plasma system.

Reactor geometry is another possible design factor that should be investigated. For planar geometry, both discharges are identical. For annular geometry, there could be a difference in the electron energy or some other variable depending on whether the inner or outer electrode is negatively charged.

A better analytical system would prove useful for measuring and identifying small fractions of the product stream that were not detected in this study. A more detailed study of the liquid and solid phases could result in useful surface treatment applications. Detailed analysis of highly reactive intermediates would help identify important reaction sequences. Single discharges in very low temperature vessels could allow these unstable intermediates to be frozen out for analysis.

Future studies should consider elevated temperatures to prevent deposition of liquids and solids on the reactor walls. A temperature above 158 °F (70 °C) would prevent the condensation of pentane and hexane on the reactor walls. Higher operating temperatures could be achieved if higher molecular weight hydrocarbons are produced since the quartz glass tubing should easily withstand temperatures up to 1800 °F. A study of longer residence times would increase methane conversion and should result in the production of hydrocarbons heavier than hexane, requiring temperatures above 158 °F. Using a multi-component feed could be an effective method for modifying the product average molecular weight. Mixing the methane feed with hydrogen should result in a lower average molecular weight for the product stream. Mixing the methane feed with higher molecular weight hydrocarbons such as ethane or propane should result in higher conversions and a higher average molecular weight for the product stream.

The successful conversion of methane during this research proves that the carbon-hydrogen bond of methane can be broken. Conversion of higher molecular weight hydrocarbons in the DBD plasma reactor should be easier than methane since carbon-carbon and carbon-hydrogen bonds in those molecules are weaker than the carbon-hydrogen bond of methane.

Many areas of investigation are still open for the reaction of methane in the DBD plasma reactor. Of particular interest would be the development of analytical techniques for measuring actual power input to the reactor. The ability to control product selectivity and average molecular weight would prove most useful for industrial-scale production of higher molecular weight hydrocarbons from methane.

## CHAPTER 6

### METHANE PLASMA MODEL FRAMEWORK

#### 6.1 Model Overview

Eighty-five kinetic equations (with 30 different chemical species) were combined with material balances to model the reaction of methane in the silent electric discharge. A *MATLAB* subroutine for stiff ordinary differential equations (ODEs) was used to solve the reaction scheme consisting of 16 electron impact reactions, 16 ion reactions, 10 wall neutralization reactions, and 43 free-radical reactions. Each of these reactions is presented in Appendix D and is of the form:

ID#	Reaction	Rate constant [k] (cm <sup>3</sup> /μmol/s)
G2	CH <sub>4</sub> + CH <sub>2</sub> <sup>·</sup> → C <sub>2</sub> H <sub>6</sub>	1.01E+08

Each of these reactions can be expressed as a rate equation of the form:

$$d(G2)/dt = k(C_{CH_4})(C_{CH_2})$$

These rate expressions must then be converted into the appropriate syntax required by the *MATLAB* program:

$$G2 = 1.01E+08 * X(4) * X(6)$$

where G2 is the rate of that reaction, 1.01E+08 is the rate constant, X(4) is the concentration of component 4 (CH<sub>4</sub> molecule), and X(6) is the concentration of component 6 (CH<sub>2</sub><sup>·</sup> radical). At this point, the rates of formation and consumption for

each component must be summed for all reactions that they participate in. For methane, this would include 33 reaction equations and the net rate equation would be:

$$\begin{aligned} X_{\text{comp}}(4) = & -G2-G3-G4-G5+G7+G11+G15+G19+G25 \\ & +G26+G6-E1-E2-E3-E4-E5-E6-E7-E8-I1-I2 \\ & -I3-I4-I5-I7-I8-I10-I11-I12-I13-I14-I15+W2; \end{aligned}$$

All *MATLAB* reaction equations and material balances are presented in Appendix C.

The model has two different reaction periods to simulate the discharge cycle in the plasma reactor. The first period simulates the discharge phase in which the electron impact reactions occur in addition to the ion, neutralization, and free-radical reactions. The second period simulates the relaxation phase in which ion, neutralization, and free-radical reactions continue to occur, but no electron impact reactions occur. These two periods alternate until the designated number of discharge periods has occurred. An extended relaxation period at the end of each simulation was included to allow the ions and free radicals to neutralize and reach an equilibrium value. These steps are shown in Figure 34. The model assumes constant temperature, pressure, and density.

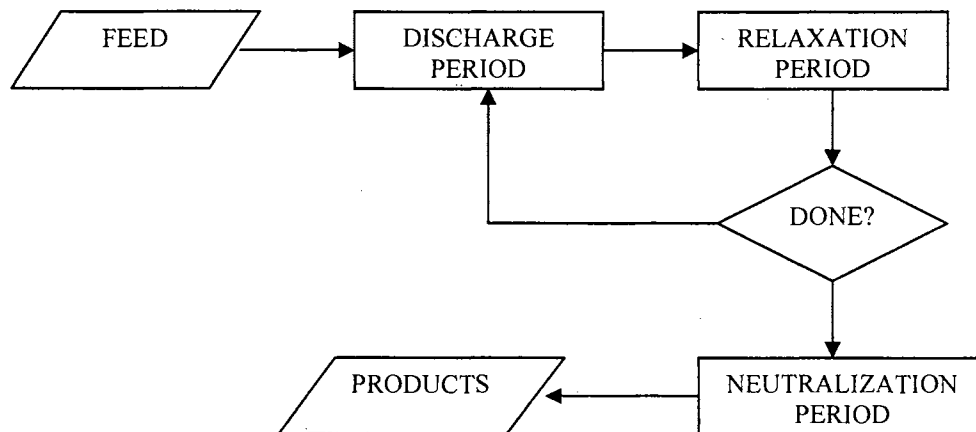


Figure 34. Flowchart Showing Separate Stages of Plasma Model.

### 6.1.1 Residence time

The residence time used in this model was the same as the residence time in the experimental studies. Constant volume and plug-flow conditions were assumed. End effects were neglected.

### 6.1.2 Discharge Frequency and Period

There are two discharges per voltage cycle. One discharge occurs when the inner electrode reaches maximum positive voltage and a second discharge occurs half a cycle later when the outer electrode reaches maximum positive voltage. The model makes no distinction between these two discharges. Since there was no diagnostic method to determine the actual discharge period in the experimental reactor, an order-of-magnitude approximation was used. Eliasson and Kogelschatz [6] have reported that a discharge period of  $1 \times 10^{-9}$  to  $1 \times 10^{-7}$  seconds is typical for silent electric discharges. The logarithmic average of these boundaries, a discharge period of  $1 \times 10^{-8}$  seconds, was used for this model.

### 6.1.3 Temperature

A standard temperature of 77 °F (298 K) was used in the reaction model. No temperature measurements could be made inside the reactor, but inlet temperatures ranged from 73 °F to 77 °F. The measured temperature increase from inlet to outlet was less than 1 °F for each of the experimental studies.



#### 6.1.4 Pressure

An operating pressure of 14.7 psi was used for the reaction model since that was the actual operating pressure for the experimental studies.

#### **6.2 Electron Density**

Since there was no diagnostic method for determining the actual discharge period in the experimental reactor, an order-of-magnitude approximation was used in the reaction model. Eliasson and Kogelschatz [6] have reported that the electron density in a silent electric discharge is on the order of  $1\text{E}14/\text{cm}^3$ . The electron density was kept constant at  $1\text{E}14/\text{cm}^3$  during the discharge phase.

#### **6.3 Electric Field**

The model has no electric field parameter. The effect of the electric field on impact rates is complex and beyond the scope of this model. Experimental values measured with electric field strength of 180 kV/cm were used to scale the electron-impact reaction rates in the model.

#### **6.4 Reactions**

Reaction rate constants for the ionic reactions, wall neutralization reactions, and free-radical reactions were taken from a variety of sources. These reactions and rate constants are presented in Appendix D. A matrix of coupled ODEs was constructed from this set of reaction rate equations (Appendices C and D) and with the electron impact reactions discussed below. The *MATLAB* subroutine 'ode23s' was used to solve this

matrix. This subroutine is based on a modified Rosenbrock formula of order 2. Subroutine 'ode23s' uses automatic step size adjustment based on the variation in the solution on the shortest length scale to maintain stability of the integration. This basis is used even when a larger step size would be allowed based on accuracy requirements. Initial efforts to solve the resulting equations failed because of the stiff nature of the coefficient matrix. The values of the rate constants were then converted from  $\text{cm}^3/\text{mol/s}$  to  $\text{cm}^3/\mu\text{mol/s}$ , making it possible to solve the reaction matrix for the full retention time.

The electron impact rate data from studies reported in the literature was measured or calculated at conditions different from the actual reaction conditions of this study. The electron impact reaction rates from the literature were scaled until the results agreed with the data from the experimental reactor at 250 Hz, 180 kV/cm, and 3.1 seconds. Four different scaling factors were used for the different sets of electron impact reactions: electron-methane impact reactions (scale1), electron-ethane impact reactions (scale2), electron-ethylene impact reactions (scale4), and electron-propane impact reactions (scale5). The values used for the electron-impact scaling factors (Appendix C) were solved sequentially, until all four values converged, using the bisection algorithm in Appendix E. These scaled rates, determined for the base experimental run (250 Hz, 180 kV/cm, and 3.1 seconds), were then used to model additional experimental runs at different retention times and operating frequencies.

The scaled rate for electron-ethylene impact reactions (scale3) was initially included, but was eventually dropped. The primary effect of the electron-ethylene impact reactions was to produce acetylene from ethylene. Individual ethylene and acetylene

concentrations could not be resolved from the experimental data so no criteria existed for determining an appropriate value for this variable (scale3).

Once the scaled reaction rates were decided, the model was compared to experimental data for a range of circuit frequencies and residence times. Comparisons were made between the model results and experimental data for 4 different conditions: 250 Hz for 2.2 seconds, 250 Hz for 5.1 seconds, 200 Hz for 3.1 seconds, and 300 Hz for 3.1 seconds. These results are presented in Chapter 7.

## CHAPTER 7

### RESULTS AND DISCUSSION MODELING

In this section, the results of the model for various conditions are presented. The effects of residence time and circuit frequency on methane conversion and product distributions are presented and compared with experimental data acquired during the first phase of this research. Detailed traces of the changing concentrations of  $\text{CH}_4$ ,  $\text{CH}_3^\bullet$ ,  $\text{C}_2\text{H}_6$ , and  $\text{C}_2\text{H}_5^\bullet$  are shown to provide general examples of the compositional changes in the reactor model with time.

#### 7.1 Base Case for Scaled Parameters

Table 8 compares the experimental concentrations measured at 250 Hz, 180 kV/cm, and 10.5 sccm with the model results at 250 Hz and 10.5 sccm. Since the model does not allow for different electric field strengths, scaling the electron impact rates to experimental data at 180 kV/cm sets this electric field as the default value for the model.

TABLE 8  
CARBON FRACTION COMPARISON:  
EXPERIMENT VS. MODEL BASE CASE AT  
250 HZ, 180 KV/CM, AND 3.1 SECONDS.

	Experiment	Model
$\text{CH}_4$	95.7%	95.7%
$\text{C}_2\text{H}_6$	2.1%	2.3%
$\text{C}_2\text{H}_4, \text{C}_2\text{H}_2$	0.6%	0.5%
$\text{C}_3\text{H}_8, \text{C}_3\text{H}_6$	1.0%	0.8%
$\text{C}_4^+$	1.1%	0.7%

Good agreement is observed between the experimental results and the model results for the base case. Figures 35-38 show how the concentrations of  $\text{CH}_4$ ,  $\text{CH}_3\cdot$ ,  $\text{C}_2\text{H}_6$ , and  $\text{C}_2\text{H}_5\cdot$  change during the first five discharge periods. Methane is consumed very rapidly during the discharge periods, but remains relatively unchanged during the relaxation periods. Methyl radicals are briefly generated during the discharge phase, but are then quickly consumed during the initial part of the relaxation phase until none remain. Ethane is produced very quickly during the initial part of the relaxation phase, but is not consumed so it continues to increase after each discharge. Ethyl radicals are generated very quickly during the discharge phase, but are only partially consumed so that the total carbon fraction continues to increase over time.

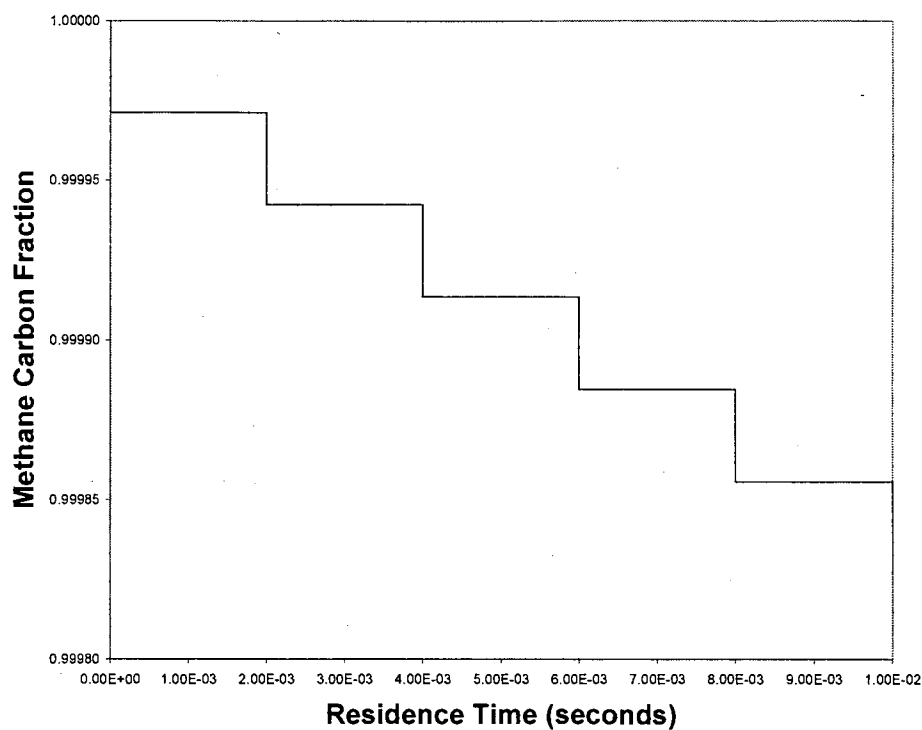


Figure 35. Detailed Trace of  $\text{CH}_4$  Carbon Fraction over a Five-Discharge Interval.

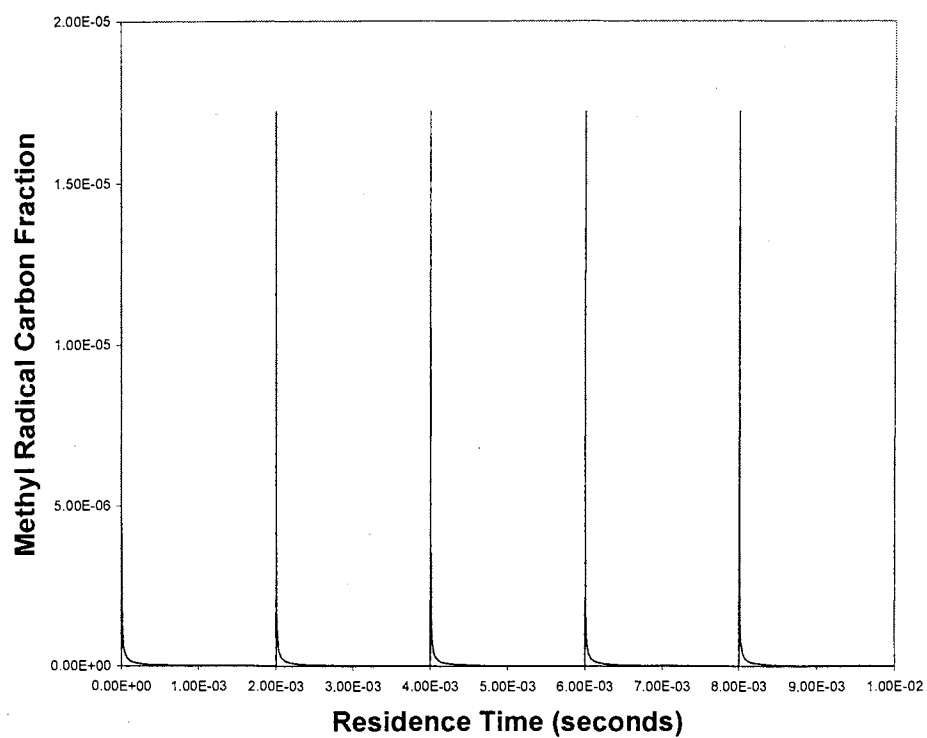


Figure 36. Detailed Trace of  $\text{CH}_3\cdot$  Carbon Fraction over a Five-Discharge Interval.

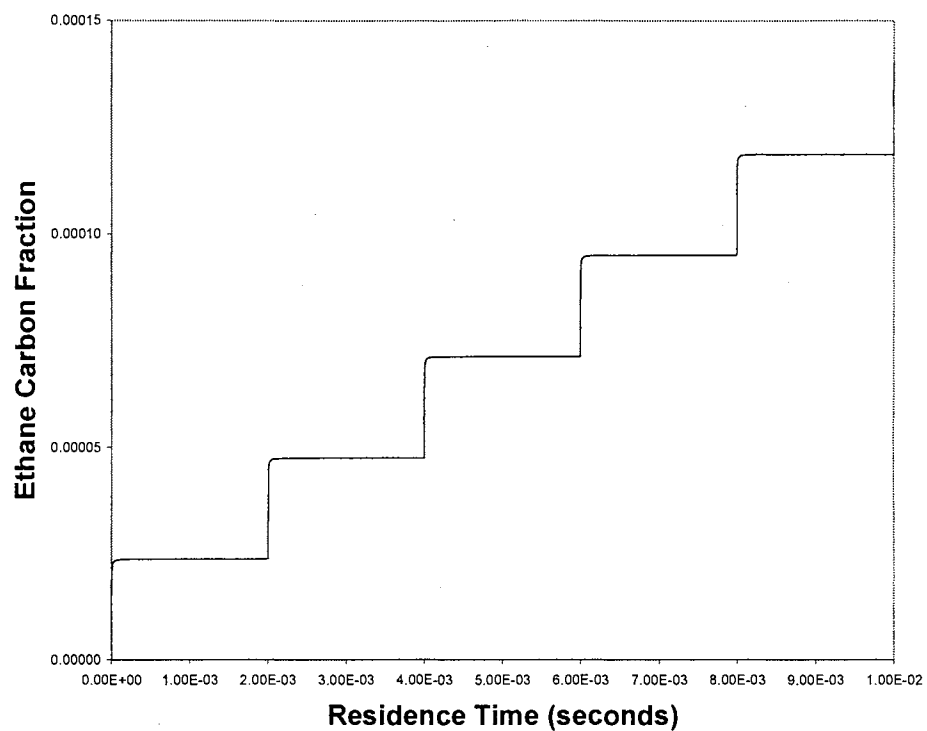


Figure 37. Detailed Trace of  $\text{C}_2\text{H}_6$  Carbon Fraction over a Five-Discharge Interval.

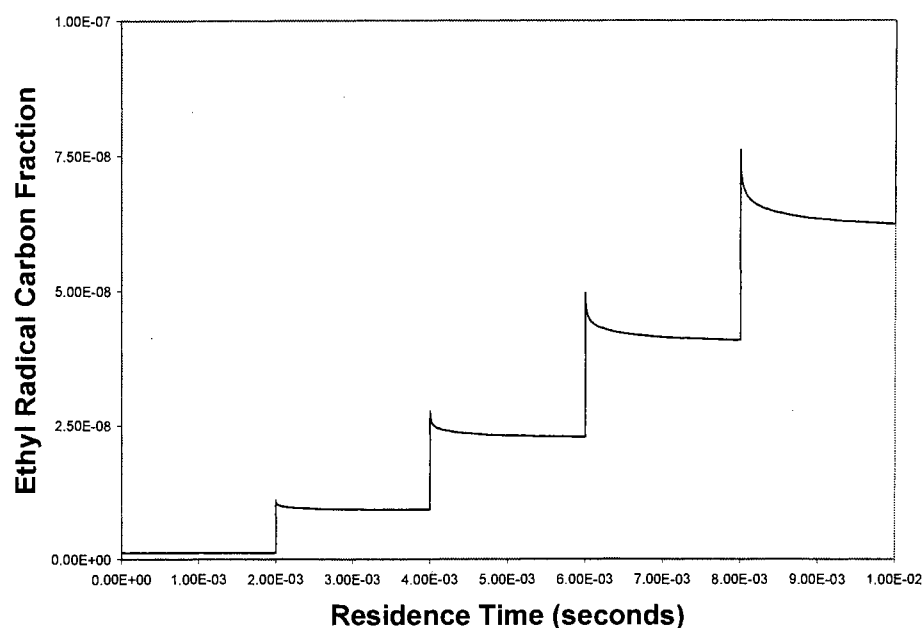


Figure 38. Detailed Trace of  $C_2H_5\bullet$  Carbon Fraction over a Five-Discharge Interval.

## 7.2 Residence Time

The base case for the scaled parameters had a residence time of 3.1 seconds at 10.5 sccm. The residence time of the model was adjusted to 2.2 seconds and compared to experimental results for the same period, at 250 Hz. The results are shown in Table 9.

TABLE 9  
CARBON FRACTION COMPARISON:  
EXPERIMENT VS. MODEL AT 250 HZ, 180 kV/CM, AND 2.2 SECONDS

	Experiment	Model
$CH_4$	97.5%	97.0%
$C_2H_6$	1.2%	1.9%
$C_2H_4, C_2H_2$	0.5%	0.4%
$C_3H_8, C_3H_6$	0.5%	0.5%
$C_4+$	0.5%	0.3%

The residence time of the model was then adjusted to 5.1 seconds and compared with the experimental results for the same period, at 250 Hz. The results are shown in Table 10.

TABLE 10  
CARBON FRACTION COMPARISON:  
EXPERIMENT VS. MODEL AT 250 HZ, 180 kV/CM, AND 5.1 SECONDS

	Experiment	Model
CH <sub>4</sub>	93.9%	92.9%
C <sub>2</sub> H <sub>6</sub>	2.9%	2.9%
C <sub>2</sub> H <sub>4</sub> , C <sub>2</sub> H <sub>2</sub>	0.9%	0.8%
C <sub>3</sub> H <sub>8</sub> , C <sub>3</sub> H <sub>6</sub>	1.4%	1.2%
C <sub>4</sub> <sup>+</sup>	1.6%	2.1%

The model predicts a slightly higher conversion of methane than measured experimentally for both retention times, but excellent qualitative agreement is shown for both cases.

Direct comparisons of the residence time effects on the model results and the experimentally obtained results for each hydrocarbon fraction are presented in Figures 39-43. The solid line shows the actual plasma composition calculated by the model. However, the fraction of ionic species is significant and will affect the overall composition once these ions have been reduced to neutral species. As shown in Figure 39, the methane carbon fraction calculated from the model does not change significantly after the neutralization period. The model predicts a nearly linear trend although the experimental data suggests a non-linear relationship between methane carbon fraction and residence time. This non-linear appearance could be due to fouling that built up within the reactor over time. Figure 40 shows very good agreement between the neutralized model values and the experimental values for ethane. The values for both sets of data increase with residence time with a decreasing slope. Figure 41 shows good agreement between the neutralized model values and the experimental values for the ethylene + acetylene carbon fractions. Figure 42 shows good qualitative agreement between the neutralized model values and the experimental values for propane. The



carbon fractions increase with time, although the rate of increase becomes less as the residence time increases. Figure 43 shows a distinct difference in the trends of the model values and the experimental values. The experimental values suggest that the rate of butane formation increases initially and then begins to decrease. The methane plasma model has no mechanism for butane consumption and this probably accounts for the continued increase in the rate of butane formation predicted by the model.

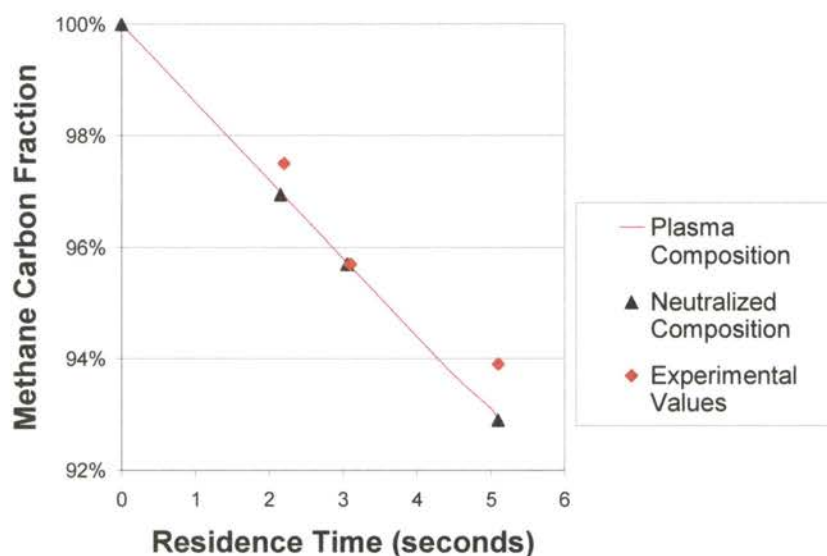


Figure 39. Effect of Residence Time on Model and Experimental Values of Methane Carbon Fraction at 250 Hz and 180 kV/cm.

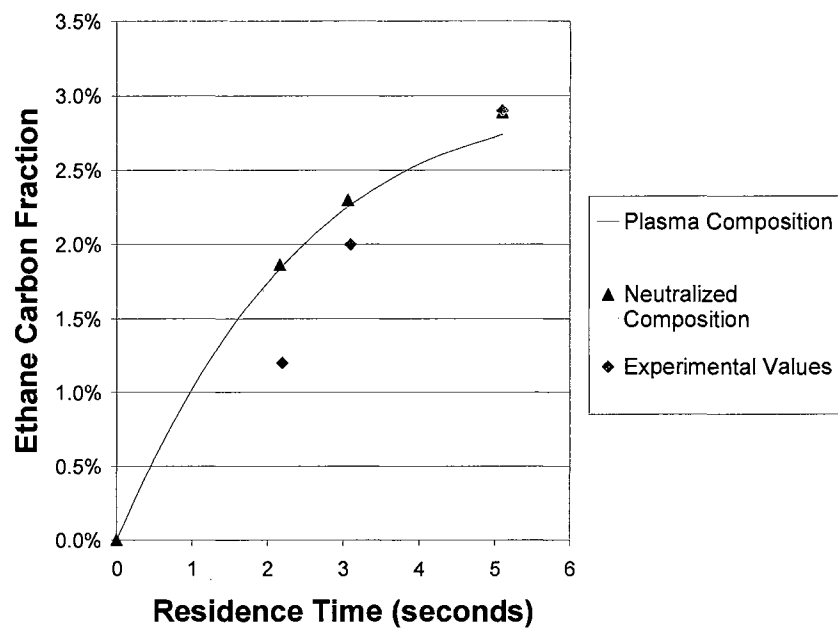


Figure 40. Effect of Residence Time on Model and Experimental Values of Ethane Carbon Fraction at 250 Hz and 180 kV/cm.

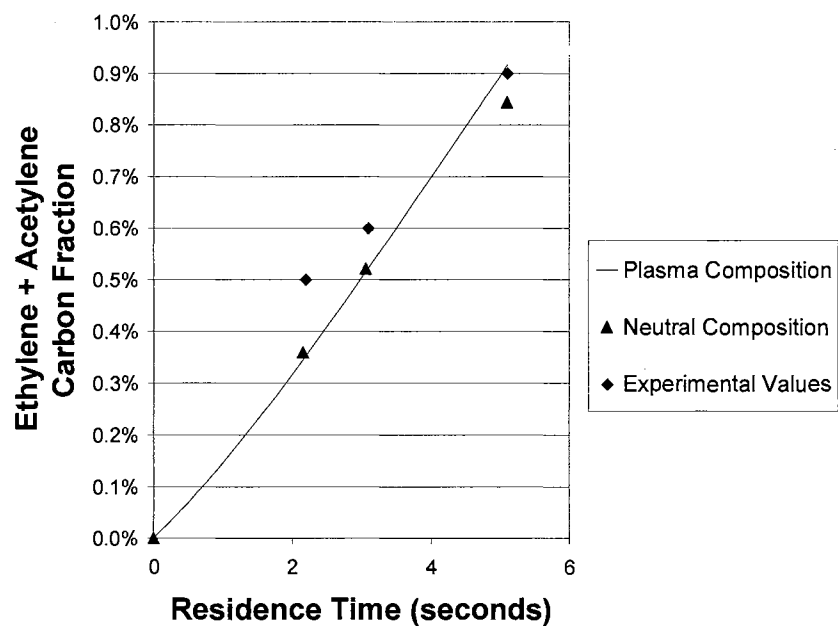


Figure 41. Effect of Residence Time on Model and Experimental Values of Ethylene + Acetylene Carbon Fraction at 250 Hz and 180 kV/cm.

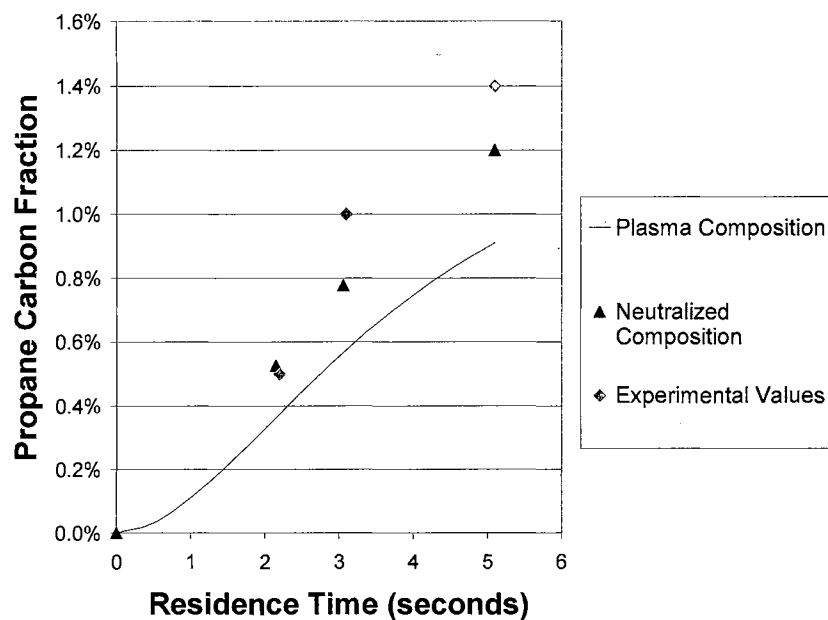


Figure 42. Effect of Residence Time on Model and Experimental Values of Propane Carbon Fraction at 250 Hz and 180 kV/cm.

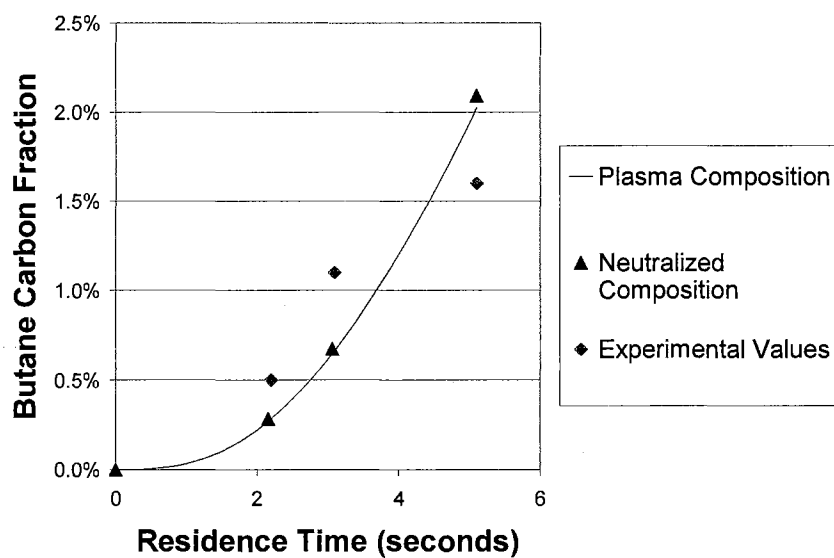


Figure 43. Effect of Residence Time on Model and Experimental Values of Butane Carbon Fraction at 250 Hz and 180 kV/cm.

### 7.3 Operating Frequency

The base case for the scaled parameters had a frequency of 250 Hz and a retention time of 3.1 seconds. The frequency of the model was adjusted to 200 Hz and compared to experimental results for the same discharge frequency, both with a retention time of 3.1 seconds. The results are shown in Table 11.

TABLE 11  
CARBON FRACTION COMPARISON:  
EXPERIMENT VS. MODEL AT 200 HZ, 180 kV/CM, AND 3.1 SECONDS

	Experiment	Model
CH <sub>4</sub>	96.9%	96.5%
C <sub>2</sub> H <sub>6</sub>	1.5%	2.0%
C <sub>2</sub> H <sub>4</sub> , C <sub>2</sub> H <sub>2</sub>	0.5%	0.4%
C <sub>3</sub> H <sub>8</sub> , C <sub>3</sub> H <sub>6</sub>	0.7%	0.6%
C <sub>4</sub> <sup>+</sup>	0.7%	0.4%

The frequency of the model was then adjusted to 300 Hz and compared with the experimental results for the same discharge frequency, still at a residence time of 3.1 seconds. The results are shown in Table 12.

TABLE 12  
CARBON FRACTION COMPARISON:  
EXPERIMENT VS. MODEL AT 300 HZ, 180 kV/CM, AND 3.1 SECONDS

	Experiment	Model
CH <sub>4</sub>	94.8%	94.9%
C <sub>2</sub> H <sub>6</sub>	2.5%	2.5%
C <sub>2</sub> H <sub>4</sub> , C <sub>2</sub> H <sub>2</sub>	0.7%	0.6%
C <sub>3</sub> H <sub>8</sub> , C <sub>3</sub> H <sub>6</sub>	1.2%	0.9%
C <sub>4</sub> <sup>+</sup>	1.3%	1.0%

The model predicts a slightly elevated selectivity of ethane at 200 Hz, resulting in slightly depressed concentrations for other products. However, good qualitative agreement is still shown. The model shows good qualitative and quantitative agreement at 300 Hz.

Direct comparisons of the hydrocarbon fractions obtained from the model and by experiment, for three different frequencies, are presented in Figures 44-49. The lower molecular weight fractions (methane, ethane, ethylene + acetylene) show better agreement at higher frequencies. The higher molecular weight fractions (propane, butane) show better agreement at lower frequencies. The plasma model also predicts carbon fractions higher than experimental values for every component except ethane. This suggests that the rate at which the model is converting ethane into higher molecular weight products is too low. Since the electron impact rates have already been optimized, this may suggest that an important ethane reaction is missing from the model or that an ethane reaction included in the model is inappropriate.

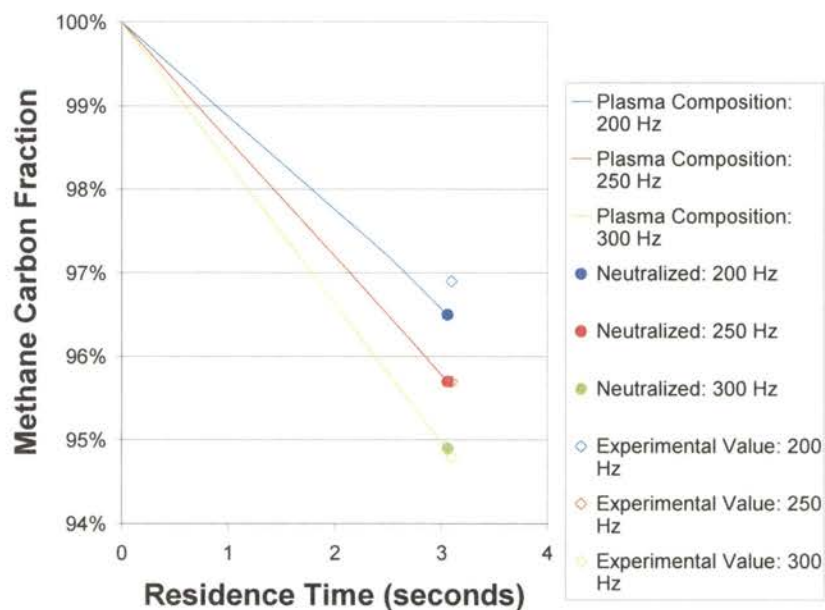


Figure 44. Effect of Frequency on Model and Experimental Values of Methane Carbon Fraction at 3.1 Seconds and 180 kV/cm.

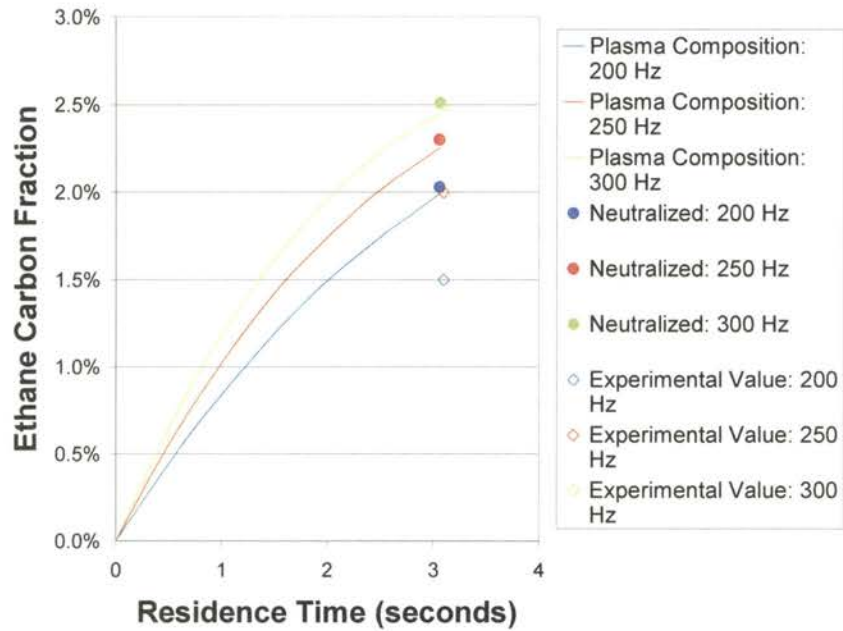


Figure 45. Effect of Frequency on Model and Experimental Values of Ethane Carbon Fraction at 3.1 Seconds and 180 kV/cm.

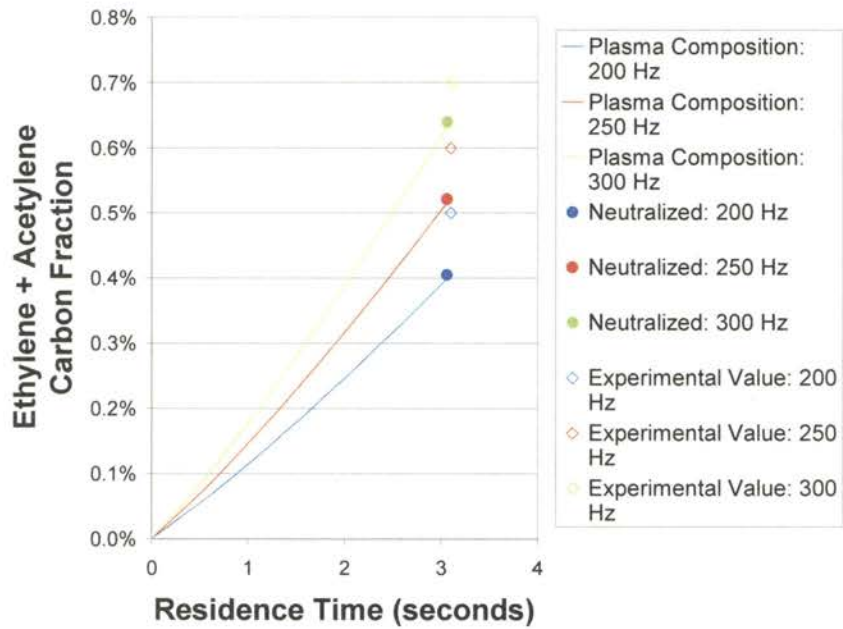


Figure 46. Effect of Frequency on Model and Experimental Values of Ethylene + Acetylene Carbon Fraction at 3.1 sec. and 180 kV/cm.

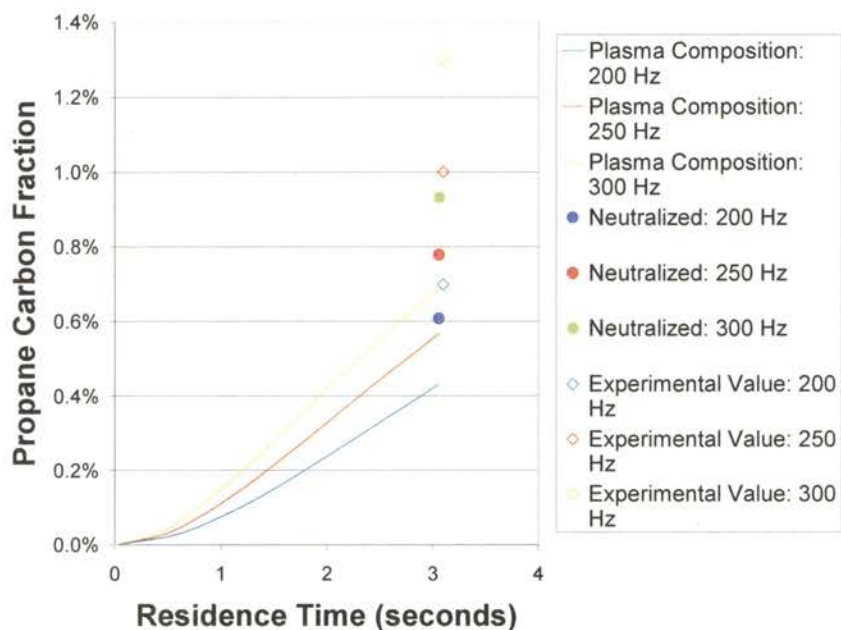


Figure 47. Effect of Frequency on Model and Experimental Values of Propane Carbon Fraction at 3.1 Seconds and 180 kV/cm.

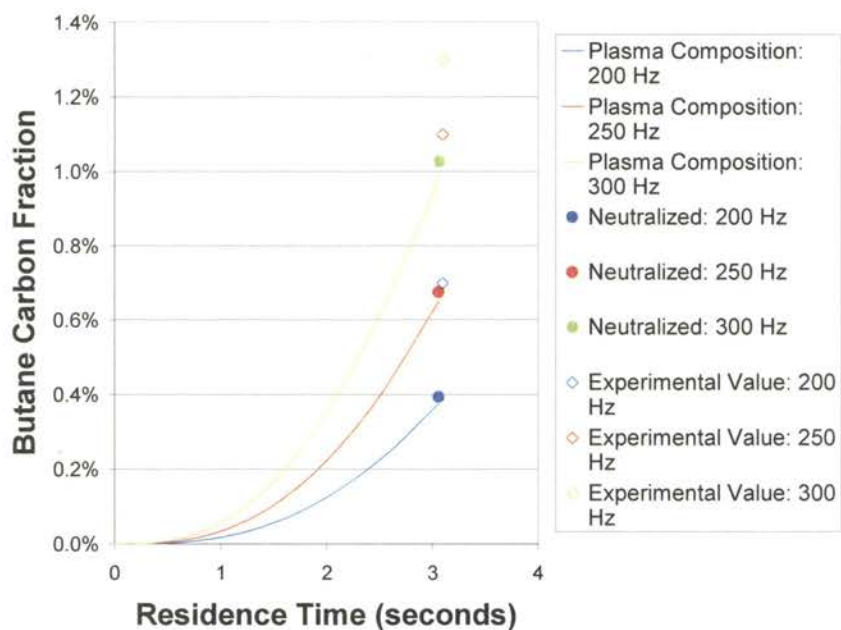


Figure 48. Effect of Frequency on Model and Experimental Values of Butane Carbon Fraction at 3.1 Seconds and 180 kV/cm.

## 7.4 Hydrogen Production

Although the previous analyses have focused on carbon fractions, the plasma model does account for hydrogen production. Table 13 compares the hydrogen mole fractions calculated from experimental data with the hydrogen mole fractions predicted by the methane plasma model. In each case, the model predicts a lower hydrogen mole fraction than what is calculated from the experimental data although the same relative trends are exhibited. The primary reason for the differences is related to the differences in hydrocarbon fractions discussed above. The model tends to underestimate the fractions of higher molecular weight hydrocarbons, which results in lower hydrogen mole fractions.

TABLE 13  
EXPERIMENTAL AND PLASMA MODEL  
HYDROGEN MOLE FRACTIONS

<b>Experimental Conditions</b>	<b>Experimental H<sub>2</sub> Mole Fraction</b>	<b>Model H<sub>2</sub> Mole Fraction</b>
200 Hz, 180 kV/cm, 3.1 seconds	0.039	0.021
250 Hz, 180 kV/cm, 3.1 seconds	0.054	0.027
300 Hz, 180 kV/cm, 3.1 seconds	0.065	0.033
250 Hz, 180 kV/cm, 5.1 seconds	0.076	0.047
250 Hz, 180 kV/cm, 2.2 seconds	0.033	0.019

## 7.5 Sensitivity Analysis

A sensitivity analysis was performed to determine if any variables were particularly sensitive to changes. Six different variables were examined: electron density, discharge period, and the four electron-impact rates (scale1, scale2, scale4, and scale5).



Each variable was altered by  $\pm 1\%$ ,  $\pm 10\%$ , and  $\pm 50\%$ . The resulting compositions were calculated for a residence time of 3.1 seconds at 250 Hz. The final compositions for these cases are shown in Table 14. These results are shown graphically in Appendix F.

Variations in electron density and discharge period produce almost identical changes in composition. Methane carbon fractions are not affected by variations in scale2, scale4, or scale5. Other fractions are affected by a change in their respective scaling factors or the scaling factors of other fractions with which they react. None of the variables show unexpected sensitivity. Methane is most sensitive to electron density, discharge period, and scale1. All three variables directly affect the rate of radical formation from methane. Ethane is most sensitive to scale1, showing a strong relationship between ethane formation and methane dissociation by electron impact. Electron density and discharge period are the variables to which ethylene is most sensitive. The propane and propylene fraction is most sensitive to scale1, indicating a strong relationship between their formation and the rate of electron-methane impacts. Clearly, the most important consideration in the model is the rate at which methane is dissociated and can be attributed to three variables: electron density, discharge period, and scale1.

TABLE 14  
HYDROCARBON SENSITIVITY TO MODEL VARIABLES  
FINAL COMPOSITION AT 250 HZ, 3.1 SECONDS

Sensitivity of Hydrocarbon Fractions to Variation of Electron Density

	+50%	+10%	+1%	-1%	-10%	-50%
Methane	93.61%	95.27%	95.65%	95.73%	96.11%	97.82%
Ethane	2.67%	2.36%	2.26%	2.24%	2.13%	1.44%
Ethylene + Acetylene	0.82%	0.57%	0.52%	0.51%	0.46%	0.23%
Propane + Propylene	0.82%	0.63%	0.57%	0.56%	0.51%	0.24%
Heavy Hydrocarbons	1.55%	0.80%	0.66%	0.63%	0.51%	0.12%

Sensitivity of Hydrocarbon Fractions to Variation of Discharge Period

	+50%	+10%	+1%	-1%	-10%	-50%
Methane	93.61%	95.27%	95.65%	95.73%	96.11%	97.82%
Ethane	2.67%	2.36%	2.26%	2.24%	2.13%	1.44%
Ethylene + Acetylene	0.82%	0.58%	0.52%	0.51%	0.46%	0.23%
Propane + Propylene	0.83%	0.63%	0.57%	0.56%	0.50%	0.23%
Heavy Hydrocarbons	1.58%	0.81%	0.66%	0.63%	0.51%	0.12%

Sensitivity of Hydrocarbon Fractions to Variation of [scale1]

	+50%	+10%	+1%	-1%	-10%	-50%
Methane	93.61%	95.27%	95.65%	95.73%	96.11%	97.82%
Ethane	3.33%	2.47%	2.27%	2.23%	2.03%	1.14%
Ethylene + Acetylene	0.76%	0.57%	0.52%	0.51%	0.47%	0.26%
Propane + Propylene	0.85%	0.62%	0.57%	0.56%	0.51%	0.29%
Heavy Hydrocarbons	0.97%	0.71%	0.65%	0.64%	0.58%	0.32%

Sensitivity of Hydrocarbon Fractions to Variation of [scale2]

	+50%	+10%	+1%	-1%	-10%	-50%
Methane	95.69%	95.69%	95.69%	95.69%	95.69%	95.69%
Ethane	2.21%	2.24%	2.25%	2.25%	2.26%	2.30%
Ethylene + Acetylene	0.57%	0.53%	0.52%	0.51%	0.50%	0.46%
Propane + Propylene	0.56%	0.57%	0.57%	0.57%	0.57%	0.57%
Heavy Hydrocarbons	0.64%	0.65%	0.65%	0.65%	0.65%	0.65%

Sensitivity of Hydrocarbon Fractions to Variation of [scale4]

	+50%	+10%	+1%	-1%	-10%	-50%
Methane	95.69%	95.69%	95.69%	95.69%	95.69%	95.69%
Ethane	1.88%	2.17%	2.24%	2.26%	2.34%	2.74%
Ethylene + Acetylene	0.51%	0.51%	0.52%	0.52%	0.52%	0.52%
Propane + Propylene	0.72%	0.60%	0.57%	0.56%	0.53%	0.35%
Heavy Hydrocarbons	0.85%	0.69%	0.65%	0.64%	0.60%	0.39%

Sensitivity of Hydrocarbon Fractions to Variation of [scale5]

	+50%	+10%	+1%	-1%	-10%	-50%
Methane	95.69%	95.69%	95.69%	95.69%	95.69%	95.69%
Ethane	2.22%	2.25%	2.25%	2.25%	2.26%	2.30%
Ethylene + Acetylene	0.51%	0.52%	0.52%	0.52%	0.52%	0.52%
Propane + Propylene	0.44%	0.54%	0.56%	0.57%	0.60%	0.77%
Heavy Hydrocarbons	0.80%	0.68%	0.65%	0.64%	0.61%	0.41%

## CHAPTER 8

### METHANE PLASMA MODEL RECOMMENDATIONS

The major shortcoming of the current methane plasma model is the inability to account for the effect of different electric field strengths. The electric field directly affects the average electron energy and thus, the electron impact reaction rates. The ability to account for changes in the electric field strength would be the most significant addition to the current model. If a method for relating the average electron energy to the electron impact reaction rates could be incorporated into the plasma model, the need to scale these electron impact reaction rates to experimentally measured electron impact reaction rates would be eliminated.

The current reaction matrix is adequate for demonstrating the potential of the model framework. The ethane carbon fraction appears to be the primary difference between the experimental data and the plasma model predictions. The inclusion of additional ethane reaction mechanisms resulting in the production of higher molecular weight hydrocarbons should be investigated to improve the reliability of the model.

The calculations required for this model are intensive. Identification and removal of unimportant reactions from the model could reduce calculation times significantly. A single simulation for a retention time of 3 seconds requires approximately 50 minutes on a PC with a Pentium III, 1.4 GHz processor.

## CHAPTER 9

### CONCLUSIONS

This research has resulted in the successful conversion of methane into higher molecular weight hydrocarbons using a Dielectric Barrier Discharge plasma reactor. The basic trends for methane conversion and product selectivity at various frequencies, electric fields, and residence times have been established.

The 2:1 production of n-butane and iso-butane from methane in a dielectric barrier discharge has not been reported previously. Thermal methods of butane production result in more isobutane than n-butane because the isobutane isomer is thermodynamically more stable. Since n-butane is more valuable and useful as a feedstock than isobutane, this process could prove economically significant.

A maximum methane conversion of 6% was achieved at 250 Hz and a residence time of 5 seconds. This roughly corresponds to the methane conversion for thermodynamic equilibrium at a temperature of 650 °C, as shown in Figure 1. Evidence suggests that the conversion of methane in a dielectric barrier discharge would reach 100% if given sufficient time. If the rate of conversion calculated at 3.1 seconds remains constant at 1.39% per second, the time for 100% conversion would be approximately 224 seconds. The primary concern with prolonged exposure would be the accumulation of heavy hydrocarbon on the reactor walls. Once hydrocarbons precipitate inside the reactor as liquids, they are quickly converted to polymer films.

A unique, kinetic plasma model has also been successfully developed during this research. This new model simulates the actual physical process of a multi-discharge

process more realistically than previous models [2, 26]. This new model also improves upon the versatility of previous methane reaction models by incorporating propane and butane as products. Excellent qualitative agreement is observed between the model results and the experimentally determined effects of frequency, electric field, and residence time on methane conversion and product formation. Very good quantitative agreement has also been observed between this model and the experimental data obtained at different residence times. The plasma model developed as a part of this work is not currently capable of simulating the experimentally measured 2:1 ratio of n-butane to isobutane. However, it does provide the framework for a future model that might be able to simulate this trend once a more robust reaction scheme for the longer hydrocarbons is added.

The two step reaction sequence used in this model appears promising and should provide novel ways of optimizing reaction schemes using dielectric barrier discharge reactors. By optimizing the period between discharges, enough time could be allowed for faster, more desirable reactions to occur, yet not enough time for undesirable ones to compete. Including additional reactants and varying operating conditions could be investigated computationally before conducting actual experimental work.

A primary focus should be to determine the best uses for plasma reactors based upon known factors instead of trying to adapt plasma reactors to do jobs for which they are poorly suited. Reaction schemes that can take advantage of the “on-off” sequence should be studied. It should be noted that the discharge frequencies used in this work could not be manipulated to selectively break chemical bonds. Electric field strength is

the only means for controlling which chemical bonds are broken. Residence time and operating frequency were effective for controlling methane conversion.

## REFERENCES

- [1] Melton, C. E. and P. S. Rudolph (1967). "Radiolysis of Methane in a Wide-Range Radiolysis Source of a Mass Spectrometer. 1. Individual and Total Cross Sections for the Production of Positive Ions, Negative Ions, and Free Radicals by Electrons." Journal of Chemical Physics **47**(5): 1771-1774.
- [2] Masi, M. et al. (1998). "Different Approaches for Methane Plasmas Modeling." Chemical Engineering Science **53**(22): 3875-3886.
- [3] Nagayama, K. et al. (1998). "Particle Simulation of Radio-Frequency Plasma Discharges of Methane for Carbon Film Deposition." IEEE Transactions on Plasma Science **26**(2): 125-134.
- [4] Piatt, M. A. (1988). Methane Destruction in an Alternating Current Plasma Reactor. Chemical Engineering. Stillwater, Oklahoma State University.
- [5] Manning, D. K. (1993). Hydrocarbon Rearrangements and Synthesis Using an Alternating Current Silent Glow Discharge Reactor. Chemical Engineering. Stillwater, Oklahoma State University.
- [6] Eliasson, B. and U. Kogelschatz (1991). "Modeling and Applications of Silent Discharge Plasmas." IEEE Transactions on Plasma Science **19**(2): 309-323.
- [7] Eliasson, B. and U. Kogelschatz (1991). "Nonequilibrium Volume Plasma Chemical Processing." IEEE Transactions on Plasma Science **19**(6): 1063-1077.
- [8] Spedding, P. L. (1969). "Chemical Reactions in Non-Disruptive Electric Discharges." The Chemical Engineer(Jan/Feb 1969): CE17.
- [9] Carman, R. J. and R. P. Mildren (2000). "Electron Energy Distribution Functions for Modeling the Plasma Kinetics in Dielectric Barrier Discharges." Journal of Physics D: Applied Physics **33**(19): L99-L103.
- [10] Glockler, G., and S. C. Lind (1939). The Electrochemistry of Gases and Other Dielectrics. New York, John Wiley & Sons, Inc.
- [11] Lind, S. C. and G. Schultze (1931). The Condensation of Hydrocarbons by Electrical Discharge. VII. A Study of the Rates of Condensation for Methane, Ethylene and Acetylene. Fifty-ninth General Meeting of the Electrochemical Society, Birmingham, Alabama.
- [12] Lind, S. C. and G. Schultze (1931). "The Condensation of Hydrocarbons by Electrical Discharge. VIII. The Condensation as a Function of Time and Pressure." J. Am. Chem. Soc. **53**: 3355-3366.

- [13] Evans, D. et al. (1993). "Plasma Remediation of Trichloroethylene in Silent Discharge Plasmas." J. Appl. Phys. **74**(9): 5378-5386.
- [14] Zhang, R. et al. (1996). "Control of Ammonia and Odors in Animal Houses by a Ferroelectric Plasma Reactor." IEEE Transactions on Industry Applications **32**(1): 113-117.
- [15] Dorai, R. and M. J. Kushner (2001). "Effect of Multiple Pulses on the Plasma Chemistry during the Remediation of NO<sub>x</sub> Using Dielectric Barrier Discharges." Journal of Physics D: Applied Physics **34**(4): 574-583.
- [16] Okazaki, K. et al. (1997). "Plasma Chemical Reactions at Atmospheric Pressure for High Efficiency Use of Hydrocarbon Fuels." Energy **22**(2/3): 369-374.
- [17] Okumoto, M. et al. (1998). "Nonthermal Plasma Approach in Direct Methanol Synthesis from CH<sub>4</sub>." IEEE Transactions on Industry Applications **34**(5): 940-944.
- [18] Legrand, J. C. et al. (1997). "Kinetics of Reactions in CH<sub>4</sub>/N<sub>2</sub> Afterglow Plasma." Vacuum **48**(7-9): 671-675.
- [19] Thanyachotpaiboon, K. et al. (1998). "Conversion of Methane to Higher Hydrocarbons in AC Nonequilibrium Plasmas." AIChE Journal **44**(10): 2252-2257.
- [20] Kleban, P. and H. Davis (1977). "Electron Transport in Methane Gas." Physical Review Letters **39**(8): 456-460.
- [21] Kleban, P. and H. Davis (1978). "Electron Drift and Diffusion in Polyatomic Gases: Calculations for CH<sub>4</sub>, CD<sub>4</sub>, and Related Models." J. Chem. Phys. **68**(7): 2999-3006.
- [22] Pitchford, L. C. et al. (1980). "Extended Boltzmann Analysis of Electron Swarm Experiments." Physical Review A **23**(1): 294-304.
- [23] Chatham, H. et al. (1984). "Total and Partial Electron Collisional Ionization Cross Sections for CH<sub>4</sub>, C<sub>2</sub>H<sub>6</sub>, SiH<sub>4</sub>, and Si<sub>2</sub>H<sub>6</sub>." J. Chem. Phys. **81**(4): 1770-1777.
- [24] Segur, P. et al. (1983). "The Application of a Modified Form of the S<sub>N</sub> Method to the Calculation of Swarm Parameters of Electrons in a Weakly Ionised Equilibrium Medium." Journal of Computational Physics **50**: 116-137.
- [25] Segur, P. et al. (1984). "Comparisons Between Different Methods of Solution of the Boltzmann Equation Adapted to the Calculation of Swarm Parameters in a Weakly Ionised Medium." Journal of Physics D: Applied Physics **17**: 2199-2214.
- [26] Penetrante, B. M. et al. (1985). "Monte Carlo and Boltzmann Calculations of the Density Gradient Expanded Energy Distribution Functions of Electron Swarms in Gases." J. Phys. D: Apply. Phys. **18**: 1087-1100.



- [27] Ohmori, K. et al. (1986). "Boltzmann Equation Analysis of Electron Swarm Behaviour in Methane." J. Phys. D: Appl. Phys. **19**: 437-455.
- [28] Verboncoeur, J. P. et al. (1996). "Comparison of Collision Rates in Particle-In-Cell, Monte Carlo, and Boltzmann Codes." J. Appl. Phys. **80**(3): 1299-1303.
- [29] Balbach, J. H. (1991). Modeling the Removal of Sulfur Dioxide and Nitrogen Oxides From Flue Gases Using Combined Plasma and Optical Processing. Electrical Engineering. Urbana, University of Illinois at Urbana-Champaign: 1-68.
- [30] Schoenbach, K. H. et al. (1997). "The Effect of Pulsed Electric Fields on Biological Cells: Experiments and Applications." IEEE Transactions on Plasma Science **25**(2): 284-292.
- [31] Desai, V. R. (1992). Decomposition of Hydrogen Sulfide in an Alternating Current, Frequency Tuned Plasma Reactor. Chemical Engineering. Stillwater, Oklahoma State University.
- [32] Mangrio, T. M. (1992). Production of Titanium Dioxide Powder by the Oxidation of Titanium Tetrachloride in a Plasma Reactor. Chemical Engineering. Stillwater, Oklahoma State University.
- [33] Robinowitz, S. B. (1992). Production of NO<sub>x</sub> in an Alternating Current Plasma Reactor. Environmental Engineering. Stillwater, Oklahoma State University.
- [34] Hurst, M. C. (1993). Destruction of Carbon Tetrachloride in an Alternating Current Plasma Reactor. Environmental Engineering. Stillwater, Oklahoma.
- [35] Sidhu, G. S. (1995). Production and Destruction of Nitrogen Oxides in Alternating Current Plasma Reactors. Chemical Engineering. Stillwater, Oklahoma State University.
- [36] Magunta, S. R. (1995). Studies on Destruction of Hydrogen Sulfide Mixed with Carbon Dioxide in an Alternating Current Plasma Arc Reactor. Chemical Engineering. Stillwater, Oklahoma State University.
- [37] Parker, G. W. (1996). Conceptual Design of an Industrially Applicable Plasma Reactor. Chemical Engineering. Stillwater, Oklahoma State University.
- [38] Lytle, P. H. (1998). Destruction of Nitrogen Oxides Using a Dielectric Barrier Discharge Plasma Reactor. Environmental Engineering. Stillwater, Oklahoma State University.
- [39] McNair, H. M. and E. J. Bonelli (1968). Basic Gas Chromatography. Berkley, CA, Consolidated Printers.

- [40] Feng, R. et al. (1998). "Automated System for Power Measurement in the Silent Discharge." IEEE Transactions on Industry Applications **34**(3): 563-569.
- [41] Rhallabi, A. and Y. Catherine (1991). "Computer Simulation of a Carbon-Deposition Plasma in CH<sub>4</sub>." IEEE Transactions on Plasma Science **19**(2): 270-277.
- [42] NIST Chemical Kinetics Database on the Web, <http://kinetics.nist.gov>, Public Beta Release 1.1, Standard Reference Database 17, Version 7.0 (Web Version).

## APPENDIX A

### Experimental Data: Frequency, Electric Field, and Residence Time

This appendix contains the seven sets of experimental data for this study. Each individual set is composed of four experimental runs. The integrated peak areas are converted into moles using relative weighting factors for each component. These mole compositions are then converted into relative mole fractions and relative carbon fractions. Average values are computed and shown in the right hand column.

TABLE A-1: 200 Hz, 180 kV/cm, and 3.1 seconds .....	90
TABLE A-2: 250 Hz, 180 kV/cm, and 3.1 seconds .....	91
TABLE A-3: 300 Hz, 180 kV/cm, and 3.1 seconds .....	92
TABLE A-4: 250 Hz, 180 kV/cm, and 5.1 seconds .....	93
TABLE A-5: 250 Hz, 180 kV/cm, and 2.2 seconds .....	94
TABLE A-6: 250 Hz, 127 kV/cm, and 3.1 seconds .....	95
TABLE A-7: 250 Hz, 153 kV/cm, and 3.1 seconds .....	96

TABLE A-1  
200 Hz, 180 kV/cm, and 3.1 seconds

Frequency		200 Hz		180 kV/cm		Sec. voltage reading	
Secondary voltage		27 kV				7.00 v" fluke	
Actual flow		3.1 seconds				Mass flow reading	
		RUN #1	RUN #2	RUN #3	RUN #4		
Tin (F) - from readout		73.5	75.1	76.4	75.0		
Tout (F) - from readout		74.1	75.6	76.6	75.4		
Tin (F) - corrected		73.3	74.8	76.0	74.7		
Tout (F) - corrected		73.7	75.1	76.0	74.9		
pressure (psig) - readout		0.015	0.015	0.015	0.015		
pressure (psia) - corrected		14.715	14.715	14.715	14.715		
moles in sample		1.74E-05	1.73E-05	1.73E-05	1.73E-05	average	stdv/ave
total methane feed		1.10E+07	1.09E+07	1.09E+07	1.09E+07	1.09E+07	0.2%
conversion of methane		3.8%	3.4%	3.0%	3.4%	feed basis	9.9%
		3.2%	3.2%	3.2%	3.2%	product basis	0.4%
Component		retention time	area	area	area	area	average
methane		1.06	1.0544E+07	1.0562E+07	1.0586E+07	1.0567E+07	stdv/ave
ethylene		1.66	34180	34584	35573	34974	0.2%
ethane		1.87	120500	119310	119470	119020	2.0%
water		2.15	27570	15757	11318	15708	0.5%
propylene		3.26	3101	2630	2779	2796	54.1%
propane		3.50	41816	40756	40783	40594	7.0%
isobutane		6.65	5709	6213	6731	6399	1.4%
n-butane		7.68	13983	14088	13663	14027	6.8%
pentane		16.08	5377	5335	5741	4981	1.4%
						5359	5.8%
Dry basis		weight factors	moles	moles	moles	moles	
methane feed		0.02813	3.08E+05	3.07E+05	3.07E+05	3.08E+05	
methane		0.02813	2.97E+05	2.97E+05	2.98E+05	2.97E+05	
ethylene		0.02089	7.14E+02	7.23E+02	7.43E+02	7.43E+02	
ethane		0.01967	2.37E+03	2.35E+03	2.35E+03	2.34E+03	
propylene		0.01552	4.81E+01	4.08E+01	4.31E+01	4.34E+01	
propane		0.01545	6.46E+02	6.30E+02	6.30E+02	6.27E+02	
isobutane		0.01224	6.99E+01	7.61E+01	8.24E+01	7.83E+01	
n-butane		0.01172	1.64E+02	1.65E+02	1.60E+02	1.64E+02	
pentane		0.00958	5.15E+01	5.11E+01	5.50E+01	4.77E+01	
						average	
H2 by difference			1.23E+04	1.22E+04	1.23E+04	1.23E+04	
total moles (no H2)			3.01E+05	3.01E+05	3.02E+05	3.01E+05	
total moles			3.13E+05	3.13E+05	3.14E+05	3.14E+05	
moles of carbon			3.06E+05	3.06E+05	3.07E+05	3.07E+05	
non-methane C fraction			3.09%	3.06%	3.08%	3.06%	
						3.07%	
Relative mole percents						average	
methane			94.78%	94.82%	94.78%	94.80%	
ethylene			0.23%	0.23%	0.24%	0.24%	
ethane			0.76%	0.75%	0.75%	0.75%	
propylene			0.02%	0.01%	0.01%	0.01%	
propane			0.21%	0.20%	0.20%	0.20%	
isobutane			0.02%	0.02%	0.03%	0.02%	
n-butane			0.05%	0.05%	0.05%	0.05%	
pentane			0.02%	0.02%	0.02%	0.02%	
total			96.07%	96.10%	96.07%	96.09%	
Relative carbon percents						average	
methane			96.91%	96.94%	96.92%	96.94%	
ethylene			0.47%	0.47%	0.48%	0.48%	
ethane			1.55%	1.53%	1.53%	1.53%	
propylene			0.05%	0.04%	0.04%	0.04%	
propane			0.63%	0.62%	0.62%	0.61%	
isobutane			0.09%	0.10%	0.11%	0.10%	
n-butane			0.21%	0.22%	0.21%	0.21%	
pentane			0.08%	0.08%	0.09%	0.08%	
total			100.00%	100.00%	100.00%	100.00%	

TABLE A-2  
250 Hz, 180 kV/cm, and 3.1 seconds

Frequency		250 Hz		180 kV/cm		Sec. voltage reading	
Secondary voltage		27 kV				7.00 v" fluke	
Actual flow		3.1 seconds				Mass flow reading	
		RUN #1	RUN #2	RUN #3	RUN #4		
Tin (F) - from readout		74.1	74.1	75.1	74.2		
Tout (F) - from readout		74.4	74.4	75.4	74.5		
Tin (F) - corrected		73.8	73.8	74.8	73.9		
Tout (F) - corrected		73.9	73.9	74.9	74.0		
pressure (psig) - readout		0.025	0.025	0.025	0.025		
pressure (psia) - corrected		14.725	14.725	14.725	14.725		
moles in sample		1.74E-05	1.74E-05	1.73E-05	1.74E-05	average	stdv/ave
total methane feed		1.10E+07	1.10E+07	1.09E+07	1.10E+07	1.10E+07	0.1%
conversion of methane		3.9%	3.7%	3.4%	3.6%	feed basis	6.3%
		4.6%	4.5%	4.4%	4.4%	product basis	2.8%
Component		retention time	area	area	area	area	average
methane		1.06	1.0531E+07	1.0561E+07	1.0574E+07	1.0563E+07	10557250
ethylene		1.66	44337	45823	45807	45767	45434
ethane		1.87	172710	166680	161880	163590	166215
water		2.15	15051	9569	7010	5955	9396
propylene		3.26	4049	4093	4079	4101	4081
propane		3.50	63702	60842	59065	59939	60887
isobutane		6.65	11479	10737	10332	10486	10759
n-butane		7.68	20735	19129	18816	18927	19402
pentane		16.08	9321	7823	7782	8775	8425
							8.9%
Dry basis		weight factors	moles	moles	moles	moles	
methane feed		0.02813	3.08E+05	3.08E+05	3.08E+05	3.08E+05	
methane		0.02813	2.96E+05	2.97E+05	2.97E+05	2.97E+05	
ethylene		0.02089	9.26E+02	9.57E+02	9.57E+02	9.56E+02	
ethane		0.01967	3.40E+03	3.28E+03	3.18E+03	3.22E+03	
propylene		0.01552	6.29E+01	6.35E+01	6.33E+01	6.37E+01	
propane		0.01545	9.84E+02	9.40E+02	9.13E+02	9.26E+02	
isobutane		0.01224	1.41E+02	1.31E+02	1.26E+02	1.28E+02	
n-butane		0.01172	2.43E+02	2.24E+02	2.21E+02	2.22E+02	
pentane		0.00958	8.93E+01	7.50E+01	7.46E+01	8.41E+01	
							average
H2 by difference			1.78E+04	1.73E+04	1.69E+04	1.71E+04	1.73E+04
total moles (no H2)			3.02E+05	3.03E+05	3.03E+05	3.03E+05	3.03E+05
total moles			3.20E+05	3.20E+05	3.20E+05	3.20E+05	3.20E+05
moles of carbon			3.10E+05	3.10E+05	3.10E+05	3.10E+05	3.10E+05
non-methane C fraction			4.44%	4.28%	4.18%	4.24%	4.28%
Relative mole percents							average
methane			92.60%	92.83%	92.98%	92.90%	92.83%
ethylene			0.29%	0.30%	0.30%	0.30%	0.30%
ethane			1.06%	1.02%	1.00%	1.01%	1.02%
propylene			0.02%	0.02%	0.02%	0.02%	0.02%
propane			0.31%	0.29%	0.29%	0.29%	0.29%
isobutane			0.04%	0.04%	0.04%	0.04%	0.04%
n-butane			0.08%	0.07%	0.07%	0.07%	0.07%
pentane			0.03%	0.02%	0.02%	0.03%	0.03%
total			94.43%	94.60%	94.71%	94.65%	94.60%
Relative carbon percents							average
methane			95.56%	95.72%	95.82%	95.76%	95.72%
ethylene			0.60%	0.62%	0.62%	0.62%	0.61%
ethane			2.19%	2.11%	2.05%	2.07%	2.11%
propylene			0.06%	0.06%	0.06%	0.06%	0.06%
propane			0.95%	0.91%	0.88%	0.90%	0.91%
isobutane			0.18%	0.17%	0.16%	0.17%	0.17%
n-butane			0.31%	0.29%	0.28%	0.29%	0.29%
pentane			0.14%	0.12%	0.12%	0.14%	0.13%
total			100.00%	100.00%	100.00%	100.00%	100.00%

TABLE A-3  
300 Hz, 180 kV/cm, and 3.1 seconds

Frequency		300 Hz		180 kV/cm		Sec. voltage reading		7.00 v" fluke	
Secondary voltage		27 kV							
Actual flow		3.1 seconds				Mass flow reading		99 flow	
		RUN #1	RUN #2	RUN #3	RUN #4				
Tin (F) - from readout		73.3	74.5	74.5	74.9				
Tout (F) - from readout		74.4	75.1	75.1	75.4				
Tin (F) - corrected		73.1	74.2	74.2	74.6				
Tout (F) - corrected		73.9	74.6	74.6	74.9				
pressure (psig) - readout		0.025	0.025	0.025	0.025				
pressure (psia) - corrected		14.725	14.725	14.725	14.725				
moles in sample		1.74E-05	1.74E-05	1.74E-05	1.73E-05	average		stdv/ave	
total methane feed		1.10E+07	1.09E+07	1.09E+07	1.09E+07	1.10E+07		0.1%	
conversion of methane		6.8%	6.3%	6.2%	6.0%	feed basis	6.3%	5.4%	
		5.7%	5.5%	5.4%	5.2%	product basis	5.5%	3.6%	
Component		retention time	area	area	area	area	average	stdv/ave	
methane		1.06	1.0217E+07	1.0255E+07	1.0267E+07	1.0287E+07	1.0257E+07	0.3%	
ethylene		1.66	51645	53657	53127	53134	52891	1.6%	
ethane		1.87	202940	194750	193050	186050	194198	3.6%	
water		2.15	19827	12019	8640	6928	11854	48.3%	
propylene		3.26	5088	5167	5137	5123	5129	0.6%	
propane		3.50	77645	73621	73379	70618	73816	3.9%	
isobutane		6.65	14752	13842	13895	12326	13704	7.4%	
n-butane		7.68	24511	22613	22628	21029	22695	6.3%	
pentane		16.08	11666	10932	10129	10739	10867	5.8%	
Dry basis		weight factors	moles	moles	moles	moles			
methane feed		0.02813	3.08E+05	3.08E+05	3.08E+05	3.08E+05			
methane		0.02813	2.87E+05	2.88E+05	2.89E+05	2.89E+05			
ethylene		0.02089	1.08E+03	1.12E+03	1.11E+03	1.11E+03			
ethane		0.01967	3.99E+03	3.83E+03	3.80E+03	3.66E+03			
propylene		0.01552	7.90E+01	8.02E+01	7.97E+01	7.95E+01			
propane		0.01545	1.20E+03	1.14E+03	1.13E+03	1.09E+03			
isobutane		0.01224	1.81E+02	1.69E+02	1.70E+02	1.51E+02			
n-butane		0.01172	2.87E+02	2.65E+02	2.65E+02	2.47E+02			
pentane		0.00958	1.12E+02	1.05E+02	9.71E+01	1.03E+02			
							average		
H2 by difference			2.13E+04	2.06E+04	2.04E+04	1.98E+04	2.05E+04		
total moles (no H2)			2.94E+05	2.95E+05	2.95E+05	2.96E+05	2.95E+05		
total moles			3.16E+05	3.16E+05	3.16E+05	3.16E+05	3.16E+05		
moles of carbon			3.04E+05	3.04E+05	3.04E+05	3.04E+05	3.04E+05		
non-methane C fraction			5.40%	5.20%	5.15%	4.98%	5.18%		
Relative mole percents							average		
methane			91.06%	91.34%	91.42%	91.68%	91.38%		
ethylene			0.34%	0.36%	0.35%	0.35%	0.35%		
ethane			1.26%	1.21%	1.20%	1.16%	1.21%		
propylene			0.0%	0.0%	0.0%	0.0%	0.03%		
propane			0.38%	0.36%	0.36%	0.35%	0.36%		
isobutane			0.06%	0.05%	0.05%	0.05%	0.05%		
n-butane			0.09%	0.08%	0.08%	0.08%	0.08%		
pentane			0.04%	0.03%	0.03%	0.03%	0.03%		
total			93.26%	93.47%	93.53%	93.72%	93.49%		
Relative carbon percents							average		
methane			94.60%	94.80%	94.85%	95.02%	94.82%		
ethylene			0.71%	0.74%	0.73%	0.73%	0.73%		
ethane			2.63%	2.52%	2.49%	2.40%	2.51%		
propylene			0.1%	0.1%	0.1%	0.1%	0.08%		
propane			1.19%	1.12%	1.12%	1.08%	1.12%		
isobutane			0.24%	0.22%	0.22%	0.20%	0.22%		
n-butane			0.38%	0.35%	0.35%	0.32%	0.35%		
pentane			0.18%	0.17%	0.16%	0.17%	0.17%		
total			100.00%	100.00%	100.00%	100.00%	100.00%		

TABLE A-4  
250 Hz, 180 kV/cm, and 5.1 seconds

Frequency		250 Hz		180 kV/cm		Sec. voltage reading		7.00 v" fluke	
Secondary voltage		27 kV							
Actual flow		5.1 seconds				Mass flow reading		49 flow	
		RUN #1	RUN #2	RUN #3	RUN #4				
Tin (F) - from readout		74.6	75	74.3	74.1				
Tout (F) - from readout		75.4	75.6	75.1	74.8				
Tin (F) - corrected		74.3	74.7	74.0	73.8				
Tout (F) - corrected		74.9	75.1	74.6	74.3				
pressure (psig) - readout		0.015	0.015	0.015	0.015				
pressure (psia) - corrected		14.715	14.715	14.715	14.715				
moles in sample		1.73E-05	1.73E-05	1.73E-05	1.73E-05	average		stdv/ave	
total methane feed		1.09E+07	1.09E+07	1.09E+07	1.09E+07	1.09E+07		0.1%	
conversion of methane		5.5%	5.3%	5.3%	5.5%	feed basis	5.4%	2.0%	
		6.6%	6.4%	6.4%	6.5%	product basis	6.5%	1.5%	
Component	retention time	area	area	area	area	average		stdv/ave	
methane	1.06	1.0339E+07	1.0351E+07	1.0361E+07	1.0342E+07	1.0348E+07		0.1%	
ethylene	1.66	62617	62930	64189	65017	63688		1.8%	
ethane	1.87	230690	225380	222100	226880	226263		1.6%	
water	2.15								
propylene	3.26	6228	6320	6290	6428	6317		1.3%	
propane	3.50	90962	89147	87156	88651	88979		1.8%	
isobutane	6.65	18251	17662	17190	17149	17563		2.9%	
n-butane	7.68	28548	27466	26925	28179	27780		2.6%	
pentane	16.08	15127	13557	13583	14016	14071		5.2%	
Dry basis	weight factors	moles	moles	moles	moles				
methane feed	0.02813	3.08E+05	3.07E+05	3.08E+05	3.08E+05				
methane	0.02813	2.91E+05	2.91E+05	2.91E+05	2.91E+05				
ethylene	0.02089	1.31E+03	1.31E+03	1.34E+03	1.36E+03				
ethane	0.01967	4.54E+03	4.43E+03	4.37E+03	4.46E+03				
propylene	0.01552	9.67E+01	9.81E+01	9.76E+01	9.98E+01				
propane	0.01545	1.41E+03	1.38E+03	1.35E+03	1.37E+03				
isobutane	0.01224	2.23E+02	2.16E+02	2.10E+02	2.10E+02				
n-butane	0.01172	3.35E+02	3.22E+02	3.16E+02	3.30E+02				
pentane	0.00958	1.45E+02	1.30E+02	1.30E+02	1.34E+02				
						average			
H2 by difference		2.50E+04	2.45E+04	2.43E+04	2.48E+04	2.46E+04			
total moles (no H2)		2.99E+05	2.99E+05	2.99E+05	2.99E+05	2.99E+05			
total moles		3.24E+05	3.24E+05	3.23E+05	3.24E+05	3.24E+05			
moles of carbon		3.10E+05	3.10E+05	3.10E+05	3.10E+05	3.10E+05			
non-methane C fraction		6.18%	6.04%	5.97%	6.10%	6.07%			
Relative mole percents						average			
methane		89.79%	89.99%	90.08%	89.89%	89.94%			
ethylene		0.40%	0.41%	0.41%	0.42%	0.41%			
ethane		1.40%	1.37%	1.35%	1.38%	1.38%			
propylene		0.0%	0.0%	0.0%	0.0%	0.03%			
propane		0.43%	0.43%	0.42%	0.42%	0.42%			
isobutane		0.07%	0.07%	0.07%	0.06%	0.07%			
n-butane		0.10%	0.10%	0.10%	0.10%	0.10%			
pentane		0.04%	0.04%	0.04%	0.04%	0.04%			
total		92.27%	92.43%	92.50%	92.35%	92.39%			
Relative carbon percents						average			
methane		93.82%	93.96%	94.03%	93.90%	93.93%			
ethylene		0.84%	0.85%	0.87%	0.88%	0.86%			
ethane		2.93%	2.86%	2.82%	2.88%	2.87%			
propylene		0.1%	0.1%	0.1%	0.1%	0.1%			
propane		1.36%	1.33%	1.30%	1.33%	1.33%			
isobutane		0.29%	0.28%	0.27%	0.27%	0.28%			
n-butane		0.43%	0.42%	0.41%	0.43%	0.42%			
pentane		0.23%	0.21%	0.21%	0.22%	0.22%			
total		100.00%	100.00%	100.00%	100.00%	100.00%			

TABLE A-5  
250 Hz, 180 kV/cm, and 2.2 seconds

Frequency		250 Hz		180 kV/cm		Sec. voltage reading	
Secondary voltage		27 kV				7.00 v" fluke	
Actual flow		2.2 seconds				Mass flow reading	
		RUN #1	RUN #2	RUN #3	RUN #4		
Tin (F) - from readout		74.1	74.1	75.1	74.2		
Tout (F) - from readout		74.4	74.4	75.4	74.5		
Tin (F) - corrected		73.8	73.8	74.8	73.9		
Tout (F) - corrected		73.9	73.9	74.9	74.0		
pressure (psig) - readout		0.025	0.025	0.025	0.025		
pressure (psia) - corrected		14.725	14.725	14.725	14.725		
moles in sample		1.737E-05	1.737E-05	1.734E-05	1.737E-05	average	stdv/ave
total methane feed		1.096E+07	1.096E+07	1.094E+07	1.096E+07	1.0957E+07	0.1%
conversion of methane		2.5%	2.2%	1.9%	2.1%	feed basis	11.7%
		2.6%	2.6%	2.5%	2.5%	product basis	2.4%
Component		retention time	area	area	area	area	average
methane		1.06	1.0688E+07	1.0717E+07	1.0734E+07	1.0734E+07	1.0718E+07
ethylene		1.66	39370	38583	37994	38225	38543
ethane		1.87	93717	91566	89680	87247	90553
water		2.15					
propylene		3.26	3086	2873	2821	2790	2893
propane		3.50	32545	31719	30957	30016	31309
isobutane		6.65	5732	5496	2864	5326	4855
n-butane		7.68	11131	10555	9997	10252	10484
pentane		16.08		4310	4124	4226	4220
Dry basis		weight factors	moles	moles	moles	moles	
methane feed		0.02813	3.08E+05	3.08E+05	3.08E+05	3.08E+05	
methane		0.02813	3.01E+05	3.01E+05	3.02E+05	3.02E+05	
ethylene		0.02089	8.23E+02	8.06E+02	7.94E+02	7.99E+02	
ethane		0.01967	1.84E+03	1.80E+03	1.76E+03	1.72E+03	
propylene		0.01552	4.79E+01	4.46E+01	4.38E+01	4.33E+01	
propane		0.01545	5.03E+02	4.90E+02	4.78E+02	4.64E+02	
isobutane		0.01224	7.02E+01	6.73E+01	3.51E+01	6.52E+01	
n-butane		0.01172	1.31E+02	1.24E+02	1.17E+02	1.20E+02	
pentane		0.00958	0.00E+00	4.13E+01	3.95E+01	4.05E+01	
						average	
H2 by difference			1.05E+04	1.05E+04	1.01E+04	1.02E+04	1.03E+04
total moles (no H2)			3.04E+05	3.05E+05	3.05E+05	3.05E+05	3.05E+05
total moles			3.14E+05	3.15E+05	3.15E+05	3.15E+05	3.15E+05
moles of carbon			3.08E+05	3.09E+05	3.09E+05	3.09E+05	3.09E+05
non-methane C fraction			2.52%	2.52%	2.42%	2.42%	2.47%
Relative mole percents						average	
methane			95.58%	95.59%	95.76%	95.74%	95.67%
ethylene			0.26%	0.26%	0.25%	0.25%	0.26%
ethane			0.59%	0.57%	0.56%	0.54%	0.57%
propylene			0.02%	0.01%	0.01%	0.01%	0.01%
propane			0.16%	0.16%	0.15%	0.15%	0.15%
isobutane			0.02%	0.02%	0.01%	0.02%	0.02%
n-butane			0.04%	0.04%	0.04%	0.04%	0.04%
pentane			0.00%	0.01%	0.01%	0.01%	0.01%
total			96.67%	96.66%	96.79%	96.77%	96.72%
Relative carbon percents						average	
methane			97.48%	97.48%	97.58%	97.58%	97.53%
ethylene			0.53%	0.52%	0.51%	0.52%	0.52%
ethane			1.20%	1.16%	1.14%	1.11%	1.15%
propylene			0.05%	0.04%	0.04%	0.04%	0.04%
propane			0.49%	0.48%	0.46%	0.45%	0.47%
isobutane			0.09%	0.09%	0.05%	0.08%	0.08%
n-butane			0.17%	0.16%	0.15%	0.16%	0.16%
pentane			0.00%	0.07%	0.06%	0.07%	0.05%
total			100.00%	100.00%	100.00%	100.00%	100.00%



TABLE A-6  
250 Hz, 127 kV/cm, and 3.1 seconds

Frequency		250 Hz		127 kV/cm		Sec. voltage reading		5.00 v" fluke	
Secondary voltage		19 kV							
Actual flow		3.1 seconds				Mass flow reading		99 flow	
		RUN #1	RUN #2	RUN #3	RUN #4				
Tin (F) - from readout		76.9	76.1	76.3	77.4				
Tout (F) - from readout		77.8	77	77.2	78.1				
Tin (F) - corrected		76.5	75.7	75.9	77.0				
Tout (F) - corrected		77.2	76.4	76.6	77.5				
pressure (psig) - readout		0.015	0.015	0.015	0.015				
pressure (psia) - corrected		14.715	14.715	14.715	14.715				
moles in sample		1.726E-05	1.728E-05	1.727E-05	1.725E-05	average		stdv/ave	
total methane feed		1.089E+07	1.090E+07	1.090E+07	1.088E+07	1.0894E+07		0.1%	
conversion of methane		2.0%	2.0%	1.9%	1.6%	feed basis		1.8%	
		1.9%	1.9%	1.9%	1.9%	product basis		1.9%	
Component	retention time	area	area	area	area	average		stdv/ave	
methane	1.06	1.0671E+07	1.0689E+07	1.0697E+07	1.0713E+07	10692500		0.2%	
ethylene	1.66	36411	36013	35838	36039	36075		0.7%	
ethane	1.87	65443	63681	65437	64459	64755		1.3%	
water	2.15	8530	5804	5191	5079	6151		26.3%	
propylene	3.26	2438	2337	2396	2313	2371		2.4%	
propane	3.50	21214	20633	21324	20946	21029		1.5%	
isobutane	6.65	1483	3510	3515	3551	3015		33.9%	
n-butane	7.68	7208	7549	7342	7433	7383		2.0%	
pentane	16.08				2764	2764		#DIV/0!	
Dry basis	weight factors	moles	moles	moles	moles				
methane feed	0.02813	3.06E+05	3.07E+05	3.07E+05	3.06E+05				
methane	0.02813	3.00E+05	3.01E+05	3.01E+05	3.01E+05				
ethylene	0.02089	7.61E+02	7.52E+02	7.49E+02	7.53E+02				
ethane	0.01967	1.29E+03	1.25E+03	1.29E+03	1.27E+03				
propylene	0.01552	3.78E+01	3.63E+01	3.72E+01	3.59E+01				
propane	0.01545	3.28E+02	3.19E+02	3.30E+02	3.24E+02				
isobutane	0.01224	1.82E+01	4.30E+01	4.30E+01	4.35E+01				
n-butane	0.01172	8.45E+01	8.85E+01	8.61E+01	8.71E+01				
pentane	0.00958	0.00E+00	0.00E+00	0.00E+00	2.65E+01				
						average			
H2 by difference		7.77E+03	7.80E+03	7.88E+03	8.05E+03	7.88E+03			
total moles (no H2)		3.03E+05	3.03E+05	3.03E+05	3.04E+05	3.03E+05			
total moles		3.10E+05	3.11E+05	3.11E+05	3.12E+05	3.11E+05			
moles of carbon		3.06E+05	3.06E+05	3.07E+05	3.07E+05	3.06E+05			
non-methane C fraction		1.83%	1.83%	1.86%	1.88%	1.85%			
Relative mole percents						average			
methane		96.69%	96.69%	96.65%	96.60%	96.66%			
ethylene		0.25%	0.24%	0.24%	0.24%	0.24%			
ethane		0.41%	0.40%	0.41%	0.41%	0.41%			
propylene		0.0%	0.0%	0.0%	0.0%	0.01%			
propane		0.11%	0.10%	0.11%	0.10%	0.10%			
isobutane		0.01%	0.01%	0.01%	0.01%	0.01%			
n-butane		0.03%	0.03%	0.03%	0.03%	0.03%			
pentane		0.00%	0.00%	0.00%	0.01%	0.00%			
total		97.50%	97.49%	97.47%	97.42%	97.47%			
Relative carbon percents						average			
methane		98.17%	98.17%	98.14%	98.12%	98.15%			
ethylene		0.50%	0.49%	0.49%	0.49%	0.49%			
ethane		0.84%	0.82%	0.84%	0.83%	0.83%			
propylene		0.0%	0.0%	0.0%	0.0%	0.0%			
propane		0.32%	0.31%	0.32%	0.32%	0.32%			
isobutane		0.02%	0.06%	0.06%	0.06%	0.05%			
n-butane		0.11%	0.12%	0.11%	0.11%	0.11%			
pentane		0.00%	0.00%	0.00%	0.04%	0.01%			
total		100.00%	100.00%	100.00%	100.00%	100.00%			

TABLE A-7  
250 Hz, 153 kV/cm, and 3.1 seconds

Frequency		250 Hz		153 kV/cm		Sec. voltage reading		6.00 v" fluke	
Secondary voltage		23 kV							
Actual flow		3.1 seconds				Mass flow reading		99 flow	
		RUN #1	RUN #2	RUN #3	RUN #4				
Tin (F) - from readout		73.6	74.1	74.6	74.1				
Tout (F) - from readout		74.2	74.8	75.3	74.7				
Tin (F) - corrected		73.3	73.8	74.3	73.8				
Tout (F) - corrected		73.8	74.3	74.8	74.2				
pressure (psig) - readout		0.025	0.025	0.015	0.025				
pressure (psia) - corrected		14.725	14.725	14.715	14.725				
moles in sample		1.738E-05	1.736E-05	1.733E-05	1.736E-05	average		stdv/ave	
total methane feed		1.097E+07	1.095E+07	1.094E+07	1.096E+07	1.0954E+07		0.1%	
conversion of methane		2.7%	2.4%	2.2%	2.3%	feed basis		2.4%	
		2.8%	2.8%	2.8%	2.7%	product basis		2.8%	
Component	retention time	area	area	area	area	average		stdv/ave	
methane	1.06	1.0666E+07	1.0692E+07	1.0698E+07	1.0708E+07	10691000		0.2%	
ethylene	1.66	43259	42025	43473	43388	43036		1.6%	
ethane	1.87	99190	96007	98156	95345	97175		1.9%	
water	2.15	9563	7160	6667	5596	7247		23.1%	
propylene	3.26	3154	3147	3231	3165	3174		1.2%	
propane	3.50	34740	33912	34168	33095	33979		2.0%	
isobutane	6.65	5878	5786	6288	5862	5954		3.8%	
n-butane	7.68	12078	11271	11810	11173	11583		3.7%	
pentane	16.08	3902	4713	5731		4782		19.2%	
Dry basis	weight factors	moles	moles	moles	moles				
methane feed	0.02813	3.08E+05	3.08E+05	3.08E+05	3.08E+05				
methane	0.02813	3.00E+05	3.01E+05	3.01E+05	3.01E+05				
ethylene	0.02089	9.04E+02	8.78E+02	9.08E+02	9.06E+02				
ethane	0.01967	1.95E+03	1.89E+03	1.93E+03	1.88E+03				
propylene	0.01552	4.90E+01	4.89E+01	5.02E+01	4.91E+01				
propane	0.01545	5.37E+02	5.24E+02	5.28E+02	5.11E+02				
isobutane	0.01224	7.20E+01	7.08E+01	7.70E+01	7.18E+01				
n-butane	0.01172	1.42E+02	1.32E+02	1.38E+02	1.31E+02				
pentane	0.00958	3.74E+01	4.52E+01	5.49E+01	0.00E+00				
						average			
H2 by difference		1.15E+04	1.13E+04	1.16E+04	1.09E+04	1.13E+04			
total moles (no H2)		3.04E+05	3.04E+05	3.05E+05	3.05E+05	3.04E+05			
total moles		3.15E+05	3.16E+05	3.16E+05	3.16E+05	3.16E+05			
moles of carbon		3.08E+05	3.09E+05	3.09E+05	3.09E+05	3.09E+05			
non-methane C fraction		2.76%	2.68%	2.76%	2.61%	2.70%			
Relative mole percents						average			
methane		95.17%	95.30%	95.15%	95.41%	95.26%			
ethylene		0.29%	0.28%	0.29%	0.29%	0.28%			
ethane		0.62%	0.60%	0.61%	0.59%	0.61%			
propylene		0.02%	0.02%	0.02%	0.02%				
propane		0.17%	0.17%	0.17%	0.16%	0.17%			
isobutane		0.02%	0.02%	0.02%	0.02%	0.02%			
n-butane		0.04%	0.04%	0.04%	0.04%	0.04%			
pentane		0.01%	0.01%	0.02%	0.00%	0.01%			
total		96.34%	96.43%	96.32%	96.54%	96.41%			
Relative carbon percents						average			
methane		97.24%	97.32%	97.24%	97.39%	97.30%			
ethylene		0.59%	0.57%	0.59%	0.59%	0.58%			
ethane		1.26%	1.22%	1.25%	1.21%	1.24%			
propylene		0.05%	0.05%	0.05%	0.05%	0.05%			
propane		0.52%	0.51%	0.51%	0.50%	0.51%			
isobutane		0.09%	0.09%	0.10%	0.09%	0.09%			
n-butane		0.18%	0.17%	0.18%	0.17%	0.18%			
pentane		0.06%	0.07%	0.09%	0.00%	0.06%			
total		100.00%	100.00%	100.00%	100.00%	100.00%			

## APPENDIX B

### Thermocouple and Mass Flow Calibration Data

The two Omega type K thermocouples were calibrated against a Hart Scientific Microtherm 1006 readout with a model 5614 resistor. The range of temperatures for calibration was 82-91 °F. The calibration data for each thermocouple was fit with a linear relationship as shown in Figures B-1 and B-2.

The Brooks mass flow controller and meter were calibrated against an Altech Digital Flow Meter. The flow rates for calibration were 6-35 sccm. The calibration data for each device was fit with a linear relationship as shown in Figure B-3.

Figure B-1: Calibration of Thermocouple #1 .....	98
Figure B-2: Calibration of Thermocouple #2 .....	98
Figure B-3: Calibration of Mass Flow Controller and Meter .....	99

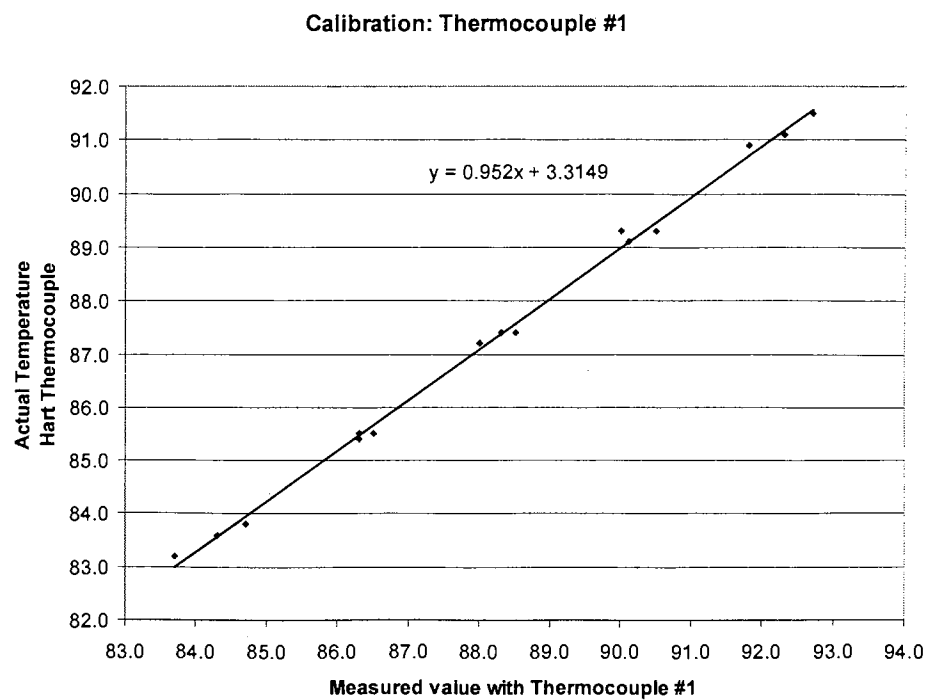


Figure B-1: Calibration of Thermocouple #1

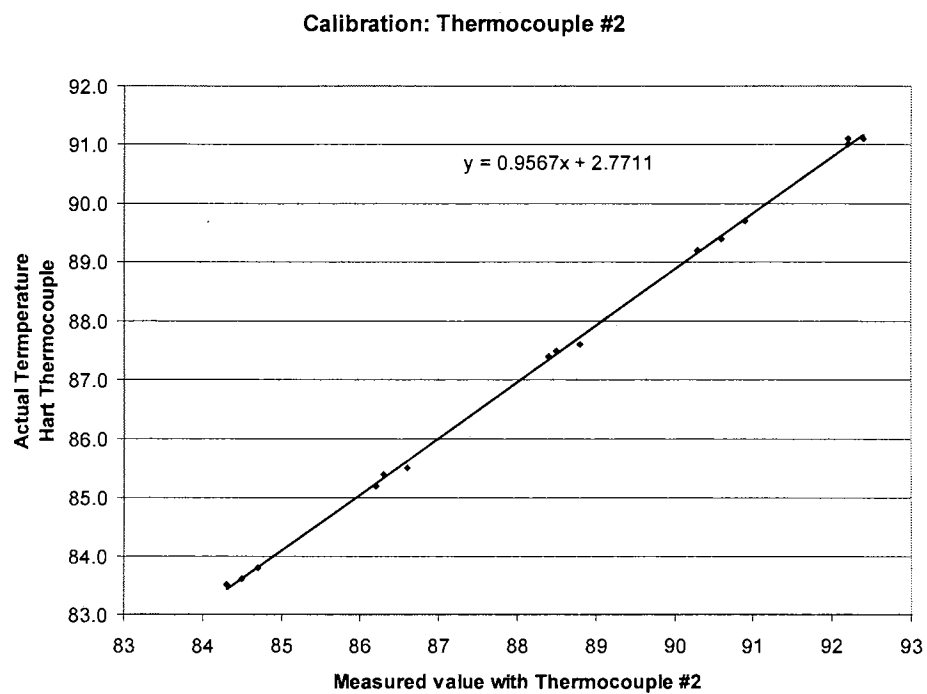


Figure B-2: Calibration of Thermocouple #2

### Calibration: Flow Controller and Meter

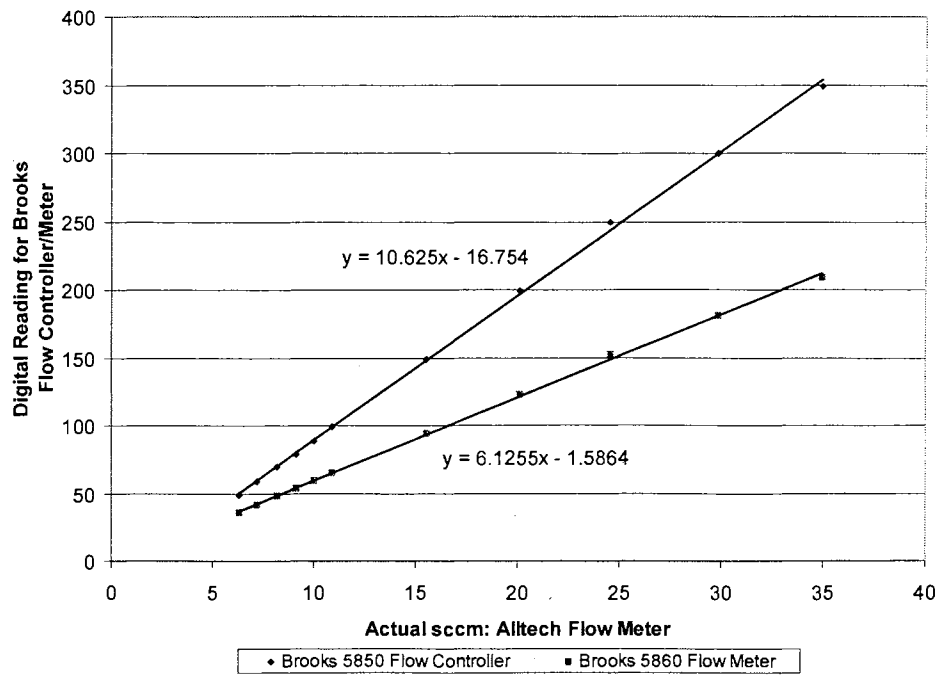


Figure B-3: Calibration of Mass Flow Controller and Meter

## APPENDIX C

### MATLAB Code for the Methane Plasma Model

The first section is the MATLAB main routine. This main routine assigns initial values for all variables and keeps track of the time steps. The main routine then uses the subroutines `plasma_on` and `plasma_off` to simulate the discharge and relaxation periods. Values at the end of each period are kept in arrays to minimize data file sizes. After the required number of discharge cycles have been completed, the `plasma_off` subroutine is run again for a period of 4E6 times the normal relaxation period so that the charged species have sufficient time to neutralize. Chemical concentrations at the end of each period are saved in a text file at the end of the simulation.

The second section is the discharge phase subroutine, `plasma_on`. This subroutine simulates the discharge period of the plasma reactor when high-energy electrons impact methane and other molecular species. There are 16 electron impact reactions, 16 ion reactions, 10 wall neutralization reactions, and 43 free-radical reactions in this subroutine.

The third section is the relaxation phase subroutine, `plasma_off`. This subroutine simulates the relaxation period of the plasma reactor when there are no high-energy electrons to impact with methane or other molecular species. There are 16 ion reactions, 10 wall neutralization reactions, and 43 free-radical reactions. The `plasma_off` subroutine is identical to the `plasma_on` subroutine except that no electron impact reactions are included.

The ID numbers corresponding to the chemical species represented in the model are listed below.

ID#	Component	ID#	Component	ID#	Component
1	= e	11	= C <sub>2</sub> H <sub>3</sub> ·	21	= CH <sub>4</sub> <sup>+</sup>
2	= H <sub>2</sub>	12	= C <sub>2</sub> H <sub>2</sub>	22	= CH <sub>3</sub> <sup>+</sup>
3	= H	13	= C <sub>3</sub> H <sub>8</sub>	23	= CH <sub>2</sub> <sup>+</sup>
4	= CH <sub>4</sub>	14	= n-C <sub>3</sub> H <sub>7</sub> ·	24	= CH <sup>+</sup>
5	= CH <sub>3</sub> ·	15	= i-C <sub>3</sub> H <sub>7</sub> ·	25	= C <sup>+</sup>
6	= CH <sub>2</sub> ·	16	= n-C <sub>4</sub> H <sub>10</sub>	26	= C <sub>2</sub> H <sub>5</sub> <sup>+</sup>
7	= CH·	17	= i-C <sub>4</sub> H <sub>10</sub>	27	= C <sub>2</sub> H <sub>4</sub> <sup>+</sup>
8	= C <sub>2</sub> H <sub>6</sub>	18	= n-C <sub>5</sub> H <sub>12</sub>	28	= C <sub>2</sub> H <sub>3</sub> <sup>+</sup>
9	= C <sub>2</sub> H <sub>5</sub> ·	19	= i-C <sub>5</sub> H <sub>12</sub>	29	= C <sub>2</sub> H <sub>2</sub> <sup>+</sup>
10	= C <sub>2</sub> H <sub>4</sub>	20	= CH <sub>5</sub> <sup>+</sup>	30	= C

Matlab Main Routine .....	101
Discharge phase "plasma_on.m" .....	103
Relaxation phase "plasma_off.m" .....	106

## Matlab Main Routine

```

*****
* assign global variables for main routine and subroutines *
* discharges = 2 x frequency x time *
* discharge and relaxation period in seconds *
* temperature in Kelvin *
*****
global Tg freq scale1 scale2 scale3 scale4 scale5;
discharges=1531;
freq=250;
ontime=.00000001;
offtime=1/freq*.5-ontime;
Tg=298;

*****
* assigned scalars for electron-impact reactions *
*****
scale1=1.63;
scale2=2.80;
scale3=0;
scale4=.45;
scale5=688;

tic
*****
* set initial values as micromole/cubic cm *
*****
xo=[ .00001 0 0 41 0 0 0 0 0 0 0 0 0 0 0 0 0 0 0 0 0 0 0
0]';
*****
* first discharge period *
*****
to=0;
tf=ontime;
[t,x]=ode23s('plasma_on',[to tf],xo);
tlast=t(length(t));
tsum=tlast;
xlast=x(length(t),:);
xsum=xlast;
*****
* loop for relaxation period and discharge period calculations*
*****
for nloops=1:discharges
    to=t(length(t));
    xo=x(length(t),:);
    tf=to+offtime;
    [t,x]=ode23s('plasma_off',[to tf],xo);
    tlast=t(length(t));
    tsum=cat(1,tsum,tlast);
    xlast=x(length(t),:);
    xsum=cat(1,xsum,xlast);
    to=t(length(t));
    xo=x(length(t),:);
    tf=to+ontime;
    [t,x]=ode23s('plasma_on',[to tf],xo);

```

```

        tlast=t(length(t));
        tsum=cat(1,tsum,tlast);
        xlast=x(length(t),:);
        xsum=cat(1,xsum,xlast);
    end
    *****
    * extended, final relaxation period for neutralization *
    *****
    to=t(length(t));
    xo=x(length(t),:);
    tf=to+4000000*offtime;
    [t,x]=ode23s('plasma_off',[to tf],xo);
    tlast=t(length(t));
    tsum=cat(1,tsum,tlast);
    xlast=x(length(t),:);
    xsum=cat(1,xsum,xlast);
    toc
    *****
    * end composition for each period are concatenated into an array *
    * results are written to a text file *
    *****
    save xsum.txt xsum -ASCII
    save tsum.txt tsum -ASCII

```



## Discharge phase "plasma\_on.m"

```

*****
* name the subroutine and assign global variables *
*****

function Xcomp = plasma_on ( t , X );
global Tg freq scale1 scale2 scale3 scale4 scale5;
Vmax=.41;

*****
* electron-impact reaction rates - micromole/cc/s *
*****

E1   =    5.01E+06    *    X(4)    *    X(1)    *scale1    ;
E2   =    3.98E+06    *    X(4)    *    X(1)    *scale1    ;
E3   =    7.94E+05    *    X(4)    *    X(1)    *scale1    ;
E4   =    3.98E+05    *    X(4)    *    X(1)    *scale1    ;
E5   =    1.58E+05    *    X(4)    *    X(1)    *scale1    ;
E6   =    1.00E+08    *    X(4)    *    X(1)    *scale1    ;
E7   =    2.00E+07    *    X(4)    *    X(1)    *scale1    ;
E8   =    7.94E+06    *    X(4)    *    X(1)    *scale1    ;
E9   =    7.47E+09    *    X(8)    *    X(1)    *scale4    ;
E10  =    5.01E+07    *    X(2)    *    X(1)    *scale1    ;
E11  =    2.51E+07    *    X(8)    *    X(1)    *scale2    ;
E12  =    2.00E+08    *    X(8)    *    X(1)    *scale2    ;
E13  =    6.31E+07    *    X(10)   *    X(1)    *scale3    ;
E14  =    1.26E+08    *    X(10)   *    X(1)    *scale3    ;
E15  =    1.00E+07    *    X(13)   *    X(1)    *scale5    ;
E16  =    1.00E+07    *    X(13)   *    X(1)    *scale5    ;

*****
* ionic reaction rates - micromole/cc/s *
*****

I1   =    2.40E+08    *    X(25)   *    X(4)          ;
I2   =    4.79E+08    *    X(25)   *    X(4)          ;
I3   =    8.51E+07    *    X(24)   *    X(4)          ;
I4   =    6.61E+08    *    X(24)   *    X(4)          ;
I5   =    3.89E+07    *    X(24)   *    X(4)          ;
I6   =    7.24E+08    *    X(24)   *    X(2)          ;
I7   =    5.01E+08    *    X(23)   *    X(4)          ;
I8   =    2.19E+08    *    X(23)   *    X(4)          ;
I9   =    9.55E+08    *    X(23)   *    X(2)          ;
I10  =    8.32E+07    *    X(23)   *    X(4)          ;
I11  =    2.40E+08    *    X(23)   *    X(4)          ;
I12  =    1.41E+08    *    X(23)   *    X(4)          ;
I13  =    7.24E+08    *    X(22)   *    X(4)          ;
I14  =    8.13E+07    *    X(22)   *    X(4)          ;
I15  =    8.91E+08    *    X(21)   *    X(4)          ;
I16  =    1.20E+07    *    X(21)   *    X(2)          ;

```

```

*****
* wall-neutralization reaction rates - micromole/cc/s *
*****

```

```

W1    =    4.27E+04    *    X(20) ;
W2    =    4.47E+04    *    X(21) ;
W3    =    4.68E+04    *    X(22) ;
W4    =    4.90E+04    *    X(23) ;
W5    =    5.01E+04    *    X(24) ;
W6    =    5.25E+04    *    X(25) ;
W7    =    3.39E+04    *    X(26) ;
W8    =    3.39E+04    *    X(27) ;
W9    =    3.47E+04    *    X(28) ;
W10   =    3.72E+04    *    X(29) ;

```

```

*****
* free-radical reaction rates - micromole/cc/s *
*****

```

```

G1    =    5.37E+12    *    X(3)  *    X(3)      ;
G2    =    1.01E+08    *    X(4)  *    X(6)      ;
G3    =    1.35E+02    *    X(4)  *    X(6)      ;
G4    =    1.58E-01    *    X(4)  *    X(6)      ;
G5    =    6.21E+07    *    X(4)  *    X(7)      ;
G6    =    6.18E-03    *    X(5)  *    X(2)      ;
G7    =    1.01E+09    *    X(5)  *    X(3)      ;
G8    =    6.12E+08    *    X(5)  *    X(5)      ;
G9    =    1.38E+00    *    X(5)  *    X(5)      ;
G10   =    4.27E+07    *    X(5)  *    X(6)      ;
G11   =    1.13E+06    *    X(5)  *    X(9)      ;
G12   =    1.62E+08    *    X(6)  *    X(3)      ;
G13   =    3.02E+03    *    X(6)  *    X(2)      ;
G14   =    4.27E+05    *    X(7)  *    X(2)      ;
G15   =    3.66E-03    *    X(8)  *    X(5)      ;
G16   =    4.05E+01    *    X(8)  *    X(3)      ;
G17   =    2.53E-03    *    X(10) *    X(3)      ;
G18   =    4.22E+07    *    X(10) *    X(3)      ;
G19   =    9.93E-04    *    X(10) *    X(5)      ;
G20   =    1.80E+06    *    X(9)  *    X(3)      ;
G21   =    3.98E+07    *    X(11) *    X(3)      ;
G22   =    7.45E+04    *    X(12) *    X(3)      ;
G23   =    2.83E+01    *    X(13) *    X(3)      ;
G24   =    5.94E+02    *    X(13) *    X(3)      ;
G25   =    6.14E-03    *    X(13) *    X(5)      ;
G26   =    5.67E-02    *    X(13) *    X(5)      ;
G27   =    2.18E-04    *    X(13) *    X(9)      ;
G28   =    1.62E-03    *    X(13) *    X(9)      ;
G29   =    2.66E+06    *    X(13) *    X(6)      ;
G30   =    1.14E+06    *    X(13) *    X(6)      ;
G31   =    1.50E+08    *    X(15) *    X(3)      ;
G32   =    3.10E+07    *    X(14) *    X(5)      ;
G33   =    2.82E+07    *    X(15) *    X(5)      ;
G34   =    1.99E+07    *    X(14) *    X(9)      *0;
G35   =    1.57E+07    *    X(15) *    X(9)      *0;
G36   =    3.37E+07    *    X(9)  *    X(5)      ;
G37   =    1.08E+07    *    X(9)  *    X(9)      *0;

```

```

G38 = 2.89E+06 * X(8) * X(6) ;
G39 = 9.27E-01 * X(10) * X(5) ;
G40 = 4.29E-03 * X(14) * X(2) ;
G41 = 3.78E-04 * X(15) * X(2) ;
G42 = 2.97E-04 * X(9) * X(2) ;
G43 = 9.78E-05 * X(11) * X(2) ;

```

```

*****
* reaction matrix of coupled ODEs (material balances)*
*****

```

```

Xcomp(1) = 0;
Xcomp(2) = +G1-G6-G13-G14+G16+G17+G20+G21+G23+G24+E3+E4
           +2*E5+E7+E8-E10+E11+E12+E14+W1-G40+I1+I3+I4-I6+I7-
           I9+2*I11+I12+I13-I16+G12-G41-G42-G43;
Xcomp(3) = -2*G1+G3+G5+G6-G7+G9+G10-G12+G13-G16-G17-G18-G20-G21
           -G22-G23-G24+G40+E2+E4+E6+E8+2*E10+I2+I3+I5+I6+I8+I9
           +I12+I16+E9+E15+E16+G41+G42+G43;
Xcomp(4) = -G2-G3-G4-G5+G7+G11+G15+G19+G25+G26+G6-E1-E2-E3-E4
           -E5-E6-E7-E8-I1-I2-I3-I4-I5-I7-I8-I10-I11-I12-I13
           -I14-I15+W2;
Xcomp(5) = +2*G4-G6-G7-2*G8-2*G9-G10-G11+G13+G14-G15-G19-G25
           -G26-G31-G32-G33-G36+E6+W3-G39+I10+I14+I15+W1;
Xcomp(6) = -G2-G3-G4-G10-G12-G13-G29-G30+E7+W4-G38;
Xcomp(7) = -G5+G12-G14+E8+W5;
Xcomp(8) = +G2+G8-G15-G16+G27+G28-E11-E12-G38-E9+G42;
Xcomp(9) = +G3+G9-G11+G15+G16+G18-G20-G27-G28-G34-G35-2*G37
           +W7+E9-G36-G42;
Xcomp(10) = +G10+G11-G17-G18-G19+G20+E12-E13-E14+W8-G39+G5+G43;
Xcomp(11) = +G17+G19-G21+G22+W9-G43;
Xcomp(12) = +G21-G22+E14+W10;
Xcomp(13) = -G23-G24-G25-G26-G27-G28-G29-G30+G31+G36+G38+G40-E15
           -E16+G41;
Xcomp(14) = +G23+G25+G27-G32-G34-G40+G39+E16;
Xcomp(15) = +G24+G26+G28-G31-G33-G35+E15-G41;
Xcomp(16) = +G32+G29+G37;
Xcomp(17) = +G33+G30;
Xcomp(18) = +G34;
Xcomp(19) = +G35;
Xcomp(20) = +I15+I16-W1;
Xcomp(21) = +E1+I14-I15-I16-W2;
Xcomp(22) = +E2+I9+I10-I13-I14-W3;
Xcomp(23) = +E3-I7-I8-I9-I10-I11-I12-W4;
Xcomp(24) = +E4-I3-I4-I5-I6-W5;
Xcomp(25) = +E5-I1-I2-W6;
Xcomp(26) = +I8+I13-W7;
Xcomp(27) = +E11+E13+I5+I7-W8;
Xcomp(28) = +I2+I4+I12-W9;
Xcomp(29) = +I1+I3+I11-W10;
Xcomp(30) = +W6;
Xcomp    = Xcomp';

```

## Relaxation phase "plasma\_off.m"

```

*****
* name the subroutine and assign global variables *
*****

function Xcomp = plasma_off ( t , X );
global Tg freq;
Vmax=.41;

*****
* electron-impact reaction rates are zero - micromole/cc/s *
*****

E1=0;
E2=0;
E3=0;
E4=0;
E5=0;
E6=0;
E7=0;
E8=0;
E9=0;
E10=0;
E11=0;
E12=0;
E13=0;
E14=0;
E15=0;
E16=0;

*****
* ionic reaction rates - micromole/cc/s *
*****

I1   =    2.40E+08    *    X(25) *    X(4)    ;
I2   =    4.79E+08    *    X(25) *    X(4)    ;
I3   =    8.51E+07    *    X(24) *    X(4)    ;
I4   =    6.61E+08    *    X(24) *    X(4)    ;
I5   =    3.89E+07    *    X(24) *    X(4)    ;
I6   =    7.24E+08    *    X(24) *    X(2)    ;
I7   =    5.01E+08    *    X(23) *    X(4)    ;
I8   =    2.19E+08    *    X(23) *    X(4)    ;
I9   =    9.55E+08    *    X(23) *    X(2)    ;
I10  =    8.32E+07    *    X(23) *    X(4)    ;
I11  =    2.40E+08    *    X(23) *    X(4)    ;
I12  =    1.41E+08    *    X(23) *    X(4)    ;
I13  =    7.24E+08    *    X(22) *    X(4)    ;
I14  =    8.13E+07    *    X(22) *    X(4)    ;
I15  =    8.91E+08    *    X(21) *    X(4)    ;
I16  =    1.20E+07    *    X(21) *    X(2)    ;

```

```
*****
* wall-neutralization reaction rates - micromole/cc/s *
*****
```

```
W1    =    4.27E-02    *    X(20) ;
W2    =    4.47E-02    *    X(21) ;
W3    =    4.68E-02    *    X(22) ;
W4    =    4.90E-02    *    X(23) ;
W5    =    5.01E-02    *    X(24) ;
W6    =    5.25E-02    *    X(25) ;
W7    =    3.39E-02    *    X(26) ;
W8    =    3.39E-02    *    X(27) ;
W9    =    3.47E-02    *    X(28) ;
W10   =    3.72E-02    *    X(29) ;
```

```
*****
* free-radical reaction rates - micromole/cc/s *
*****
```

```
G1    =    5.37E+12    *    X(3)  *    X(3)      ;
G2    =    1.01E+08    *    X(4)  *    X(6)      ;
G3    =    1.35E+02    *    X(4)  *    X(6)      ;
G4    =    1.58E-01    *    X(4)  *    X(6)      ;
G5    =    6.21E+07    *    X(4)  *    X(7)      ;
G6    =    6.18E-03    *    X(5)  *    X(2)      ;
G7    =    1.01E+09    *    X(5)  *    X(3)      ;
G8    =    6.12E+08    *    X(5)  *    X(5)      ;
G9    =    1.38E+00    *    X(5)  *    X(5)      ;
G10   =    4.27E+07    *    X(5)  *    X(6)      ;
G11   =    1.13E+06    *    X(5)  *    X(9)      ;
G12   =    1.62E+08    *    X(6)  *    X(3)      ;
G13   =    3.02E+03    *    X(6)  *    X(2)      ;
G14   =    4.27E+05    *    X(7)  *    X(2)      ;
G15   =    3.66E-03    *    X(8)  *    X(5)      ;
G16   =    4.05E+01    *    X(8)  *    X(3)      ;
G17   =    2.53E-03    *    X(10) *    X(3)      ;
G18   =    4.22E+07    *    X(10) *    X(3)      ;
G19   =    9.93E-04    *    X(10) *    X(5)      ;
G20   =    1.80E+06    *    X(9)  *    X(3)      ;
G21   =    3.98E+07    *    X(11) *    X(3)      ;
G22   =    7.45E+04    *    X(12) *    X(3)      ;
G23   =    2.83E+01    *    X(13) *    X(3)      ;
G24   =    5.94E+02    *    X(13) *    X(3)      ;
G25   =    6.14E-03    *    X(13) *    X(5)      ;
G26   =    5.67E-02    *    X(13) *    X(5)      ;
G27   =    2.18E-04    *    X(13) *    X(9)      ;
G28   =    1.62E-03    *    X(13) *    X(9)      ;
G29   =    2.66E+06    *    X(13) *    X(6)      ;
G30   =    1.14E+06    *    X(13) *    X(6)      ;
G31   =    1.50E+08    *    X(15) *    X(3)      ;
G32   =    3.10E+07    *    X(14) *    X(5)      ;
G33   =    2.82E+07    *    X(15) *    X(5)      ;
G34   =    1.99E+07    *    X(14) *    X(9)      *0;
G35   =    1.57E+07    *    X(15) *    X(9)      *0;
G36   =    3.37E+07    *    X(9)  *    X(5)      ;
G37   =    1.08E+07    *    X(9)  *    X(9)      *0;
```

```

G38 = 2.89E+06 * X(8) * X(6) ;
G39 = 9.27E-01 * X(10) * X(5) ;
G40 = 4.29E-03 * X(14) * X(2) ;
G41 = 3.78E-04 * X(15) * X(2) ;
G42 = 2.97E-04 * X(9) * X(2) ;
G43 = 9.78E-05 * X(11) * X(2) ;

```

```

*****
* reaction matrix of coupled ODEs (material balances)*
*****

```

```

Xcomp(1) = 0;
Xcomp(2) = +G1-G6-G13-G14+G16+G17+G20+G21+G23+G24+E3+E4+2*E5
           +E7+E8-E10+E11+E12+E14+W1-G40+I1+I3+I4-I6+I7-I9+2*I11
           +I12+I13-I16+G12-G41-G42-G43;
Xcomp(3) = -2*G1+G3+G5+G6-G7+G9+G10-G12+G13-G16-G17-G18-G20-G21
           -G22-G23-G24+G40+E2+E4+E6+E8+2*E10+I2+I3+I5+I6+I8
           +I9+I12+I16+E9+E15+E16+G41+G42+G43;
Xcomp(4) = -G2-G3-G4-G5+G7+G11+G15+G19+G25+G26+G6-E1-E2-E3-E4
           -E5-E6-E7-E8-I1-I2-I3-I4-I5-I7-I8-I10-I11-I12-I13
           -I14-I15+W2;
Xcomp(5) = +2*G4-G6-G7-2*G8-2*G9-G10-G11+G13+G14-G15-G19-G25
           -G26-G31-G32-G33-G36+E6+W3-G39+I10+I14+I15+W1;
Xcomp(6) = -G2-G3-G4-G10-G12-G13-G29-G30+E7+W4-G38;
Xcomp(7) = -G5+G12-G14+E8+W5;
Xcomp(8) = +G2+G8-G15-G16+G27+G28-E11-E12-G38-E9+G42;
Xcomp(9) = +G3+G9-G11+G15+G16+G18-G20-G27-G28-G34-G35-2*G37
           +W7+E9-G36-G42;
Xcomp(10) = +G10+G11-G17-G18-G19+G20+E12-E13-E14+W8-G39+G5+G43;
Xcomp(11) = +G17+G19-G21+G22+W9-G43;
Xcomp(12) = +G21-G22+E14+W10;
Xcomp(13) = -G23-G24-G25-G26-G27-G28-G29-G30+G31+G36+G38+G40-E15
           -E16+G41;
Xcomp(14) = +G23+G25+G27-G32-G34-G40+G39+E16;
Xcomp(15) = +G24+G26+G28-G31-G33-G35+E15-G41;
Xcomp(16) = +G32+G29+G37;
Xcomp(17) = +G33+G30;
Xcomp(18) = +G34;
Xcomp(19) = +G35;
Xcomp(20) = +I15+I16-W1;
Xcomp(21) = +E1+I14-I15-I16-W2;
Xcomp(22) = +E2+I9+I10-I13-I14-W3;
Xcomp(23) = +E3-I7-I8-I9-I10-I11-I12-W4;
Xcomp(24) = +E4-I3-I4-I5-I6-W5;
Xcomp(25) = +E5-I1-I2-W6;
Xcomp(26) = +I8+I13-W7;
Xcomp(27) = +E11+E13+I5+I7-W8;
Xcomp(28) = +I2+I4+I12-W9;
Xcomp(29) = +I1+I3+I11-W10;
Xcomp(30) = +W6;
Xcomp    = Xcomp';

```

## APPENDIX D

### Reactions Used in the Methane Plasma Model.

The reactions are divided into four sections: electron impact reactions, ionic reactions, wall reactions, and free-radical reactions. The two main sources for these reactions and rate constants are compilations of other sources.

Table D-1: Electron Impact Reactions.....	110
Table D-2: Ionic Reactions.....	110
Table D-3: Wall Neutralization Reactions.....	110
Table D-4: Free-Radical Reactions.....	111

Table D-1: Electron Impact Reactions

ID#	Reaction	Rate constant [k] (cm <sup>3</sup> /μmol/s)	Ref.
E1	$\text{CH}_4 + e \rightarrow \text{CH}_4^+ + 2e$	5.01E+06	[2]
E2	$\text{CH}_4 + e \rightarrow \text{CH}_3^+ + \text{H} + 2e$	3.98E+06	[2]
E3	$\text{CH}_4 + e \rightarrow \text{CH}_2^+ + \text{H}_2 + 2e$	7.94E+05	[2]
E4	$\text{CH}_4 + e \rightarrow \text{CH}^+ + \text{H}_2 + \text{H} + 2e$	3.98E+05	[2]
E5	$\text{CH}_4 + e \rightarrow \text{C}^+ + 2\text{H}_2 + 2e$	1.58E+05	[2]
E6	$\text{CH}_4 + e \rightarrow \text{CH}_3\cdot + \text{H} + e$	1.00E+08	[2]
E7	$\text{CH}_4 + e \rightarrow \text{CH}_2\cdot + \text{H}_2 + e$	2.00E+07	[2]
E8	$\text{CH}_4 + e \rightarrow \text{CH}\cdot + \text{H}_2 + \text{H} + e$	7.94E+06	[2]
E9	$\text{C}_2\text{H}_6 + e \rightarrow \text{C}_2\text{H}_5\cdot + \text{H} + e$	7.47E+09	[41]
E10	$\text{H}_2 + e \rightarrow 2\text{H} + e$	5.01E+07	[2]
E11	$\text{C}_2\text{H}_6 + e \rightarrow \text{C}_2\text{H}_4^+ + \text{H}_2 + 2e$	2.51E+07	[2]
E12	$\text{C}_2\text{H}_6 + e \rightarrow \text{C}_2\text{H}_4 + \text{H}_2 + e$	2.00E+08	[2]
E13	$\text{C}_2\text{H}_4 + e \rightarrow \text{C}_2\text{H}_4^+ + 2e$	6.31E+07	[2]
E14	$\text{C}_2\text{H}_4 + e \rightarrow \text{C}_2\text{H}_2 + \text{H}_2 + e$	1.26E+08	[2]
E15	$\text{C}_3\text{H}_8 + e \rightarrow i\text{-C}_3\text{H}_7\cdot + \text{H} + e$	1.00E+08	[2]
E16	$\text{C}_3\text{H}_8 + e \rightarrow n\text{-C}_3\text{H}_7\cdot + \text{H} + e$	1.00E+08	[2]

Table D-2: Ionic Reactions

I1	$\text{C}^+ + \text{CH}_4 \rightarrow \text{C}_2\text{H}_2^+ + \text{H}_2$	2.40E+08	1
I2	$\text{C}^+ + \text{CH}_4 \rightarrow \text{C}_2\text{H}_3^+ + \text{H}$	4.79E+08	1
I3	$\text{CH}^+ + \text{CH}_4 \rightarrow \text{C}_2\text{H}_2^+ + \text{H}_2 + \text{H}$	8.51E+07	1
I4	$\text{CH}^+ + \text{CH}_4 \rightarrow \text{C}_2\text{H}_3^+ + \text{H}_2$	6.61E+08	1
I5	$\text{CH}^+ + \text{CH}_4 \rightarrow \text{C}_2\text{H}_4^+ + \text{H}$	3.89E+07	1
I6	$\text{CH}^+ + \text{H}_2 \rightarrow \text{CH}_2^+ + \text{H}$	7.24E+08	1
I7	$\text{CH}_2^+ + \text{CH}_4 \rightarrow \text{C}_2\text{H}_4^+ + \text{H}_2$	5.01E+08	1
I8	$\text{CH}_2^+ + \text{CH}_4 \rightarrow \text{C}_2\text{H}_5^+ + \text{H}$	2.19E+08	1
I9	$\text{CH}_2^+ + \text{H}_2 \rightarrow \text{CH}_3^+ + \text{H}$	9.55E+08	1
I10	$\text{CH}_2^+ + \text{CH}_4 \rightarrow \text{CH}_3^+ + \text{CH}_3$	8.32E+07	1
I11	$\text{CH}_2^+ + \text{CH}_4 \rightarrow \text{C}_2\text{H}_2^+ + 2\text{H}_2$	2.40E+08	1
I12	$\text{CH}_2^+ + \text{CH}_4 \rightarrow \text{C}_2\text{H}_3^+ + \text{H}_2 + \text{H}$	1.41E+08	1
I13	$\text{CH}_3^+ + \text{CH}_4 \rightarrow \text{C}_2\text{H}_5^+ + \text{H}_2$	7.24E+08	1
I14	$\text{CH}_3^+ + \text{CH}_4 \rightarrow \text{CH}_4^+ + \text{CH}_3$	8.13E+07	1
I15	$\text{CH}_4^+ + \text{CH}_4 \rightarrow \text{CH}_5^+ + \text{CH}_3$	8.91E+08	1
I16	$\text{CH}_4^+ + \text{H}_2 \rightarrow \text{CH}_5^+ + \text{H}$	1.20E+07	1

Table D-3: Wall Neutralization Reactions

W1	$\text{CH}_5^+ \rightarrow \text{CH}_3\cdot + \text{H}_2$	4.27E+04	[2]
W2	$\text{CH}_4^+ \rightarrow \text{CH}_4$	4.47E+04	[2]
W3	$\text{CH}_3^+ \rightarrow \text{CH}_3\cdot$	4.68E+04	[2]
W4	$\text{CH}_2^+ \rightarrow \text{CH}_2\cdot$	4.90E+04	[2]
W5	$\text{CH}^+ \rightarrow \text{CH}\cdot$	5.01E+04	[2]
W6	$\text{C}^+ \rightarrow \text{C}$	5.25E+04	[2]
W7	$\text{C}_2\text{H}_5^+ \rightarrow \text{C}_2\text{H}_5\cdot$	3.39E+04	[2]
W8	$\text{C}_2\text{H}_4^+ \rightarrow \text{C}_2\text{H}_4$	3.39E+04	[2]
W9	$\text{C}_2\text{H}_3^+ \rightarrow \text{C}_2\text{H}_3\cdot$	3.47E+04	[2]
W10	$\text{C}_2\text{H}_2^+ \rightarrow \text{C}_2\text{H}_2$	3.72E+04	[2]



Table D-4: Free-Radical Reactions

ID#	Reaction	Rate constant [k] (cm <sup>3</sup> /μmol/s)	Ref.
G1	2H + M → H <sub>2</sub>	5.37E+12	[2]
G2	CH <sub>4</sub> + CH <sub>2</sub> · → C <sub>2</sub> H <sub>6</sub>	1.01E+08	[2]
G3	CH <sub>4</sub> + CH <sub>2</sub> · → C <sub>2</sub> H <sub>5</sub> · + H	1.35E+02	[2]
G4	CH <sub>4</sub> + CH <sub>2</sub> · → 2CH <sub>3</sub> ·	1.58E-01	[2]
G5	CH <sub>4</sub> + CH· → C <sub>2</sub> H <sub>4</sub> + H	6.21E+07	[2]
G6	CH <sub>3</sub> · + H <sub>2</sub> → CH <sub>4</sub> + H	4.18E-03	[2]
G7	CH <sub>3</sub> · + H → CH <sub>4</sub>	1.01E+09	[2]
G8	CH <sub>3</sub> · + CH <sub>3</sub> · → C <sub>2</sub> H <sub>6</sub>	6.12E+08	[2]
G9	CH <sub>3</sub> · + CH <sub>3</sub> · → C <sub>2</sub> H <sub>5</sub> · + H	1.38E+00	[2]
G10	CH <sub>3</sub> · + CH <sub>2</sub> · → C <sub>2</sub> H <sub>4</sub> + H	4.27E+07	[2]
G11	CH <sub>3</sub> · + C <sub>2</sub> H <sub>5</sub> · → C <sub>2</sub> H <sub>4</sub> + CH <sub>4</sub>	1.13E+06	[2]
G12	CH <sub>2</sub> · + H → CH· + H <sub>2</sub>	1.62E+08	[2]
G13	CH <sub>2</sub> · + H <sub>2</sub> → CH <sub>3</sub> · + H	3.02E+03	[2]
G14	CH· + H <sub>2</sub> → CH <sub>3</sub> ·	4.27E+05	[2]
G15	C <sub>2</sub> H <sub>6</sub> + CH <sub>3</sub> · → CH <sub>4</sub> + C <sub>2</sub> H <sub>5</sub> ·	3.66E-03	[2]
G16	C <sub>2</sub> H <sub>6</sub> + H → C <sub>2</sub> H <sub>5</sub> · + H <sub>2</sub>	4.05E+01	[2]
G17	C <sub>2</sub> H <sub>4</sub> + H → C <sub>2</sub> H <sub>3</sub> · + H <sub>2</sub>	2.53E-03	[2]
G18	C <sub>2</sub> H <sub>4</sub> + H → C <sub>2</sub> H <sub>5</sub> ·	4.22E+07	[2]
G19	C <sub>2</sub> H <sub>4</sub> + CH <sub>3</sub> · → C <sub>2</sub> H <sub>3</sub> · + CH <sub>4</sub>	9.93E-04	[2]
G20	C <sub>2</sub> H <sub>5</sub> · + H → C <sub>2</sub> H <sub>4</sub> + H <sub>2</sub>	1.80E+06	[2]
G21	C <sub>2</sub> H <sub>3</sub> · + H → C <sub>2</sub> H <sub>2</sub> + H <sub>2</sub>	3.98E+07	[2]
G22	C <sub>2</sub> H <sub>2</sub> + H → C <sub>2</sub> H <sub>3</sub> ·	7.45E+04	[2]
G23	C <sub>3</sub> H <sub>8</sub> + H → H <sub>2</sub> + n-C <sub>3</sub> H <sub>7</sub> ·	2.83E+01	[42]
G24	C <sub>3</sub> H <sub>8</sub> + H → H <sub>2</sub> + i-C <sub>3</sub> H <sub>7</sub> ·	5.94E+02	[42]
G25	C <sub>3</sub> H <sub>8</sub> + CH <sub>3</sub> · → CH <sub>4</sub> + n-C <sub>3</sub> H <sub>7</sub> ·	6.14E-03	[42]
G26	C <sub>3</sub> H <sub>8</sub> + CH <sub>3</sub> · → CH <sub>4</sub> + i-C <sub>3</sub> H <sub>7</sub> ·	5.67E-02	[42]
G27	C <sub>3</sub> H <sub>8</sub> + C <sub>2</sub> H <sub>5</sub> · → C <sub>2</sub> H <sub>6</sub> + n-C <sub>3</sub> H <sub>7</sub> ·	2.18E-04	[42]
G28	C <sub>3</sub> H <sub>8</sub> + C <sub>2</sub> H <sub>5</sub> · → C <sub>2</sub> H <sub>6</sub> + i-C <sub>3</sub> H <sub>7</sub> ·	1.62E-03	[42]
G29	C <sub>3</sub> H <sub>8</sub> + CH <sub>2</sub> · → n-C <sub>4</sub> H <sub>10</sub>	2.66E+06	[42]
G30	C <sub>3</sub> H <sub>8</sub> + CH <sub>2</sub> · → i-C <sub>4</sub> H <sub>10</sub>	1.14E+06	[42]
G31	i-C <sub>3</sub> H <sub>7</sub> · + CH <sub>3</sub> · → C <sub>3</sub> H <sub>8</sub>	1.50E+08	[42]
G32	n-C <sub>3</sub> H <sub>7</sub> · + CH <sub>3</sub> · → n-C <sub>4</sub> H <sub>10</sub>	3.10E+07	[42]
G33	i-C <sub>3</sub> H <sub>7</sub> · + CH <sub>3</sub> · → i-C <sub>4</sub> H <sub>10</sub>	2.82E+07	[42]
G34	n-C <sub>3</sub> H <sub>7</sub> · + C <sub>2</sub> H <sub>5</sub> · → n-C <sub>5</sub> H <sub>12</sub>	1.99E+07	[42]
G35	i-C <sub>3</sub> H <sub>7</sub> · + C <sub>2</sub> H <sub>5</sub> · → i-C <sub>5</sub> H <sub>12</sub>	1.57E+07	[42]
G36	C <sub>2</sub> H <sub>5</sub> · + CH <sub>3</sub> · → C <sub>3</sub> H <sub>8</sub>	3.37E+07	[42]
G37	C <sub>2</sub> H <sub>5</sub> · + C <sub>2</sub> H <sub>5</sub> · → n-C <sub>4</sub> H <sub>10</sub>	1.08E+07	[42]
G38	C <sub>2</sub> H <sub>6</sub> + CH <sub>2</sub> · → C <sub>3</sub> H <sub>8</sub>	2.89E+06	[42]
G39	C <sub>2</sub> H <sub>4</sub> + CH <sub>3</sub> · → n-C <sub>3</sub> H <sub>7</sub> ·	9.27E-01	[42]
G40	n-C <sub>3</sub> H <sub>7</sub> · + H <sub>2</sub> → C <sub>3</sub> H <sub>8</sub> + H	4.29E-03	[42]
G41	i-C <sub>3</sub> H <sub>7</sub> · + H <sub>2</sub> → C <sub>3</sub> H <sub>8</sub> + H	3.78E-04	[42]
G42	C <sub>2</sub> H <sub>5</sub> · + H <sub>2</sub> → C <sub>2</sub> H <sub>6</sub> + H	2.97E-04	[42]
G43	C <sub>2</sub> H <sub>3</sub> · + H <sub>2</sub> → C <sub>2</sub> H <sub>4</sub> + H	9.78E-05	[42]

## APPENDIX E

### Example Bisection Subroutine for Scaling Impact Rates

This is an example subroutine that shows how bisection was used to scale the electron impact rates. The first section initializes the program variables. The second section defines the target composition (carbon fraction) of the chemical species corresponding to the electron impact rate being scaled. A call must then be made to the main routine (Appendix C) to calculate the final composition of the target compound at the upper limit of the rate being scaled. A second call is then made to the main routine to calculate the final composition of the target compound at the lower limit of the rate being scaled. The subroutine then uses a bisection method to narrow down the range of the scaled rate until the precision requirements have been met.

```

*****
* example bisection subroutine for scaling electron-impact rates *
* concentrations are carbon fractions                               *
*****

global Tg freq scale1 scale2 scale3 scale4 scale5;
discharges=1531;
freq=250;
ontime=.00000001;
offtime=1/freq*.5-ontime;
Tg=298;
scale1=1.63;
scale2=2.8;
scale3=0;
scale4=.45;
scale5=688;

*****
* set target composition and precision *
*****

target=.97;
xacc=.0001;

scale1=1000;
scale1a=scale1;

*****
* call main routine                                               *
* calculate composition of target compound (x4) at upper limit    *
* compare to target                                              *
*****

f=x4-target

scale1=.1;
scale1b=scale1;

*****
* call main routine                                               *
* calculate composition of target compound (x4) at lower limit    *
* compare to target                                              *
*****

fmid=x4-target
if f <= 0.0
  rsbis=scale1a
  dx=scale1b-scale1a
else
  rsbis=scale1b
  dx=scale1a-scale1b
end
biloops=0
while biloops < 40
  biloops=biloops+1
  dx=dx*.5

```

```

xmid=rsbis+dx

scalel=xmid;
scalelb=scalel;

*****
* call main routine *
* calculate composition of target compound (x4) at midpoint *
* compare to target *
*****

    fmid=x4-target
    if fmid <=0.0
        rsbis=xmid
    end
    absfmid=abs(fmid);
    if absfmid < xacc
        biloops=40
    end
end

*****
* save results *
*****

```

## APPENDIX F

### Sensitivity Analysis: Electron Density, Discharge Period, Scale1, Scale2, Scale 4, and Scale5

This appendix contains graphical representations of the sensitivity data for each hydrocarbon fraction of the methane plasma model. Each variable was varied by  $\pm 50\%$ ,  $\pm 10\%$ , and  $\pm 1\%$  from the values used in the model. For this sensitivity analysis the model frequency was 250 Hz and the residence time was 3.1 seconds.

Figure F-1: Methane Fraction Sensitivity to Electron Density .....	116
Figure F-2: Ethane Fraction Sensitivity to Electron Density .....	116
Figure F-3: Ethylene + Acetylene Fraction Sensitivity to Electron Density .....	117
Figure F-4: Propane + Propylene Fraction Sensitivity to Electron Density .....	117
Figure F-5: Heavy Hydrocarbon Fraction Sensitivity to Electron Density .....	118
Figure F-6: Methane Fraction Sensitivity to Discharge Period .....	118
Figure F-7: Ethane Fraction Sensitivity to Discharge Period .....	119
Figure F-8: Ethylene + Acetylene Fraction Sensitivity to Discharge Period .....	119
Figure F-9: Propane + Propylene Fraction Sensitivity to Discharge Period.....	120
Figure F-10: Heavy Hydrocarbon Fraction Sensitivity to Discharge Period.....	120
Figure F-11: Methane Fraction Sensitivity to Scale1 .....	121
Figure F-12: Ethane Fraction Sensitivity to Scale1 .....	121
Figure F-13: Ethylene + Acetylene Fraction Sensitivity to Scale1 .....	122
Figure F-14: Propane + Propylene Fraction Sensitivity to Scale1.....	122
Figure F-15: Heavy Hydrocarbon Fraction Sensitivity to Scale1 .....	123
Figure F-16: Methane Fraction Sensitivity to Scale2 .....	123
Figure F-17: Ethane Fraction Sensitivity to Scale2 .....	124
Figure F-18: Ethylene + Acetylene Fraction Sensitivity to Scale2 .....	124
Figure F-19: Propane + Propylene Fraction Sensitivity to Scale2.....	125
Figure F-20: Heavy Hydrocarbon Fraction Sensitivity to Scale2.....	125
Figure F-21: Methane Fraction Sensitivity to Scale4 .....	126
Figure F-22: Ethane Fraction Sensitivity to Scale4 .....	126
Figure F-23: Ethylene + Acetylene Fraction Sensitivity to Scale4 .....	127
Figure F-24: Propane + Propylene Fraction Sensitivity to Scale4.....	127
Figure F-25: Heavy Hydrocarbon Fraction Sensitivity to Scale4.....	128
Figure F-26: Methane Fraction Sensitivity to Scale5 .....	128
Figure F-27: Ethane Fraction Sensitivity to Scale5 .....	129
Figure F-28: Ethylene + Acetylene Fraction Sensitivity to Scale5 .....	129
Figure F-29: Propane + Propylene Fraction Sensitivity to Scale5.....	130
Figure F-30: Heavy Hydrocarbon Fraction Sensitivity to Scale5.....	130
TABLE F-I: Summary of Hydrocarbon Fraction Sensitivities.....	132

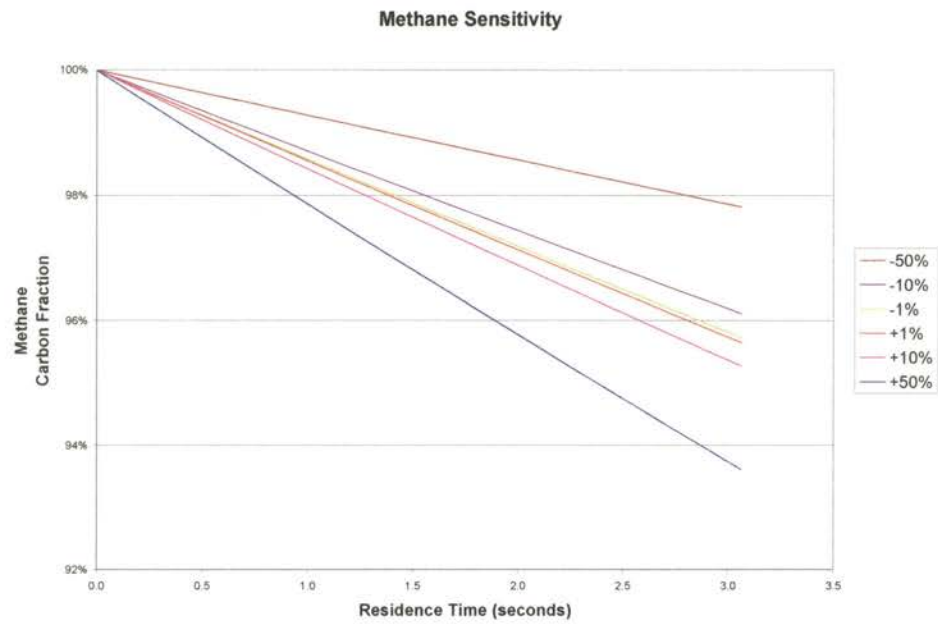


Figure F-1: Methane Fraction Sensitivity to Electron Density

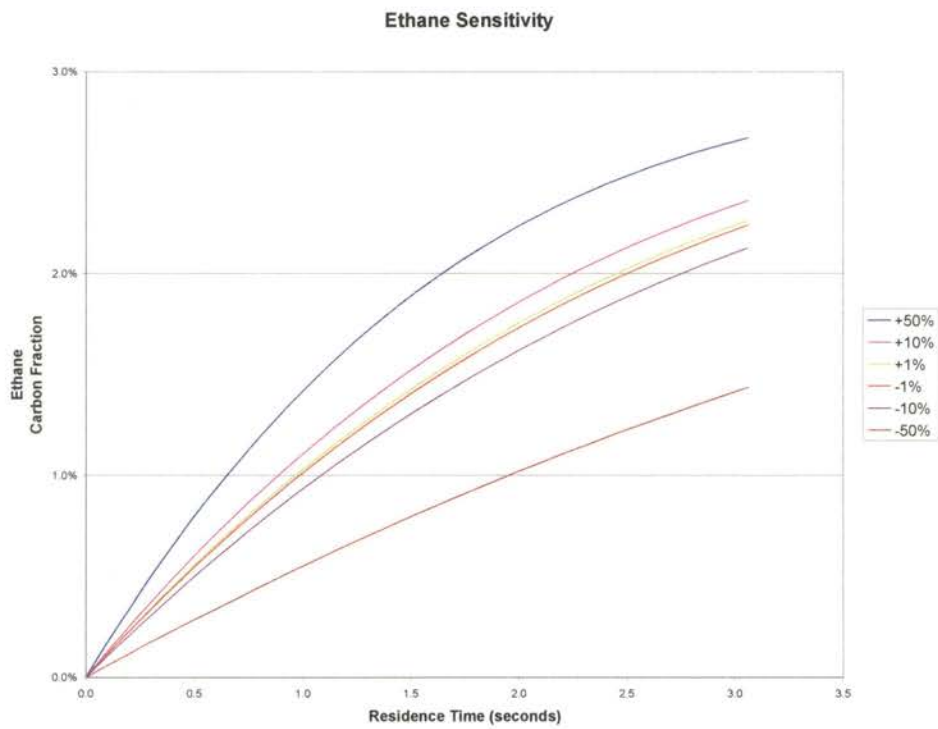


Figure F-2: Ethane Fraction Sensitivity to Electron Density

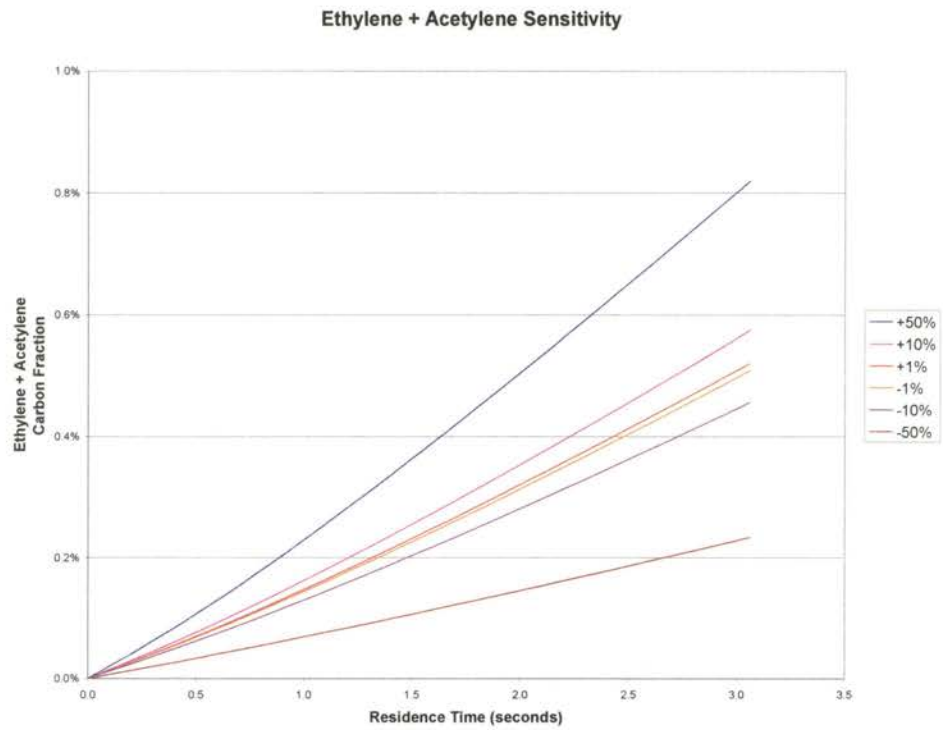


Figure F-3: Ethylene + Acetylene Fraction Sensitivity to Electron Density

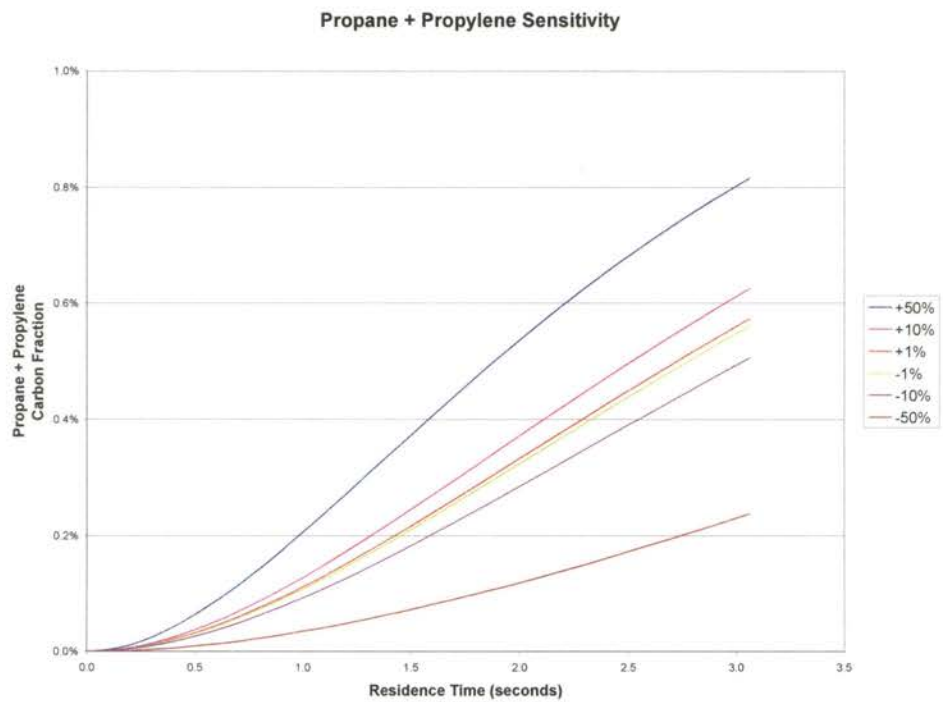


Figure F-4: Propane + Propylene Fraction Sensitivity to Electron Density

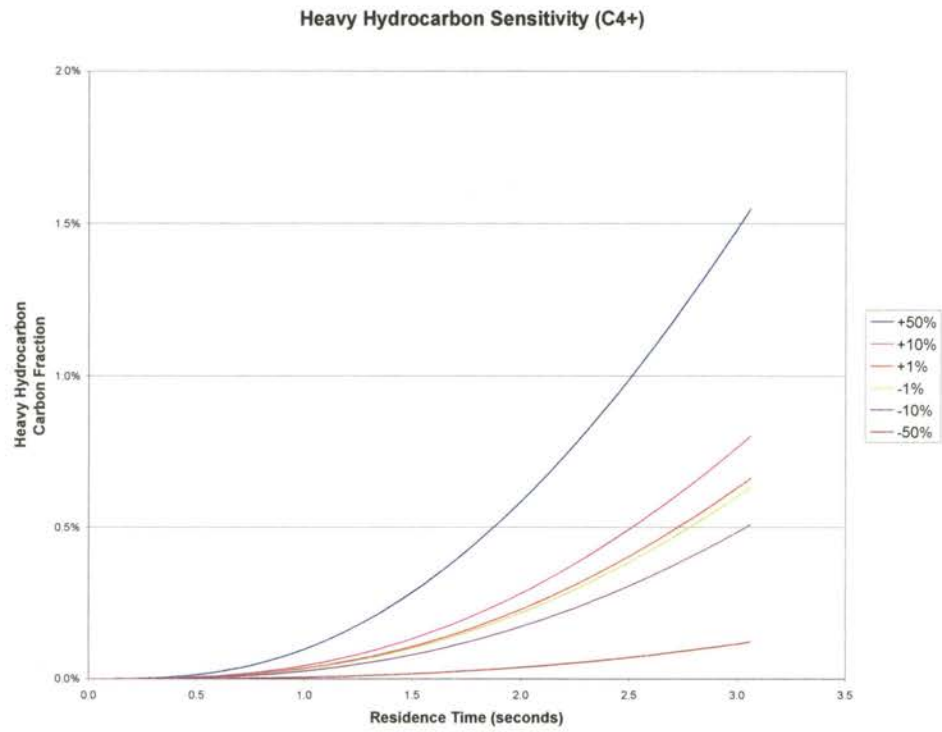


Figure F-5: Heavy Hydrocarbon Fraction Sensitivity to Electron Density

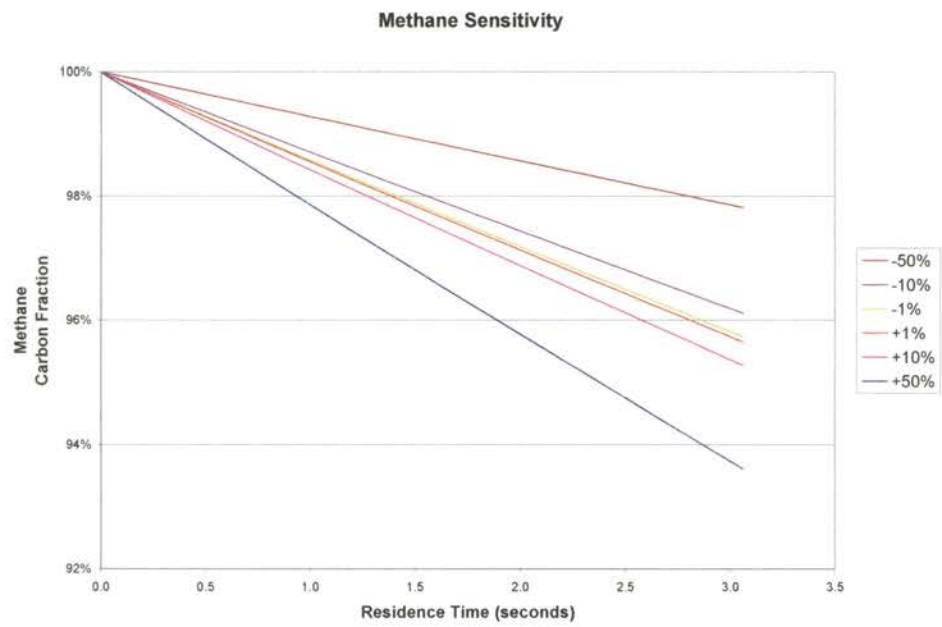


Figure F-6: Methane Fraction Sensitivity to Discharge Period



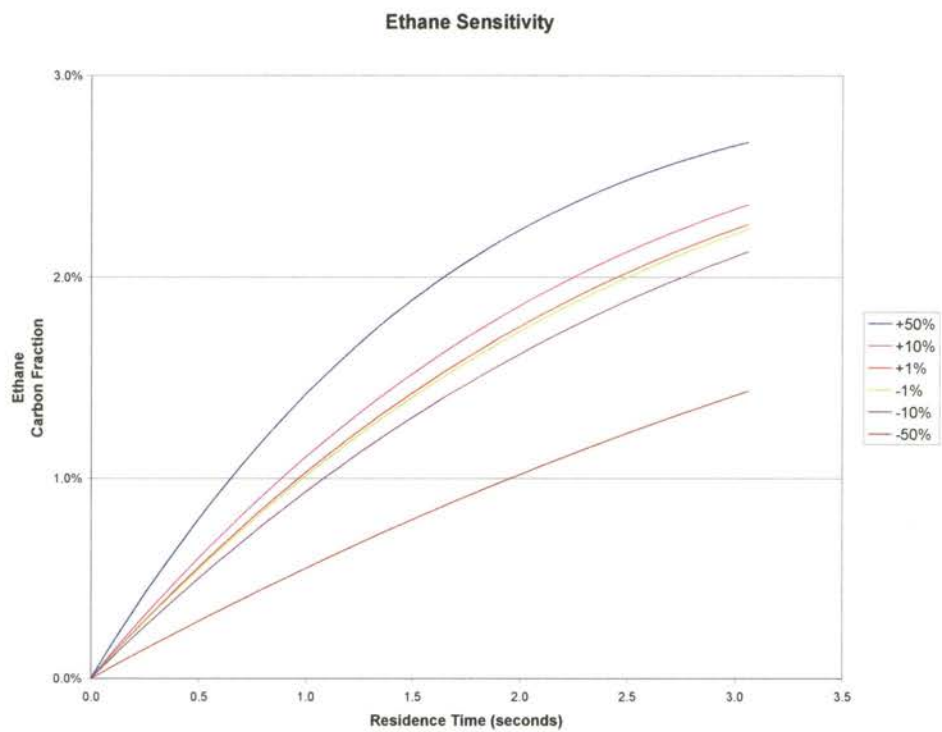


Figure F-7: Ethane Fraction Sensitivity to Discharge Period

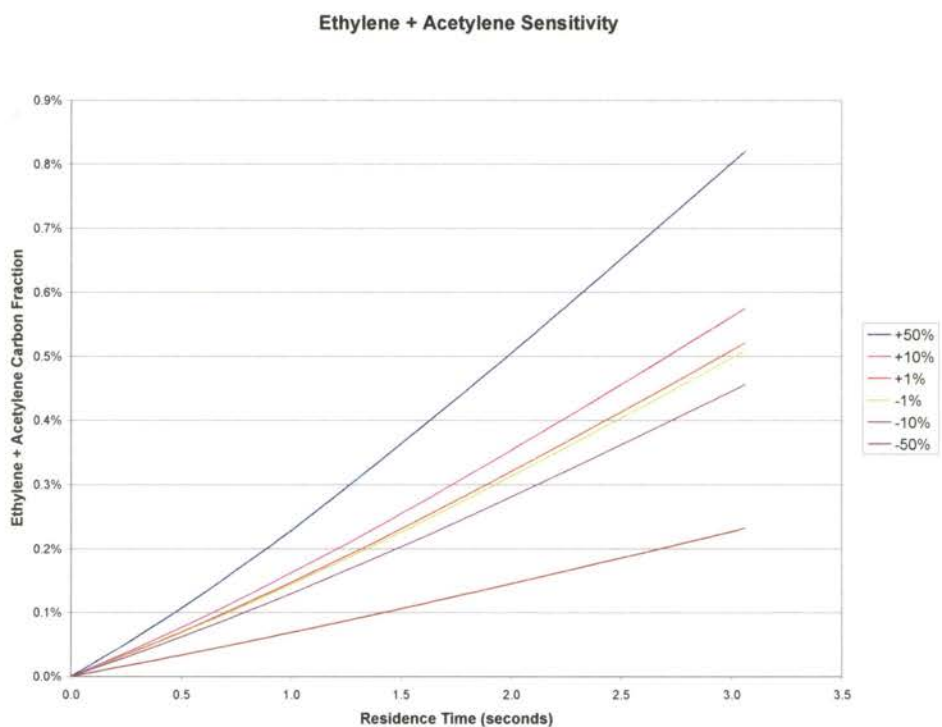


Figure F-8: Ethylene + Acetylene Fraction Sensitivity to Discharge Period

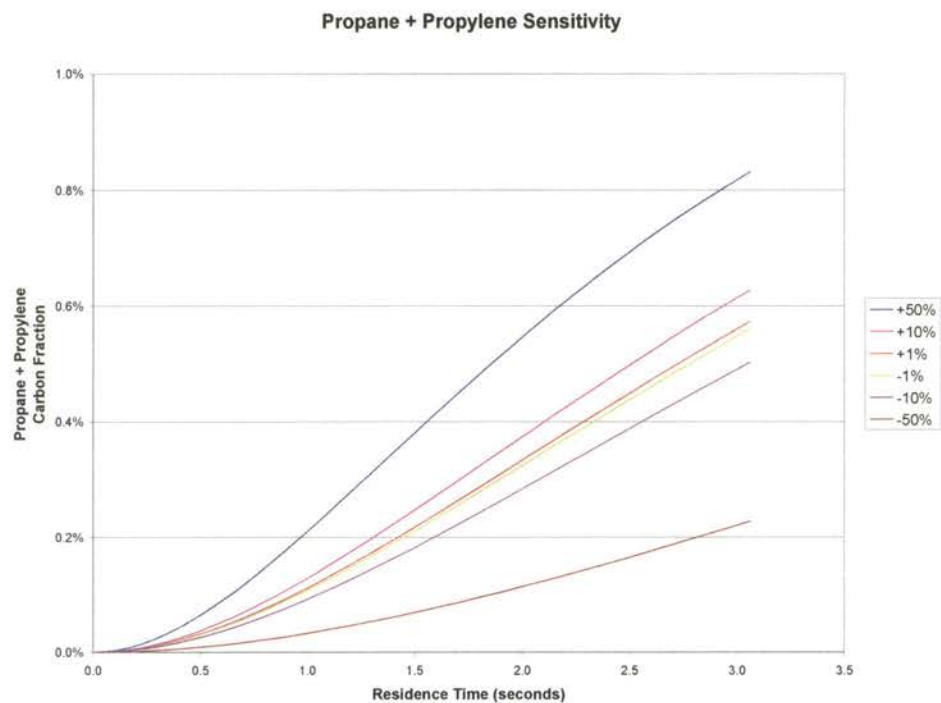


Figure F-9: Propane + Propylene Fraction Sensitivity to Discharge Period

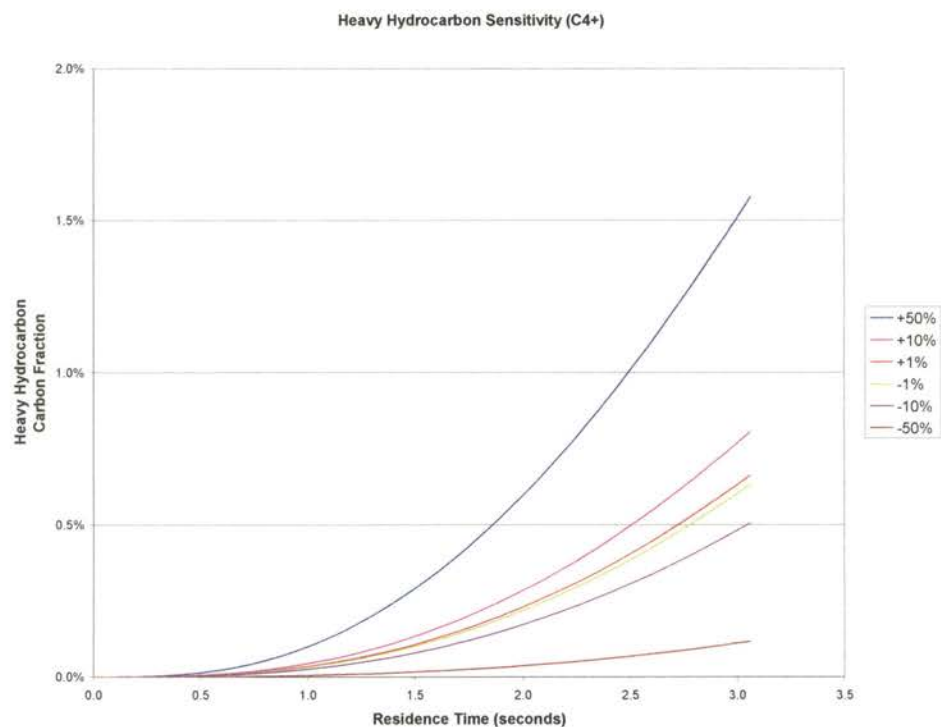


Figure F-10: Heavy Hydrocarbon Fraction Sensitivity to Discharge Period

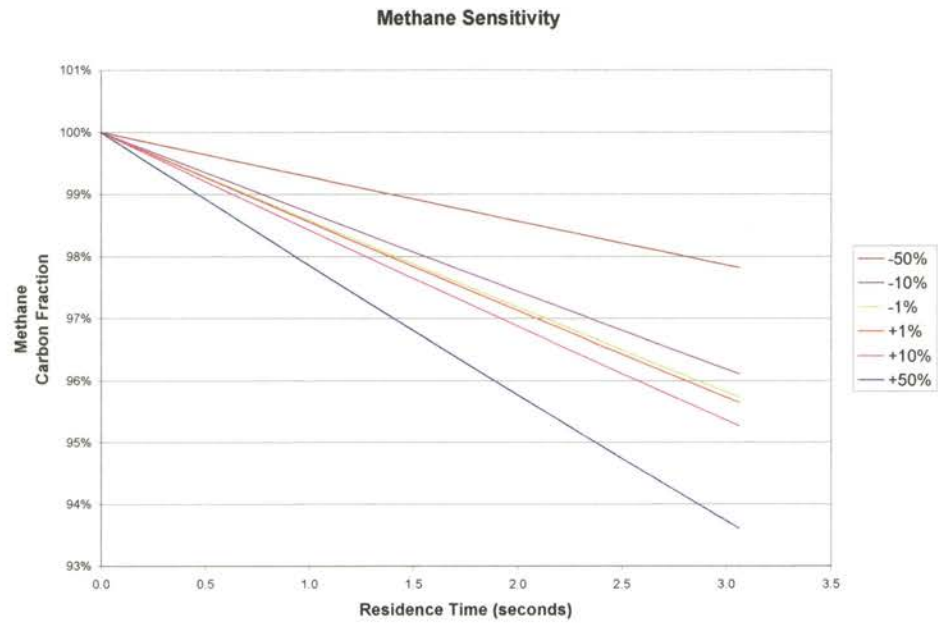


Figure F-11: Methane Fraction Sensitivity to Scale1

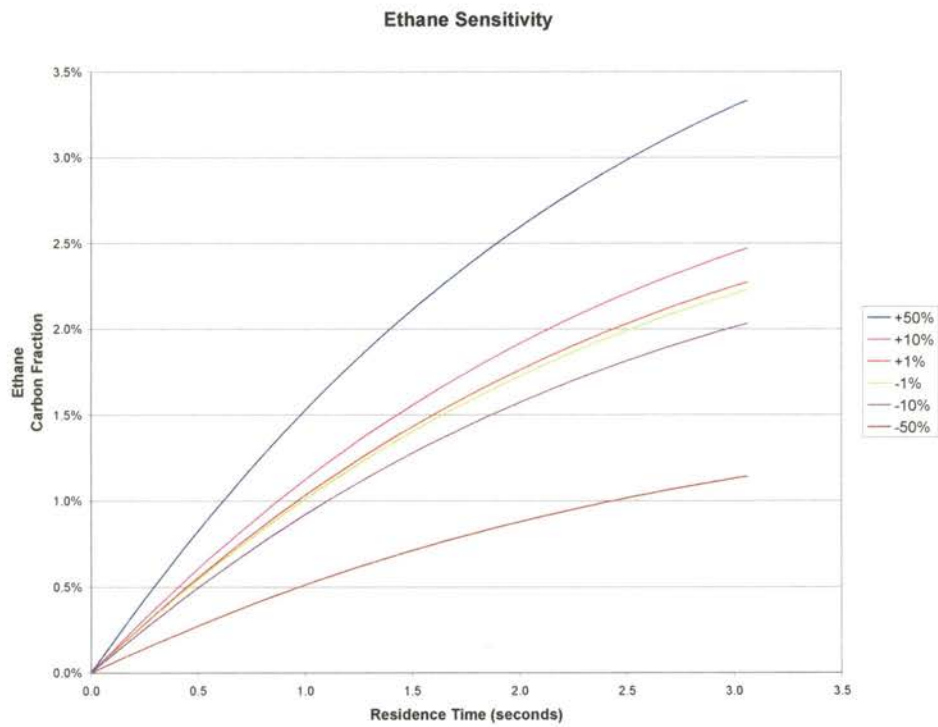


Figure F-12: Ethane Fraction Sensitivity to Scale1

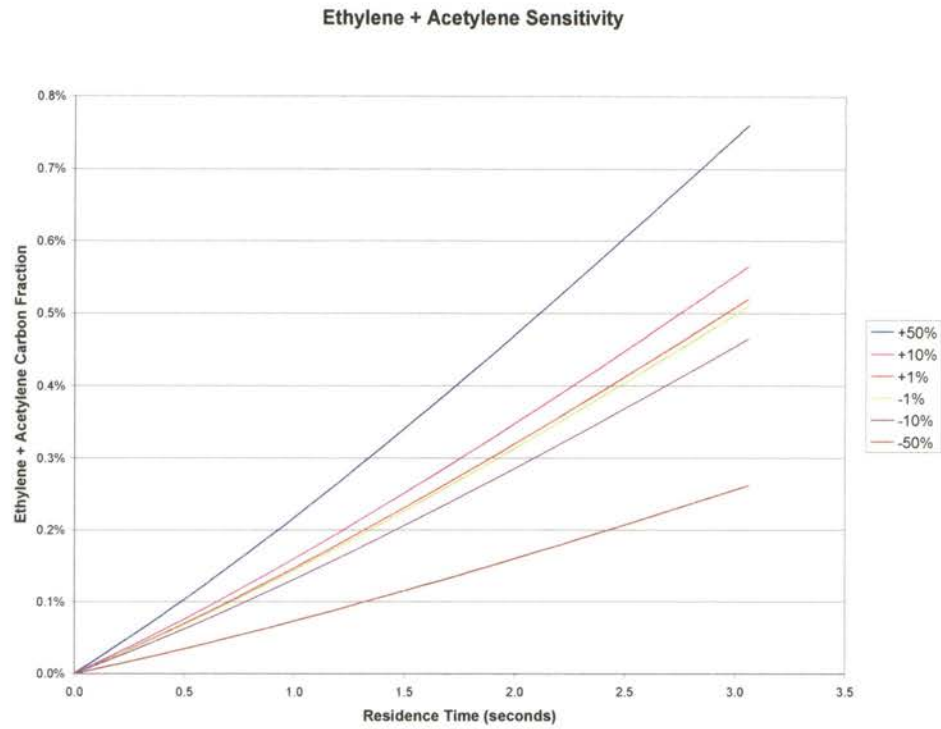


Figure F-13: Ethylene + Acetylene Fraction Sensitivity to Scale1

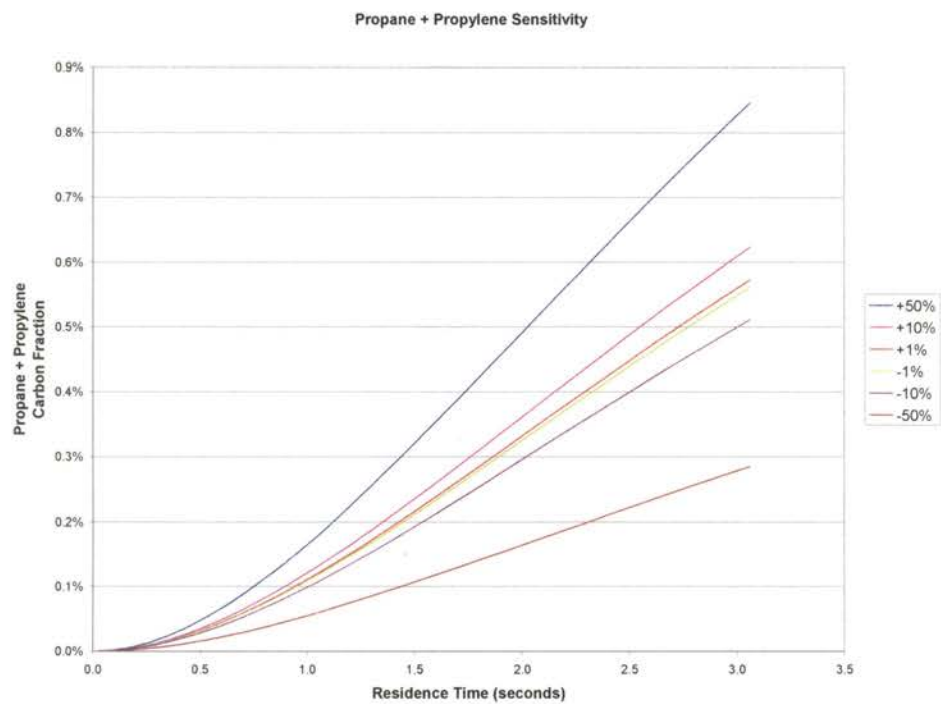


Figure F-14: Propane + Propylene Fraction Sensitivity to Scale1

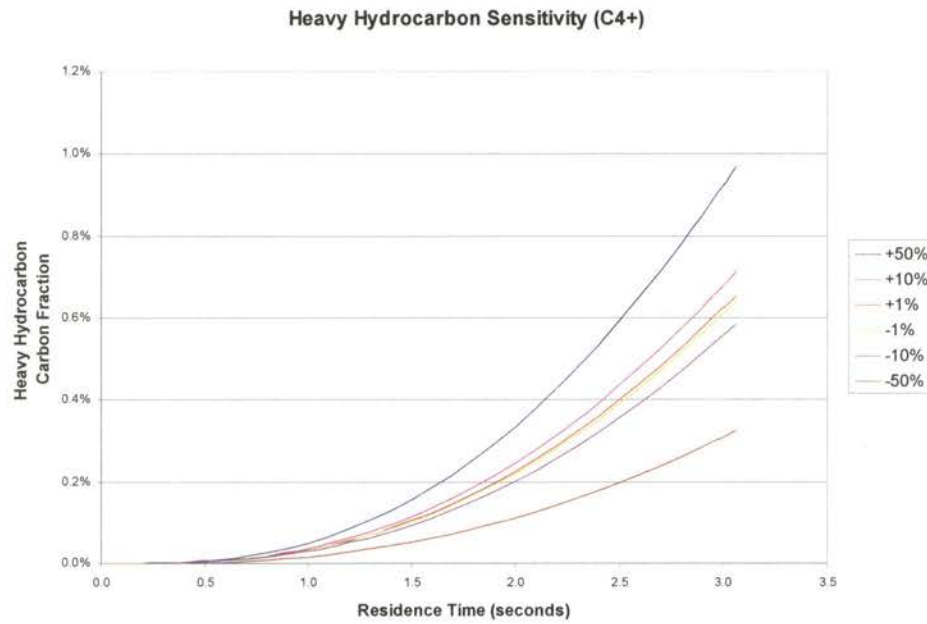


Figure F-15: Heavy Hydrocarbon Fraction Sensitivity to Scale1

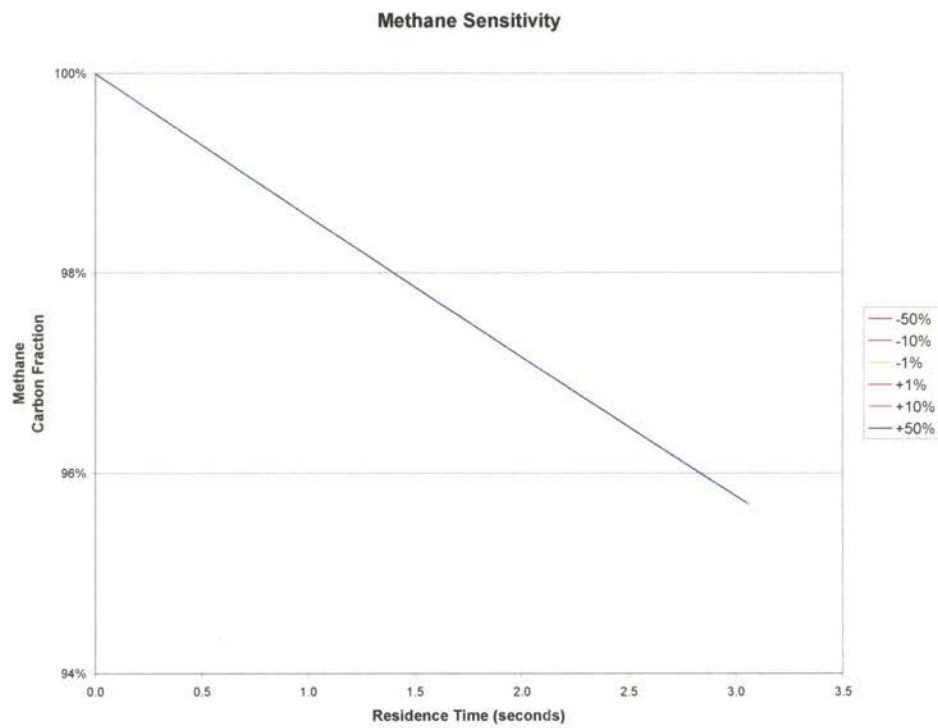


Figure F-16: Methane Fraction Sensitivity to Scale2

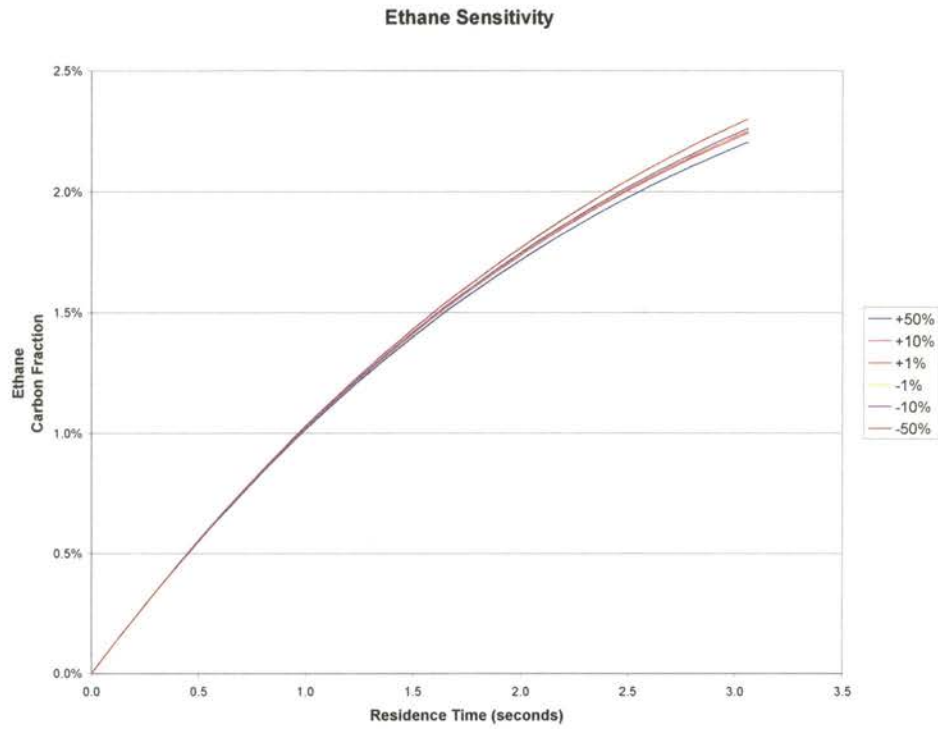


Figure F-17: Ethane Fraction Sensitivity to Scale2

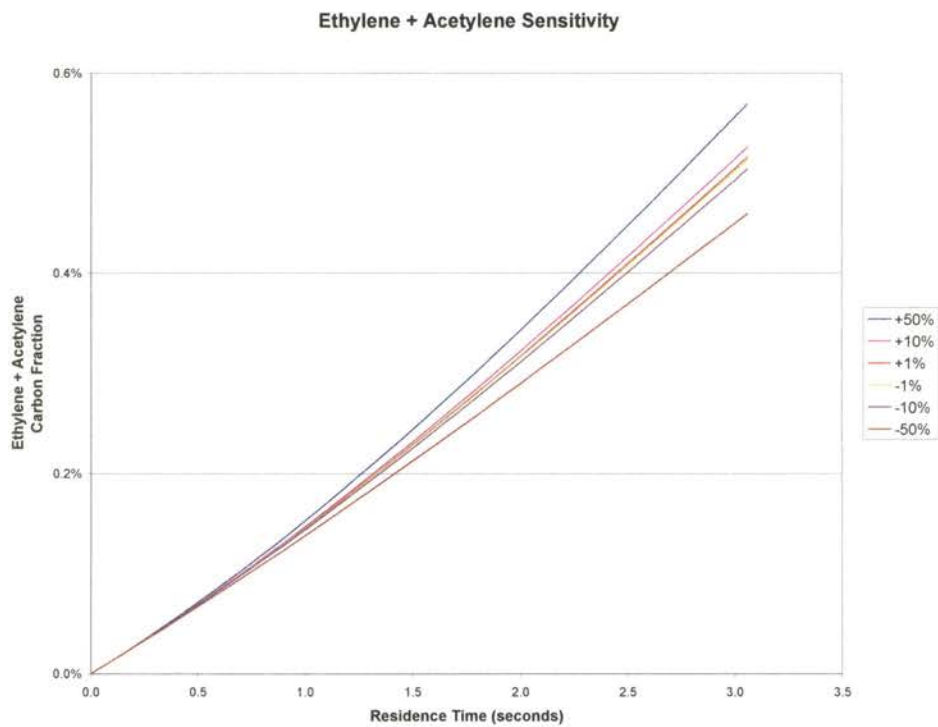


Figure F-18: Ethylene + Acetylene Fraction Sensitivity to Scale2

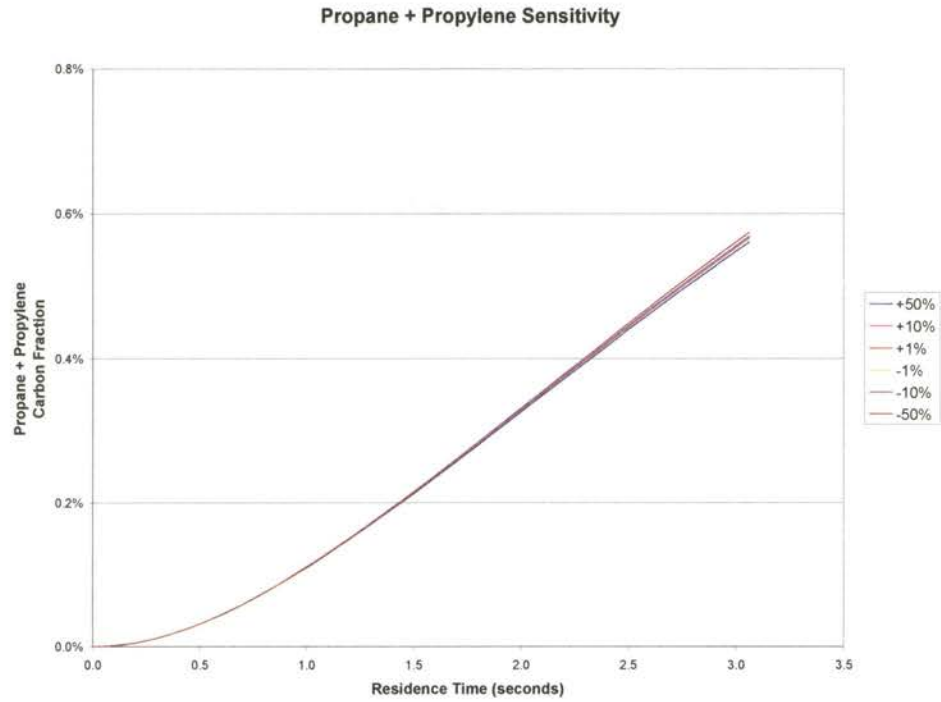


Figure F-19: Propane + Propylene Fraction Sensitivity to Scale2

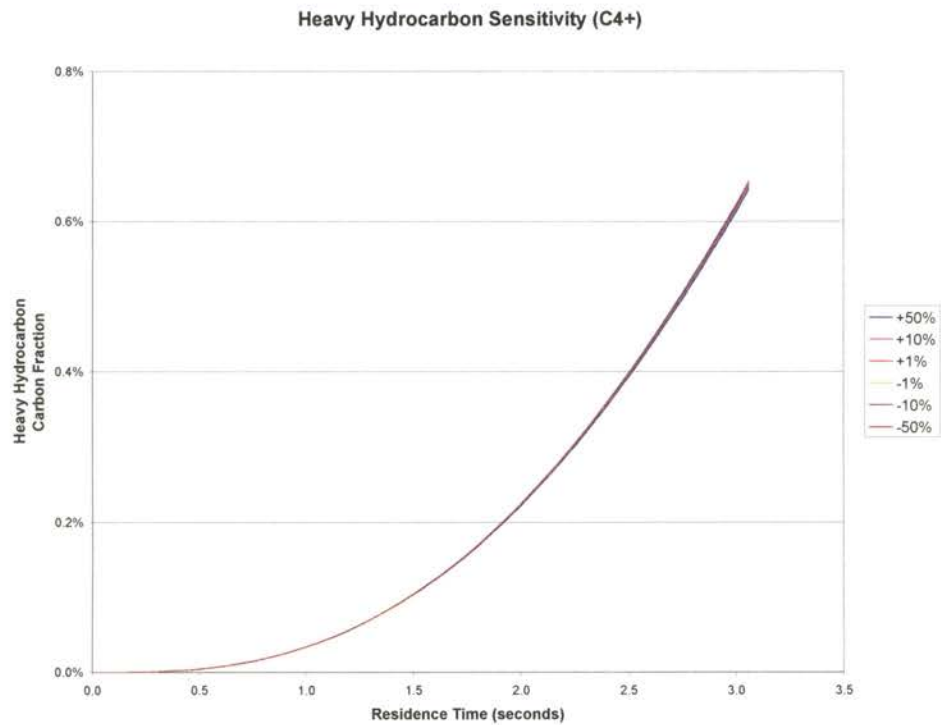


Figure F-20: Heavy Hydrocarbon Fraction Sensitivity to Scale2

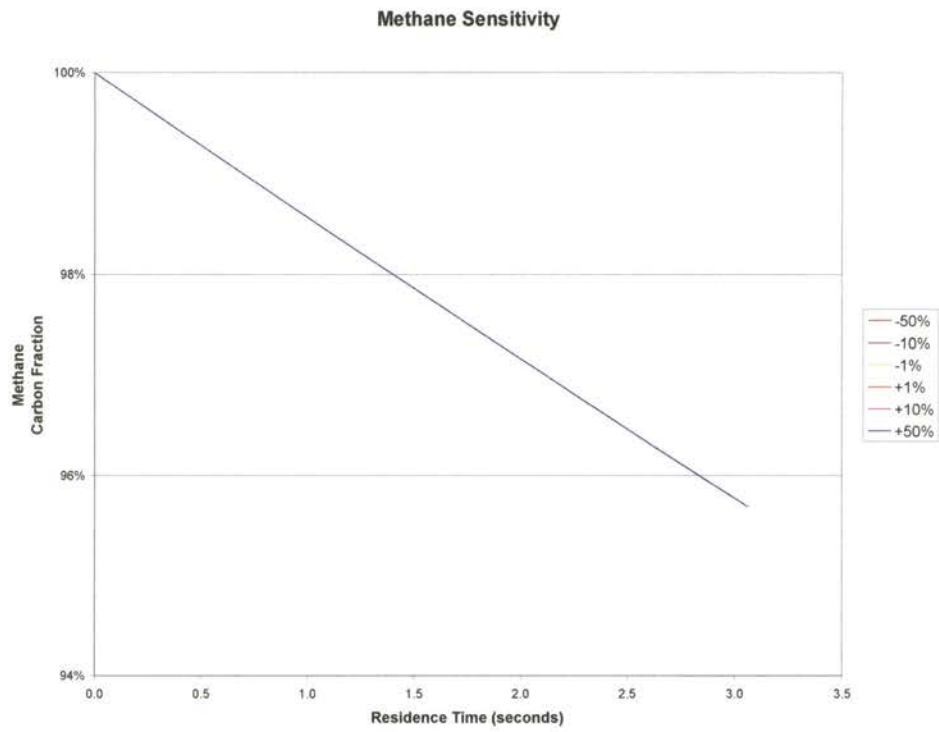


Figure F-21: Methane Fraction Sensitivity to Scale4

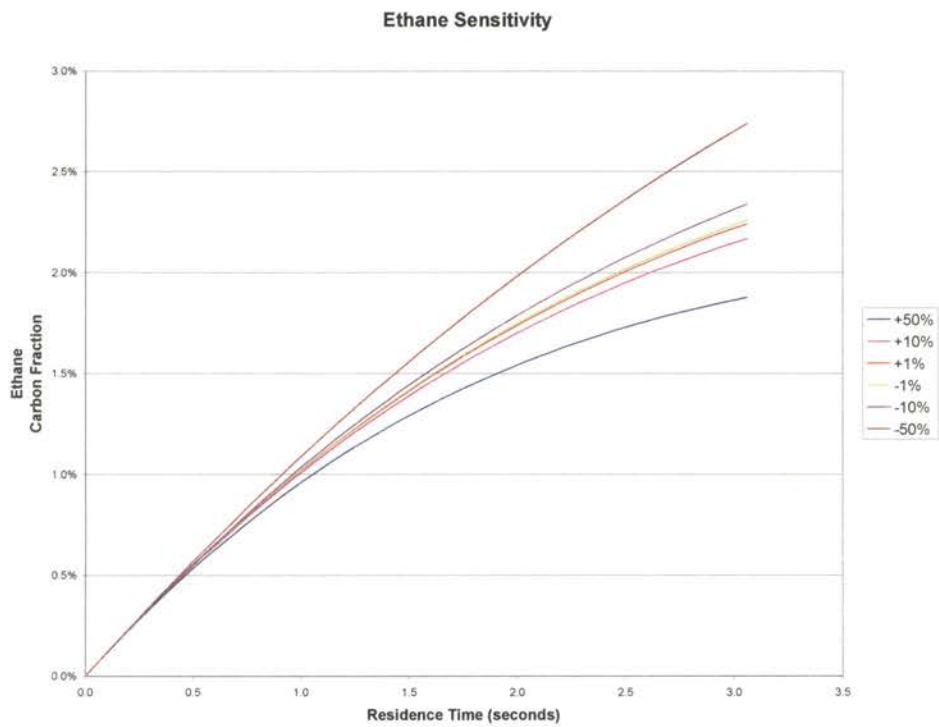


Figure F-22: Ethane Fraction Sensitivity to Scale4



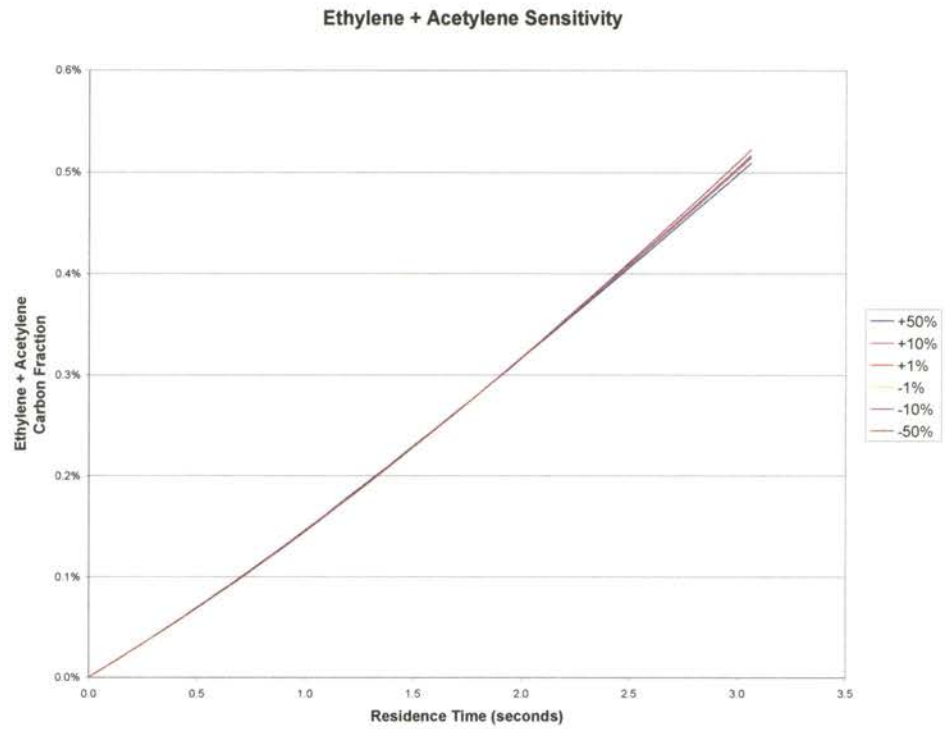


Figure F-23: Ethylene + Acetylene Fraction Sensitivity to Scale4

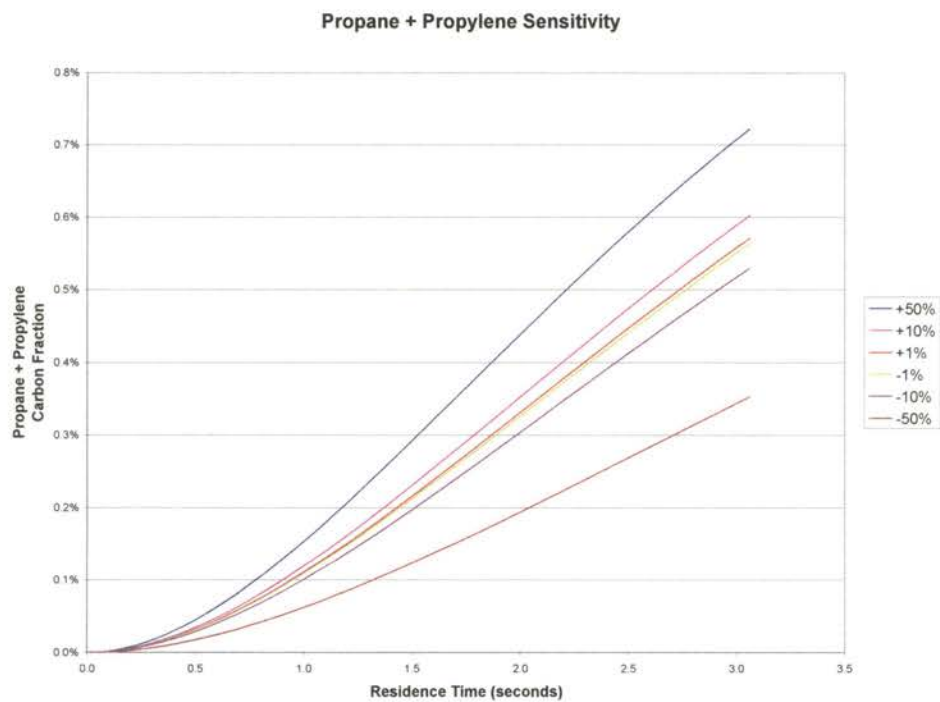


Figure F-24: Propane + Propylene Fraction Sensitivity to Scale4

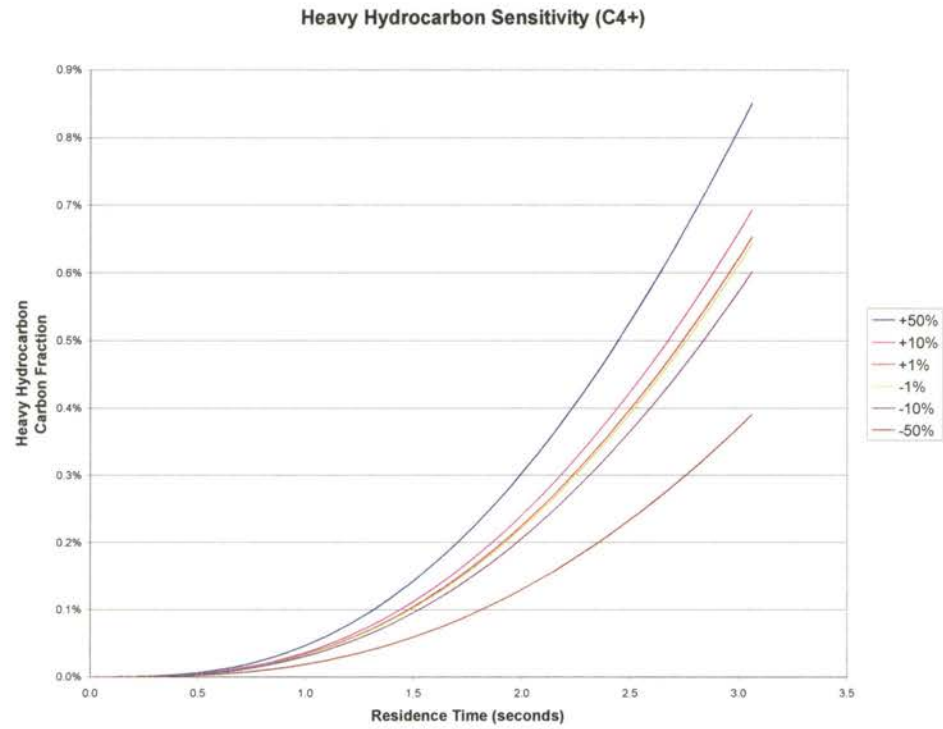


Figure F-25: Heavy Hydrocarbon Fraction Sensitivity to Scale4

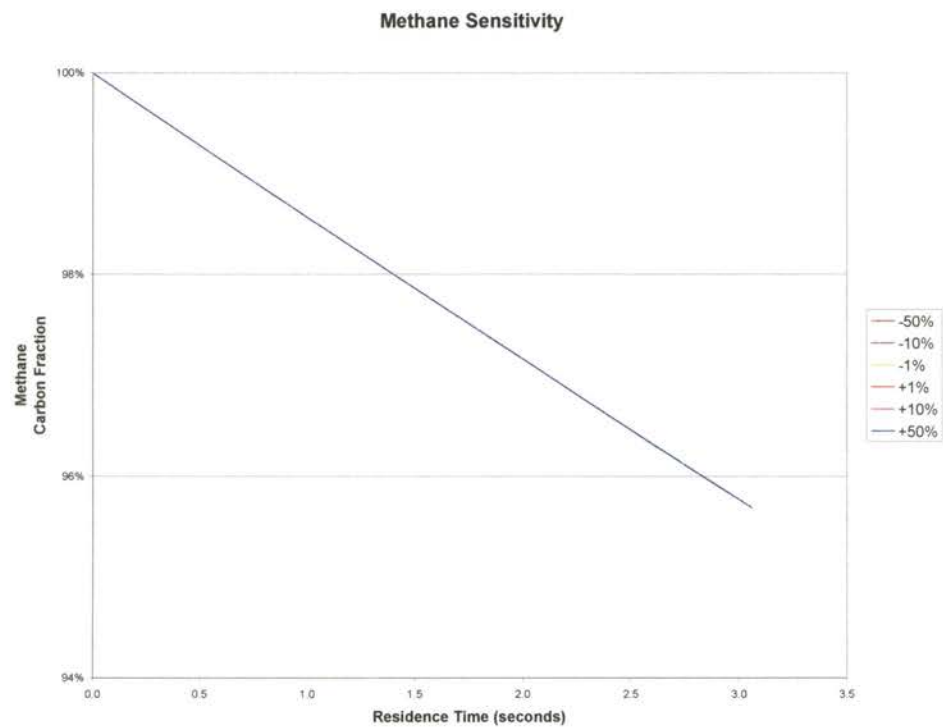


Figure F-26: Methane Fraction Sensitivity to Scale5

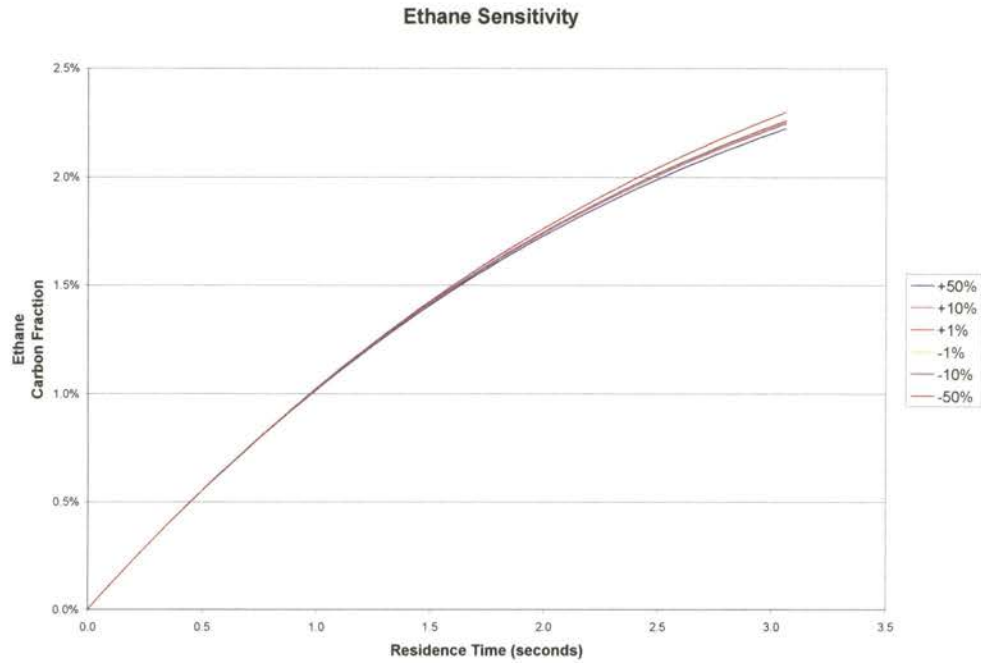


Figure F-27: Ethane Fraction Sensitivity to Scale5

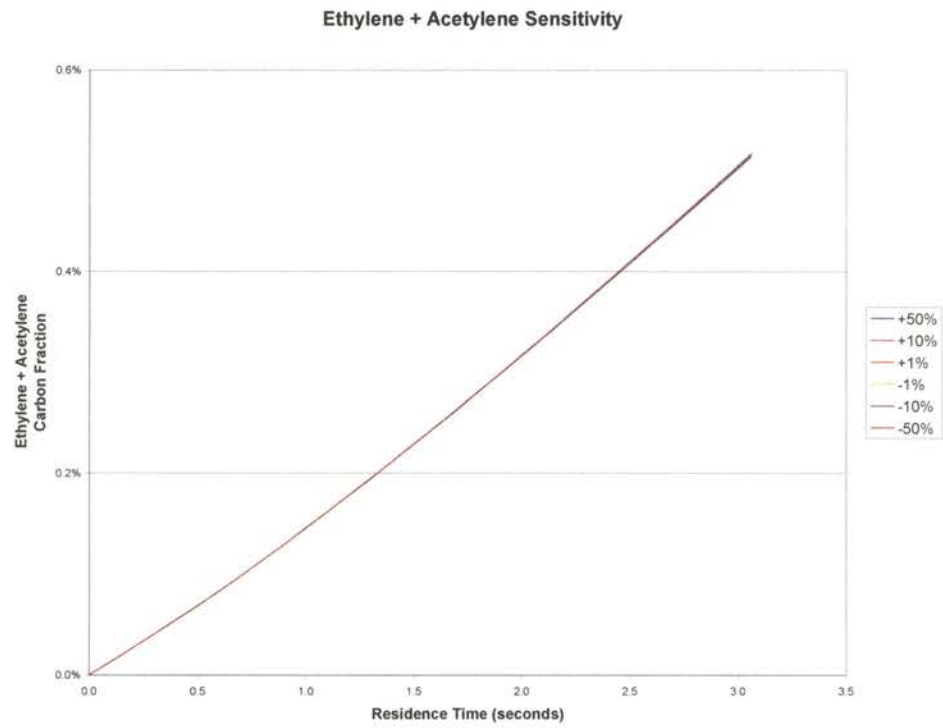


Figure F-28: Ethylene + Acetylene Fraction Sensitivity to Scale5

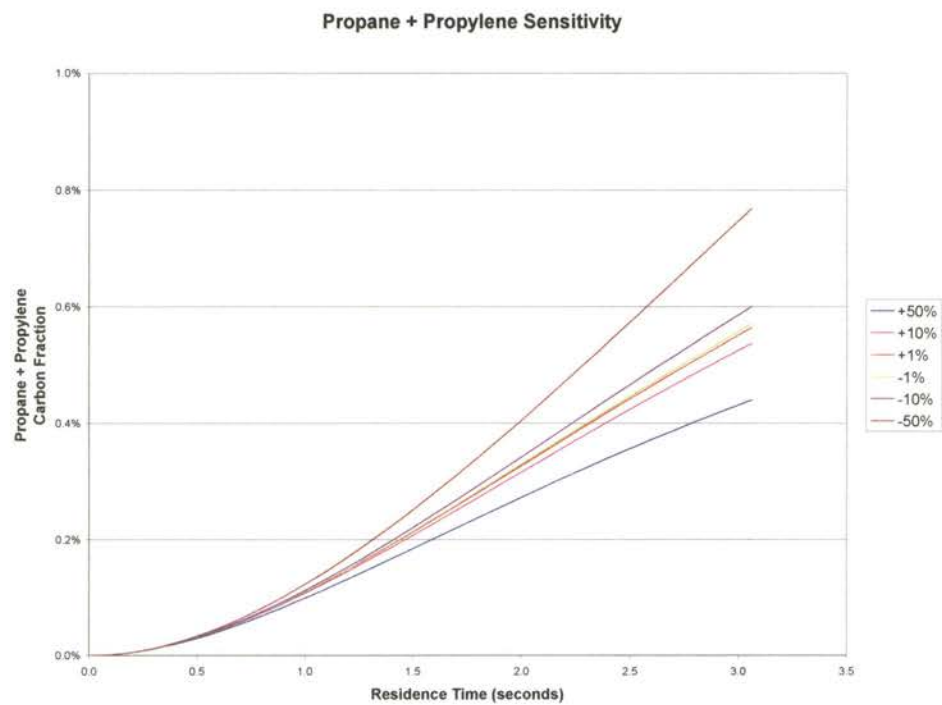


Figure F-29: Propane + Propylene Fraction Sensitivity to Scale5

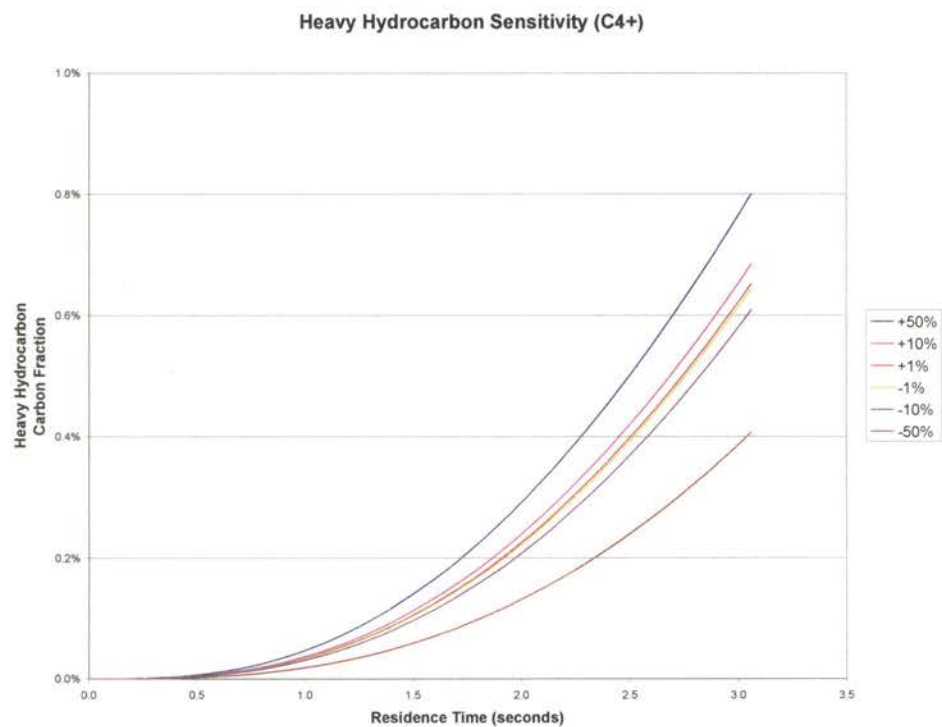


Figure F-30: Heavy Hydrocarbon Fraction Sensitivity to Scale5

TABLE F-I  
Summary of Hydrocarbon Fraction Sensitivities

Sensitivity of Hydrocarbon Fractions to Variation in Electron Density

	+50%	+10%	+1%	-1%	-10%	-50%
Methane	93.61%	95.27%	95.65%	95.73%	96.11%	97.82%
Ethane	2.67%	2.36%	2.26%	2.24%	2.13%	1.44%
Ethylene + Acetylene	0.82%	0.57%	0.52%	0.51%	0.46%	0.23%
Propane + Propylene	0.82%	0.63%	0.57%	0.56%	0.51%	0.24%
Heavy Hydrocarbons	1.55%	0.80%	0.66%	0.63%	0.51%	0.12%

Sensitivity of Hydrocarbon Fractions to Variation in Discharge Period

	+50%	+10%	+1%	-1%	-10%	-50%
Methane	93.61%	95.27%	95.65%	95.73%	96.11%	97.82%
Ethane	2.67%	2.36%	2.26%	2.24%	2.13%	1.44%
Ethylene + Acetylene	0.82%	0.58%	0.52%	0.51%	0.46%	0.23%
Propane + Propylene	0.83%	0.63%	0.57%	0.56%	0.50%	0.23%
Heavy Hydrocarbons	1.58%	0.81%	0.66%	0.63%	0.51%	0.12%

Sensitivity of Hydrocarbon Fractions to Variation in [scale1]

	+50%	+10%	+1%	-1%	-10%	-50%
Methane	93.61%	95.27%	95.65%	95.73%	96.11%	97.82%
Ethane	3.33%	2.47%	2.27%	2.23%	2.03%	1.14%
Ethylene + Acetylene	0.76%	0.57%	0.52%	0.51%	0.47%	0.26%
Propane + Propylene	0.85%	0.62%	0.57%	0.56%	0.51%	0.29%
Heavy Hydrocarbons	0.97%	0.71%	0.65%	0.64%	0.58%	0.32%

Sensitivity of Hydrocarbon Fractions to Variation in [scale2]

	+50%	+10%	+1%	-1%	-10%	-50%
Methane	95.69%	95.69%	95.69%	95.69%	95.69%	95.69%
Ethane	2.21%	2.24%	2.25%	2.25%	2.26%	2.30%
Ethylene + Acetylene	0.57%	0.53%	0.52%	0.51%	0.50%	0.46%
Propane + Propylene	0.56%	0.57%	0.57%	0.57%	0.57%	0.57%
Heavy Hydrocarbons	0.64%	0.65%	0.65%	0.65%	0.65%	0.65%

Sensitivity of Hydrocarbon Fractions to Variation in [scale4]

	+50%	+10%	+1%	-1%	-10%	-50%
Methane	95.69%	95.69%	95.69%	95.69%	95.69%	95.69%
Ethane	1.88%	2.17%	2.24%	2.26%	2.34%	2.74%
Ethylene + Acetylene	0.51%	0.51%	0.52%	0.52%	0.52%	0.52%
Propane + Propylene	0.72%	0.60%	0.57%	0.56%	0.53%	0.35%
Heavy Hydrocarbons	0.85%	0.69%	0.65%	0.64%	0.60%	0.39%

Sensitivity of Hydrocarbon Fractions to Variation in [scale5]

	+50%	+10%	+1%	-1%	-10%	-50%
Methane	95.69%	95.69%	95.69%	95.69%	95.69%	95.69%
Ethane	2.22%	2.25%	2.25%	2.25%	2.26%	2.30%
Ethylene + Acetylene	0.51%	0.52%	0.52%	0.52%	0.52%	0.52%
Propane + Propylene	0.44%	0.54%	0.56%	0.57%	0.60%	0.77%
Heavy Hydrocarbons	0.80%	0.68%	0.65%	0.64%	0.61%	0.41%

## VITA 2

Gregory D. Holland

Candidate for the Degree of

Doctor of Philosophy

Dissertation: REACTION OF METHANE IN A DIELECTRIC BARRIER  
DISCHARGE PLASMA REACTOR

Major Field: Chemical Engineering

Biographical:

Personal Data: Born in Panama City Beach, Florida, October 1, 1972, the son of  
Lonnie and Linda Holland.

Education: Graduated from Choctaw High School, Choctaw, Oklahoma in  
May 1990; received Bachelor of Science Degree in Chemical  
Engineering from Oklahoma State University in December 1994;  
completed requirements for Doctor of Philosophy degree in  
Chemical Engineering at Oklahoma State University in December  
2002.